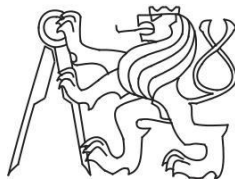


CZECH TECHNICAL UNIVERSITY IN PRAGUE

Faculty of Mechanical Engineering

Department of Automotive, Combustion Engine and Railway Engineering

Study program: Master of Automotive Engineering Field of study: Advanced
Powertrains



Test Stand for Measurement and Sampling of Brake Wear Particle Emissions.

Diploma Thesis

Author : Mr Arjun Chettiyattil Pankaj
Supervisor : Ing. Jindřich Hořenín
Year : 2019

Disclaimer

I hereby declare that this thesis work is my independent work and I have used only the documents listed in the attachments. It consists of no material previously published or written by another person.

Prague 19.08.2019

Arjun Chettiyattil Pankaj

Acknowledgement

I would like to express my gratitude to my supervisor Ing. Jindřich Hořenín. for all the guidance, support and patience throughout my master thesis. I am equally thankful for doc. Michal Vojtíšek, Ph.D, Ing. Vojtěch Klír, Ph.D. for guiding me with timely remarks which uplifted my works. I would like to thank my family and friends for their support, love and being my side throughout my master studies.

Abstract

The thesis deals with the practical design of an airtight enclosure around the braking mechanism with the filtered air has drawn into the chamber and provides cooling to the braking mechanism. This flow scavenges the wear particle produced by brake wear. The air is drawn into the designed pipe system with dilution tunnel and multiple sampling points for the isokinetic sampling process, then it is directed to the exhaust system by a variable speed centrifugal fan. This thesis includes the literature survey, description of two different design variants with pressure drop calculations, technical drawings and part lists.

Keywords: Brake wear, Airtight Chamber, Dilution tunnel, Isokinetic sampling, Variable speed centrifugal fan

Contents

Abstract.....	4
Symbols.....	8
Abbreviation	10
Chapter 1; Introduction	11
Vehicle Emissions.....	11
Importance of Non-Exhaust Emission.....	11
Test stand for measurement and sampling of brake wear particle emission	12
Scope.....	12
Chapter 2; Literature Reviews	13
Various Methods of Non-Exhaust Emissions	13
Brake Wear	13
Tyre Wear.....	13
Road Surface Wear	14
Resuspension of Road Dust.....	14
Health Effect	14
Emission Test Cycles	15
NEDC (New European Driving Cycle)	16
CADC (Common Artemis Driving Cycle).....	17
WLTC (World Harmonized Light Vehicle Test Cycle).....	18
Measuring Non-Exhaust Emission	20
Direct Measurements	20
Receptor Modelling.....	21
Road Tunnel Sampling	21
Chapter 3; Experimental Set up.....	21
Asynchronous Motor	22
Fly Wheels.....	22
Disc Brake.....	23
Brake Rotor	23
Brake Pad	24
Thermocouple Temperature Sensor	24
Infrared Temperature Sensors.....	24
Brake Fluid Temperature Sensor	25
Speed Sensor.....	25
Chapter 4; Design Concepts.....	26
Full Flow Dilution Tunnel	26

Requirements and Restrictions.....	26
Scheme and Description	27
HEPA Filter	28
Chamber enclosing the Brake disc.....	29
Duct system.....	29
Dilution Tunnel.....	29
Sampling probe	29
Temperature sensor.....	29
Centrifugal blower	29
Chimney	29
Chapter 5; Calculations	30
Determination of Total Energy Dissipated in Selected Cycles	30
WLTC	30
ARTEMIS.....	31
Calculation of Diameter of The Pipe	31
Calculation of Flow Rate.	32
3D models and Design description	33
Design Variant 1	33
Chamber.....	37
Pipe Design.....	42
Flange	43
Elbow.....	43
Tunnel	44
Sampling Point	45
Sampling Probe	45
Pitot Tube.....	47
6.3.5 Temperature Sensor	47
Structure for Mounting Fan	48
Pipe Clamp	48
Gasket Sheet	49
Rubber Cable Gland	50
6.5 Fasteners.....	50
Hex nut - DIN 934, ČSN 02 1401	51
Flat washers -DIN 125 A, ČSN 02 1702 -STAINLESS	51
Design Variant 2	51
Pipe design	52

Tunnel	55
Mounting of the Blower.....	56
5.3 Calculation of Pressure drop.....	56
.Pressure Drop at HEPA filter	56
Pressure drop during the flow through the pipe	56
Manual Pressure drop Calculation of design Variet 1	57
Manual Pressure drop Calculation of design Variet 2	59
Total pressure drop calculation using Ansys.....	60
Pump Selection	70
Frequency converter	72
SUMMARY AND CONCLUSION	74
THESIS CONTRIBUTION	76
Future suggestions	76
References	77
List of Figures	80
List of Tables	82
List of Graphs	83
List of Attachments	84
Attachments.....	86

Symbols

ΔP_1	Total pressure drop in duct (Pa)
ΔP	Total Pressure Drop(Pa)
ΔP_2	Pressure drop at HEPA filter(Pa)
ΔT	Change in temperature($^{\circ}\text{C}$)
A	Area (m^2)
Al,	Aluminium
Ba	Barium
C	Specific Heat capacity of air(kJ/kg-k)
Ca	Calcium
Cd^{2+}	Cadmium Ion
CO	Carbon monoxide
Cu	Copper
d	Diameter (m)
D_1	Initial Diameter(m)
D_2	Final Diameter(m)
Fe	Iron
f_{Re}	Friction factor
Hg^2	Mercury Ion
H_t	Total head loss (m)
J	rotational moment of inertia (kgm^2)
k_l	Resistance coefficient due to bend
K_s	Resistance coefficient due to square reduction
M	Total mass of the vehicle(kg)
Mn^{2+}	Manganese Ion
Na	Sodium

Ni ²⁺	Nickel Ion
NO _x	Nitrogen oxides
Pb	Lead
PM ₁₀	Particulate matter of size 10 micrometres or less
PM _{2.5}	Particulate matter of size 2.5micrometers or less
R _e	External radius(m)
Re	Reynolds number
R _i	Inner radius(m)
S	Sulphur
Sb	Stibnite
Ti	Titanium
T _{in}	Inlet Temperature(°C)
T _{out}	Outlet Temperature(°C)
v ₁	Final velocity (m/s)
V _{max}	Maximum vehicle velocity(m/s)
V _o	Initial velocity(m/s)
Zn	Zinc
μ	Dynamic viscosity of air(kg/m-s)
ρ _{air}	Density of air (kg/m ³)

Abbreviation

CADC	Common Artemis Driving Cycle
HEPA	High Efficiency Particulate Air
KE	Kinetic energy
NEDC	New European Driving Cycle
PMR	power to mass ratio
RPM	Revolutions per minute
UK	United Kingdom
UNECEPMP	United Nations Economic Commission for Europe
VOCs	Volatile organic compounds
WHO	World Health Organization
WLTC	World Harmonized Light Vehicle Test Cycle
3D	Three dimensional

Chapter 1; Introduction

Vehicle Emissions

The major reason for Urban air pollution is road vehicle emission. The most critical toxic emissions from light-duty, gasoline-powered vehicles are volatile organic compounds (VOCs), carbon monoxide (CO), and oxides of nitrogen (NO_x), however, for heavy-duty, diesel vehicles, the biggest concerns are Nitrogen oxides (NO_x) and fine particulate matter (PM_{2.5}). VOCs and NO_x respond to the sunlight and undergoes chemical reaction to produce ozone and photochemical aerosols. As contrasted with earlier days, the emission of VOCs, CO, NO_x, and PM are reduced by more than 99 % by introducing new technological development. [1] precise, computer-based fuel-air mixture control and three-way catalyst after-treatment combined with improved fuel quality etc are the examples to the developments. These technologies rarely permit some vehicles to have exhaust which lower in these toxic compounds than in the ambient air! Emissions of VOCs and CO from highway vehicles have fallen significantly since the light-duty fleet has turned over, on about a 15-year cycle. [2]

Emissions regulation of heavy-duty vehicles has lagged that of light-duty vehicles and combined with the slower turnover of the heavy-duty fleet, the reduction in highway emissions of NO_x and PM 2.5 has trailed that of CO and VOCs. [1] Diesel control technology capable of achieving nearly the reductions seen in light-duty vehicles appeared only recently. Heavy-duty vehicles with traps, which are very effective in reducing PM_{2.5} and ultrafine particles (<100 nm in diameter), resulting in particulate mass emissions that are more than 98% below those from uncontrolled vehicles. [2] The first half of this reduction comes from improved combustion; the second from the trap. Selective catalytic reduction technology introduced combined with previous combustion improvements and exhaust-gas recirculation, delivers similar levels of control of NO_x. [3]

Importance of Non-Exhaust Emission

It is all well perceived that 50% of the overall road transport contribution to PM₁₀ and PM_{2.5} emissions are by non-exhaust emissions.[3].Among the non-exhaust particle generation possibilities, disc brake wear plays an important role. As exhaust emission controls become stricter, relative contributions of non-exhaust sources, including brake wear, to traffic-related emissions will become more significant and will raise questions as to the necessity of regulations pertaining to non-exhaust emissions.[4]

Regulations for brake pad performance are influenced by many bodies across the world, including the Particle Measurement Programme by the United Nations Economic Commission for Europe (UNECEPMP). In order to continuously improve their products and ensure regulatory compliance, brake pad manufacturers conduct brake performance tests. These standardized tests can be carried out on vehicles and on dynamometers (separate from a vehicle). An overview of brake testing procedures for passenger cars and light-duty trucks with hydraulic braking systems can be found in the review of Agudelo and Ferro (2005).

Due to their adverse health effects emissions have been regulated for over three decades. Brake wear particulate matter is the most important non-exhaust source, however current knowledge is mainly limited to observational studies. [5] [3]

Test stand for measurement and sampling of brake wear particle emission

In this thesis, I have designed an experimental set up for measuring and sampling the brake wear particle produced as a result of the simulation of different driving cycles. The driving cycles will be simulated using the test bench available at the laboratory. Wear particle generated as the result of the simulation will undergo sampling process using a full flow dilution tunnel with a centrifugal blower to generate the flow and the airtight chamber to enclose the brake rotor. The design of the chamber and the tunnel system has done considering several criterions which are describing in the following chapters.

Scope

Goals of this thesis are as follows

- To give an overview of non-exhaust vehicle emission and its importance
- Design an airtight enclosure around the braking mechanism, drawing filtered air which provides cooling of the brake disc as well as to scavenge wear particles produced.
- Design of the pipe system which carries the particles from the enclosure to the dilution tunnel from where the isokinetic sampling is performed along with the flow ambient condition measurements.
- Description of design, technical drawings and list of parts.

Chapter 2; Literature Reviews

Various Methods of Non-Exhaust Emissions

Since there are friction and aberration during the driving of a vehicle at several places, there are several sources of Non-Exhaust emission in vehicles and driving scenarios. Each of them depends on various factors including the driving pattern as well as the weather condition.

Brake Wear

As we know, the function of the brake is to reduce the vehicle speed by converting the kinetic energy of the wheel to thermal energy. During this process debris and particles are produced as a result of the friction between the brake linings and brake pistons. Studies show more than 75 % of the brake friction lining will wear out during its lifetime. [6] Which says a major percentage of the material is converted to the microparticle. These particles will be directly emitted to atmosphere or deposited on the road which will again suspend in the atmosphere because of the road traffic. The rate of wear is depending on several factors like the material composition of the friction lining, temperature between the friction surfaces, the grain structure of the friction material, speed of rotation of the wheel, load on the wheel, the material used as the brake piston etc. Brake materials made by the combination of modifiers, binders, carbon material, lubricants and fillers. Al, Ba, Cu, Fe, Sb, Ti and Zn are the major components of brake wear emission. Brake wear contributes 14% of the total PM10 emission. [7]

Tyre Wear

During driving tire is abrade against the road. The friction between the road and tire treads will lead to the wear of tire material hence the production of wear dust. Tyres are composed of different materials including steel reinforcements, several types of rubber, carbon black, different inorganic and organic materials. A high concentration of Al, Ca, Fe, Na, Zn, and organic compounds like Styrene-butadiene rubber, benzothiazole and polycyclic aromatic hydrocarbons are found in tyre wear emission. [7] According to vehicle dynamics during the process of braking a major part of the vehicle weight to the front axle. Apart from this, for front-wheel vehicles, the engine is positioned in the front side of the vehicle which leads to additional loading at the front axle.[8] This is the reason why front-wheel vehicles contribute more than 60% of the tyre emission per vehicle. Tyre wear is increasing day by day since the number of tyres in use is growing at a vigorous rate. Studies show if the number of vehicles is increasing as in current rate then the number of tyres in use can be around

200million by 2021 (Environment Agency,1999). Tyre wear contributes 11% of the total PM10 emission. [9]

Road Surface Wear

There is a constant interaction between road surface and tyre. This relative movement causes a shear force between the road surface and the tyre which produces the wear particle. Studded tyres and traction materials used in Nordic countries escalates the rate of road wear. European roads are mostly concrete and asphalt-based surfaces. Where concrete surfaces are consisting of sand, cement and stones. However, the asphalt road surfaces are consisting of bitumen This will contribute a major share towards the road surface wear dust. Al, Ca, Cr, Fe, Ni, Si and Zn are the major elements of road wear particle. 10% of the total PM10 emission is contributed by road surface particle. [9]

Resuspension of Road Dust

This is considered as the major cause of the total PM10 emission. Due to the turbulence and the effect of wind the deposited road dust is again suspended to the atmosphere and it continues as a cyclic process. The concentration and components of the road dust are strongly depending on local factors and emission. However, there are many practical problems in measurement and sampling of road dust and which lead to uncertainty. The study conducted by Abu-Allaban, (2003); Stocker and Carruthers, (2007) estimate the range of 10-90 % of the total PM10 contribution is by resuspension of road dust. [9]

Health Effect

Several factors are considered for the investigation of the toxicity of the non-exhaust emission. Factors like particle size, chemical composition, chemistry and surface charges are important among them. A study conducted by WHO in 2013 depicts the short- and long-term exposure of non-exhaust PM emission can cause respiratory and cardiovascular deceases, as well as the number of mortalities from cardiovascular and respiratory malfunctioning also lung cancers. The upper respiratory tract can filter coarse particle however ultra-fine particle can penetrate deep into the respiratory tract and cause many serious problems due to their higher surface area and reactivity. These ultra-fine particles sometimes can diffuse into the cardiovascular system and can be transported to the other organs in the human body such as brain, kidneys, liver. [1] An experiment on animals shows the transportation of ions like Mn^{2+} , Cd^{2+} ,

Ni^{2+} , Hg^{2+} and Al^{3+} to the brain.[10]. Fine particle matter of metals, especially transition metals have a very adverse effect on human health. Metals like Fe, Cu, Cr and Ni can produce reactive oxygen species which are highly chemically active and causes oxidative stress in biological cells.

The chemical reaction of these active species is influenced by the presence of metals such as Zn, Pb and Al either as a positive catalyst or as a negative catalyst. Since Fe and Cu are the major part of the brake wear particulate matter, the relevance of this topic is very high.[11]

Apart from this heavy metal have a negative response towards the human body. Researches show

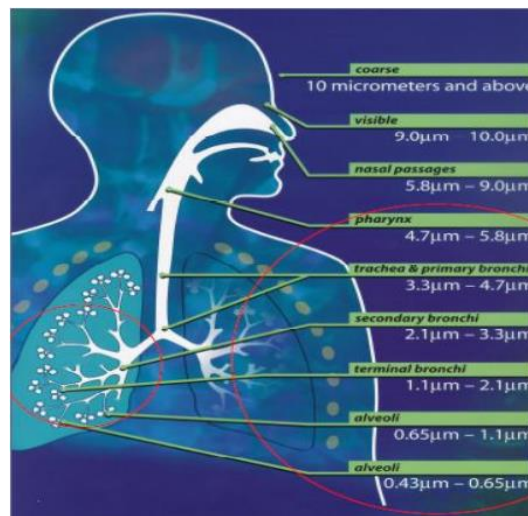


Figure 1: The penetration ability of particulate matter

a direct relationship between the amount of Pb in blood and cardiovascular diseases and mortality rate. Also, monthly mortality rate and the amount of Cu and S in blood shows a direct relationship too. However, the combined effect of these elements in blood found to be more dangerous than the element alone in blood. It shows the complex mixture of these particles is more fatal.[12]

Emission Test Cycles

This is a protocol involved in the emission standards for the repeatable and comparable measurement of the vehicle exhaust emission. There are different cycles for various type of engines like heavy-duty engines, light-duty engines, diesel engines, gasoline engines etc.

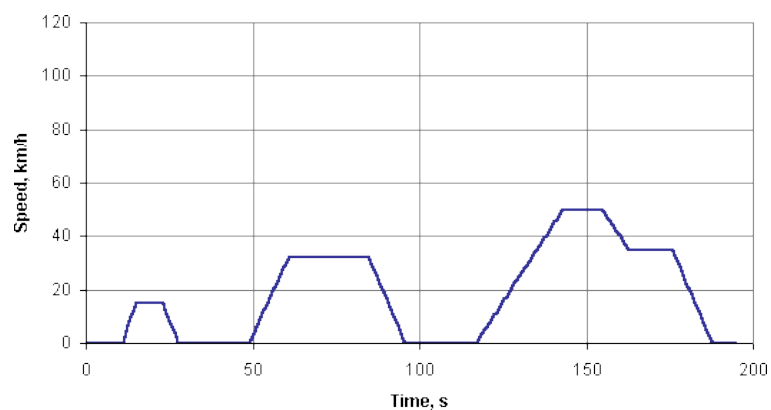
Engine or vehicle is operated under specific conditions during the operation of each cycle for the measurement of exhaust emission. Different countries, international governments and organizations are following various test cycles which are according to their driving conditions and driving behaviours. [13][14] Operating temperature, speed and load are the important parameters of the test cycle. Simulating all possible driving conditions which a vehicle or engine

operates is impossible. However, the standardising of the driving conditions can be done by the emission test cycles. [13]

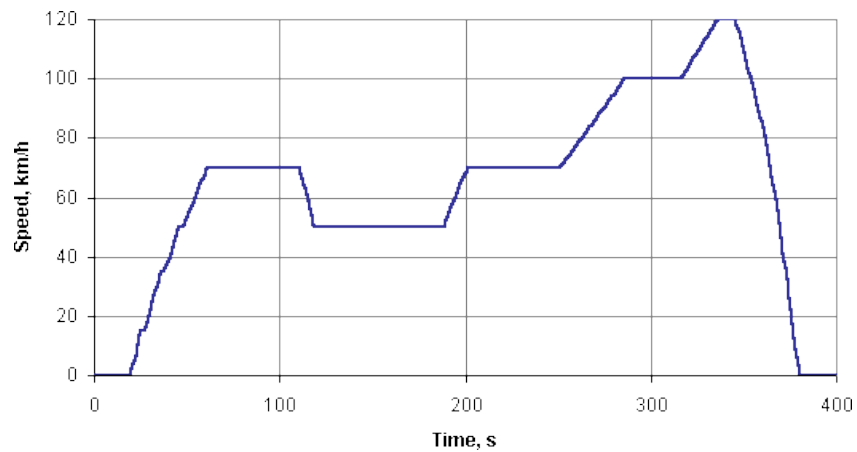
Here we are using a light-duty emission test cycle for the experiment since the number of the light-duty vehicle are higher compared to that of heavy-duty vehicles.

NEDC (New European Driving Cycle)

This emission test cycle of EU type was used for the emission control of light duty-vehicles. This is performed on a chassis dynamometer. This test cycle is the combination of the urban driving cycle (Graph: 1) and extra-urban driving cycle(Graph 2). The entire cycle contains 4 urban cycle segments repeated without interruption and followed by one extra-urban driving cycle. The vehicle should be allowed to soak for 6 Hrs at 20-30°C and then allowed to idle for 40s. An amendment in 2000 allowed to run the cycle without the 40s idling time and it is known as NEDC afterwards. The representation of the cycles is done by the speed vs time graph. [13]



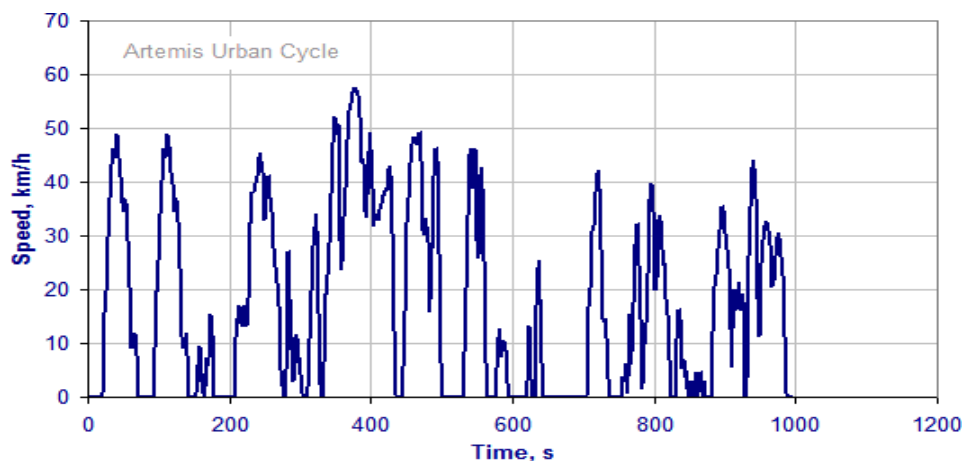
Graph : 1 NEDC-Urban Driving Cycle



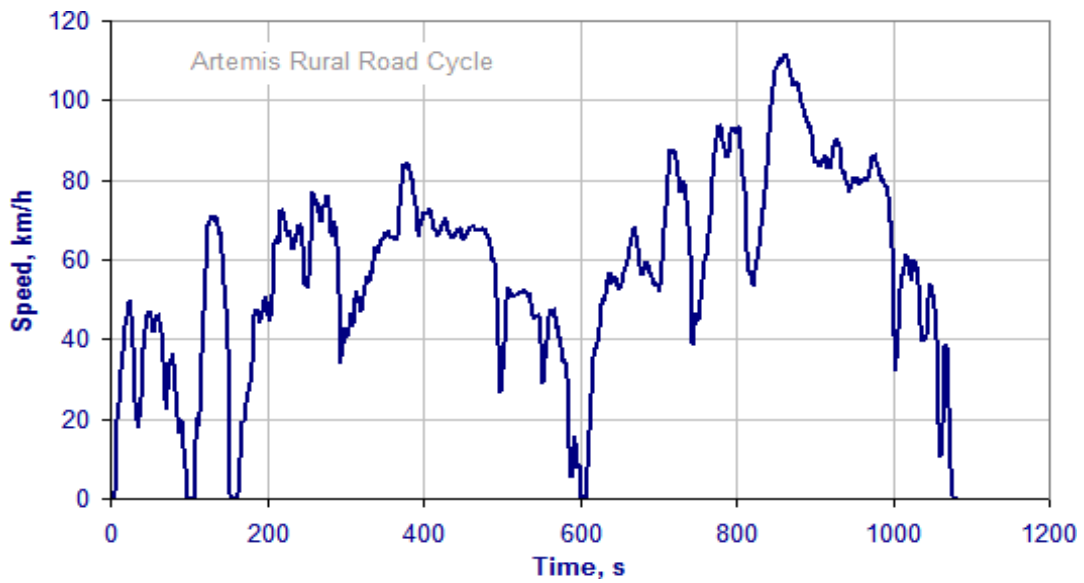
Graph : 2 NEDC-Extra Urban Driving Cycle

CADC (Common Artemis Driving Cycle)

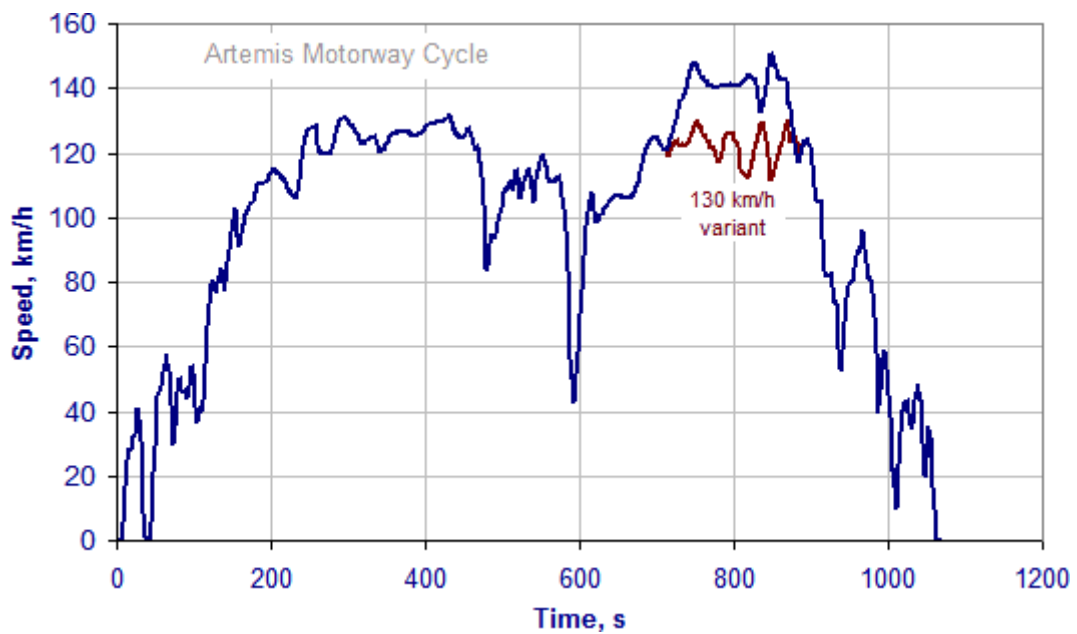
Artemis driving cycle is developed by the statistical analysis of large data of real-world driving pattern in Europe. This is done by assessment and reliability of transport emission model and inventory system project. The cycle is subdivided into 3 groups; urban(Graph 3), rural(Graph 4) and motorways(Graph 5). The motorway group is again sub-classified into two based on the maximum speed limit. One variant is with a maximum speed of 130 km/h and another with a maximum speed limit of 150km/h. Apart from this, Artemis cycle included the gear shifting strategies. [13]



Graph : 3 Artemis Urban cycle



Graph : 4 Artemis Rural roads



Graph: 5 Artemis Motorways

WLTC (World Harmonized Light Vehicle Test Cycle)

This light-duty chassis dynamometer test cycle for measurement of emission was developed by the working group in the UN which working on pollution and energy. WLTC is a part of Worldwide

harmonized Light vehicles Test Procedures, published as UNECE Global Technical Regulation No 15. WLTC is replacing NEDC and the transition is going on.

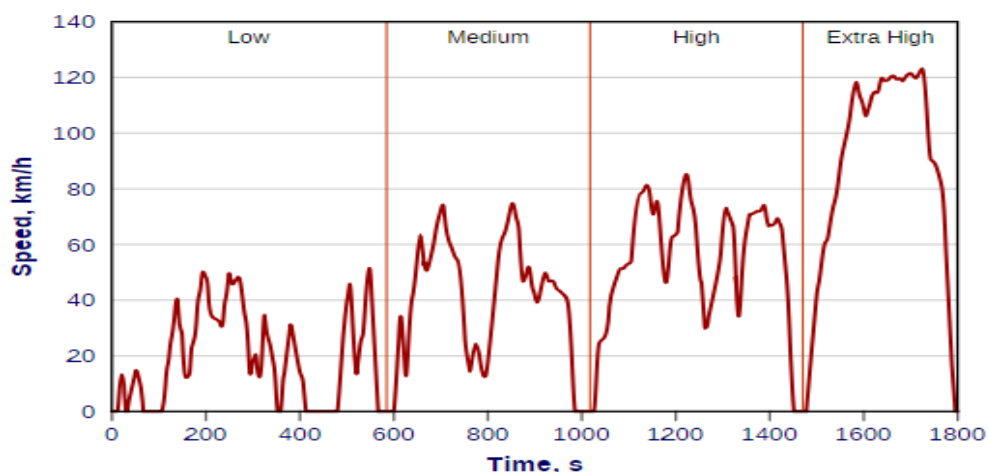
WLTC is applicable for vehicles with different power to mass ratio (PMR).

$$PMR = \frac{\text{Rated Power}(w)}{\text{Curb weight}(kg)}$$

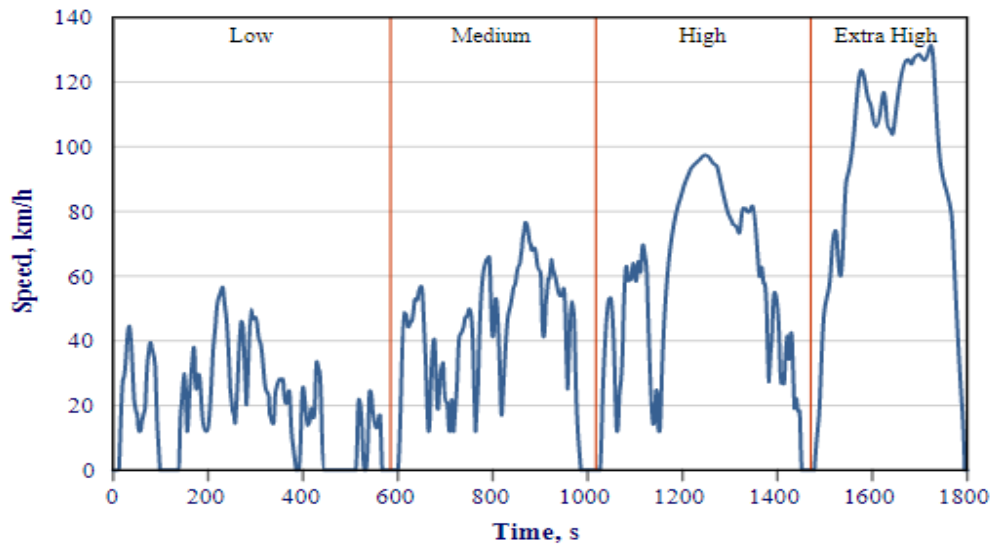
However, EU regulations appear inconsistent with GTR 15 and replace the curb mass with “mass in running order”, which includes the driver and is 75 kg higher. The cycle definition also depends on the maximum speed of the vehicle given by the manufacturer but not restricted by any other traffic regulations.

The cycle is subdivided into three classes. Class 1(Graph 6), class 2(Graph 7), class 3 (Graph 8) cycles, respectively for vehicles with $PMR \leq 22$, $22 \leq PMR \leq 34$, $PMR > 34$. Further class 3 cycle is classified again into two based on the maximum vehicle velocity. Group A is for a vehicle with maximum velocity $V_{max} \geq 120$ km/h and Group B for vehicles with $V_{max} < 120$ km/h.[13]

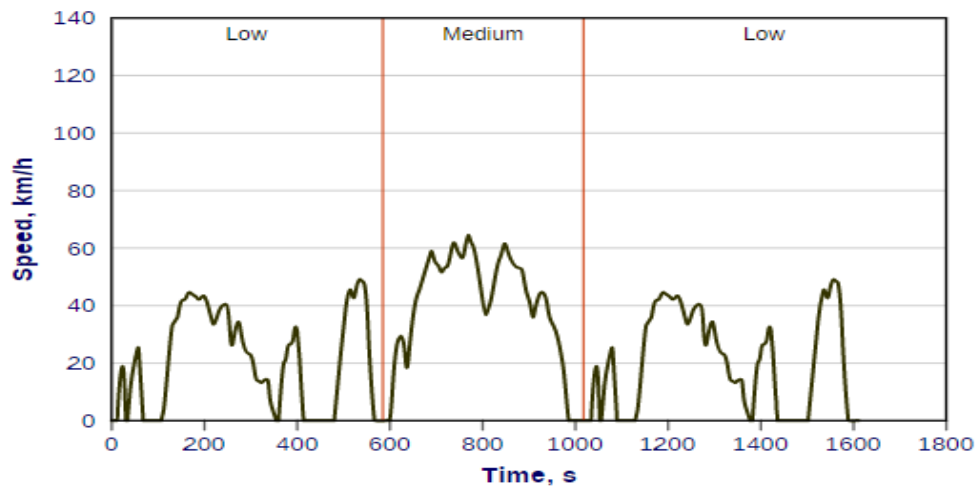
From the above chassis dynamometer test cycles, NEDC is eliminated from the experimental procedure since it is replaced by WLTC. Further WLTC class 3B conditions are considered for the experiment apart from the Artemis cycle since it simulates high-speed driving condition. So, the breaking effect, as well as the brake wear, will be more considerable. Artemis is selected since it is more realistic towards the European driving cycle since it is developed from statistical data. [13]



Graph 6 : WLTC Class3a



Graph 7: WLTC Class 3b



Graph 8: WLTC class 1

Measuring Non-Exhaust Emission

The uncertainty associated with the concentration of non-exhaust emission can vary depending on the origin of the pollutants. Therefore the emission factor is almost sight specific. This makes the non-exhaust emission quantification a difficult task. Direct measurement, receptor modelling and road tunnel sampling are the two approaches to calculate the non-exhaust emission factor for atmospheric dispersion model.[15]

Direct Measurements

Dynamometer and laboratory testing are the major direct measurement methods and have been used by many researchers. Different experimental set up must be developed to simulate the driving condition and followed by the measurement of the emission particle. Usually, use a

dynamometer or an engine bed to simulate the driving condition. The emission factors are determined by simulating the driving condition for a selected period. [15]

However, it is impossible to simulate the exact driving conditions as in real case since it is influenced by other factors like weather condition, road condition and driving style.

Receptor Modelling

This method of emission study has been developed to identify and classify the various sources contribute towards the particulate matter emission in the real-world scenario. This technique develops on the base of a theory which says a given source of emission can be identified by analysing the particle emitted, the size of the particle, density and their chemical characteristics. [16]. Researchers in UK have used the receptor modelling technique to reduce the uncertainties related to non-exhaust emission.

Road Tunnel Sampling

The combination of road tunnel sampling and the statistical techniques have been used to identify non-exhaust emission sources and calculate the non-exhaust emission factor. The sampling would do in a road tunnel at different traffic conditions using air sampling equipment. Analytical data and source apportionment techniques are used to calculate the source-specific emission factor. [15]

For the brake wear particle emission measurement, we are using a direct measurement method. The driving cycles would be simulated using the experimental set up available at the laboratory.

Chapter 3; Experimental Set up

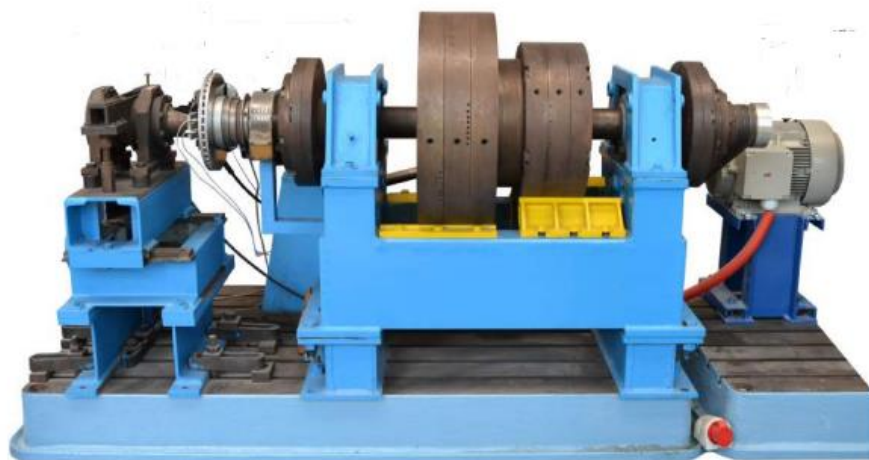


Figure 2: The brake inertia measurement test bench

Asynchronous Motor

The power to the flywheel is provided by a 4-pole asynchronous motor of model 7AA160L04. The speed of the motor can be controlled using a frequency converter. The electric motor drives the flywheel shaft by a belt transmission. The transmission ratio of the belt transmission is 0.8 with an efficiency of 92%. [17] The specifications of the motor and transmission are given in the following table 1 and table 2 respectively.

3~ Motor Type 7AA160L04			
Voltage	400 / 690 V, 50 Hz	Voltage	460 V, 60 Hz
Connection	Δ/Y	Connection	Δ
Current	29 / 15,9 A	Current	28,5 A
RPM	1460 min ⁻¹	RPM	1760 min ⁻¹
Power	15 kW	Power	17,3 kW
cos ϕ	0,84	cos ϕ	0,85
Efficiency	88,70 %	Efficiency	90,50 %

Table 1: Motor specifications

Transmission ratio of belt (i)	RPM (min ⁻¹)		Angular velocity (s ⁻¹)	
	Motor speed	Shaft speed	Motor	Shaft
0.8	1460	1825	153	191
0.8	1760	2200	184	230

Table 2: Transmission Specification

Fly Wheels

The flywheel shaft in this set up contains nine separate weights. The flywheel simulates approximately one-third of the weight of a lightweight passenger car Here the total weight of the flywheel is $m=505.09$ kg with a rotational moment of inertia of $J=42.13$ kgm². This is

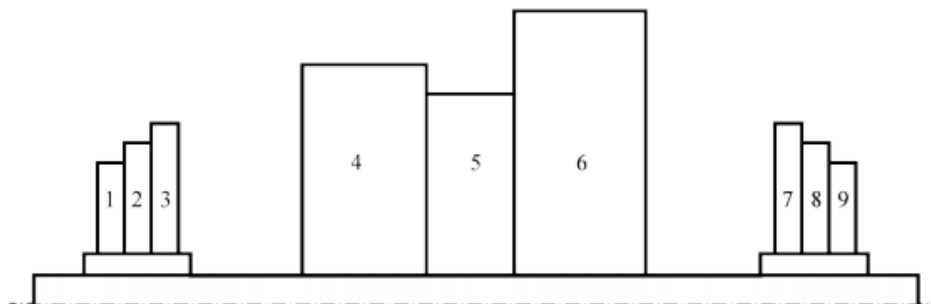


Figure 3: Arrangement of individual fly wheels

approximately 30% of the weight of Skoda Fabia II. which is 1674kg. Figure 3 shows the arrangement of individual flywheels and their parameters.

Flywheel	1	2	3	4	5	6	7	8	9
r_1 [mm]	72	72	72	50	50	50	72	72	72
r_2 [mm]	107	142	187	240	194	328	191	147	107
m [kg]	5,1	12,2	47,7	251,4	68,5	559,8	50,2	13,0	1,7
J [$\text{kg}\cdot\text{m}^{-1}$]	0,0424	0,1545	0,9586	7,5542	1,3737	1,3737	1,0451	0,1736	0,0141

Table 3: Parameters of individual flywheels

Disc Brake

The test rig is equipped with a single-piston brake with a floating calliper [17]

Brake Rotor

The test rig currently has a disc (figure 4) with a diameter of 288mm and a thickness of 25 mm. [17] This is from Skoda and used in multiple models However the test rig is compatible with the

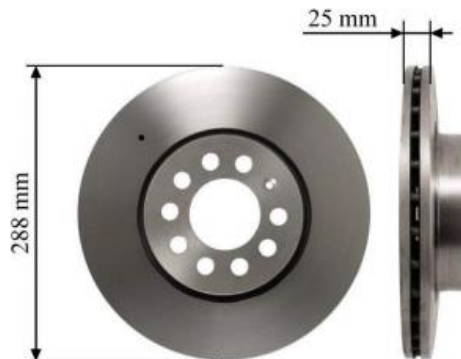


Figure 4: Brake disc dimensions currently available on the test rig

installation of various disc brakes used in different light-duty vehicles. Hence the experiment can also be performed with different disc brakes.

Brake Pad

Figure 5 illustrates the basic dimensions of the disc pad used currently in the test rig.

Where $d=54\text{mm}$, $R_e =143\text{mm}$, $R_i=84\text{mm}$.



Figure 5: Basic dimensions of currently using brake pad.

Thermocouple Temperature Sensor

This temperature sensor is in a hole drilled on the brake disc in order to measure the temperature on the surface as closer to the friction area. Hence it assures the most possible accurate measurement. The thermocouple used here is K type and the signal transmission is done with the help of a silver ring and carbon brush set up. [17]

Infrared Temperature Sensors

There are two infrared temperature sensors to measure the temperature of the brake disc apart from the thermocouple temperature sensor. These two sensors can be positioned relative to the diameter of the disc brake. Since infrared sensors are non-contact type sensors it is not going to affect by the state of measuring surface and there is no need of special an arrangement to transfer the signal from a rotating part to stationary part.

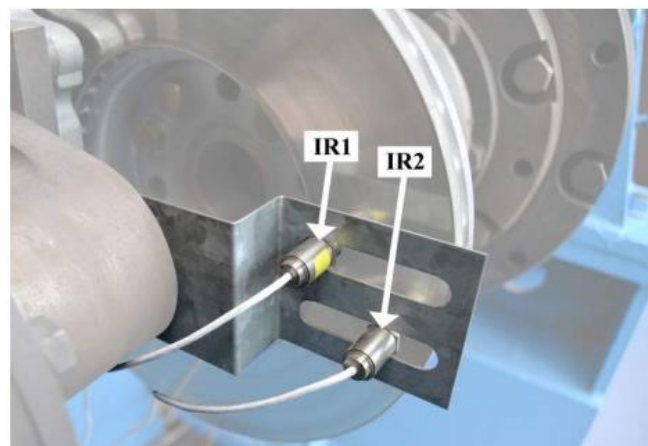


Figure 6: Infrared sensor set up.

Brake Fluid Temperature Sensor

It used to measure the brake fluid temperature to ensure the uniform warming up of the brake fluid. [17]

Speed Sensor

The SLE10B6VY encoder is used for speed sensing. The beam of light transmitted by the sensor is interrupted by a 60-hole aperture which is mounted on the flywheel shaft. Table 4 lists the parameters of the speed sensor used. [17]

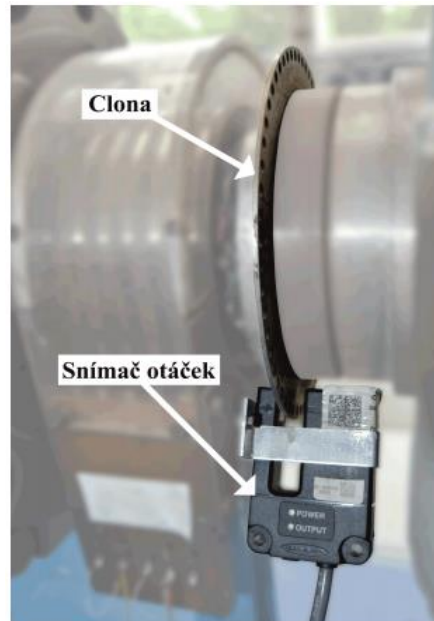


Figure 7:Speed sensor set

SLE10B6VY	
Power supply	10-30V
Output	Bipolar NPN or PNP
Spectral Range	8 to 14 μm
Slot dimension	10 mm

Table 4: Speed sensor Specification

Chapter 4; Design Concepts

Full Flow Dilution Tunnel

In the measurement of gaseous emission, some specific property of the gases measured is used, which enables the manufacturing of the measuring equipment with enough precision. However, the non-exhaust emission particles do not exhibit any unique properties as gaseous exhaust particle, hence the gravimetric method is the most common in practice of measurement of non-exhaust particle emission from vehicles. In gravimetric method total mass of the particle collected at the filter is estimated in the precisely measured and conditioned polluted gas, diluted with dry clean air.[18]

In full flow dilution tunnel, the whole exhaust gas from the vehicle is diluted using the dilution tunnel set up and then the required quantity is drawn for the sampling and measuring purpose. Whereas in partial flow dilution tunnel, a small portion of the exhaust gas is drawn and then it undergoes dilution using a dilution tunnel set up and further proceeded to the sampling and measurement purposes. In this project, we are using a full flow dilution tunnel. [19]

Requirements and Restrictions

1. The dilution of the emitted gas-particle by ambient air should not lead to any condensation and the conditions should be similar to the ambient conditions after the production of the wear particle. That means the temperature of the mixture should not be less than 20°C in order to avoid the thermophoresis effect. [20]

So the system should be designed in such a way that allows the continues flow of ambient atmospheric air to the chamber after filtering.

2. The tunnel should be sufficiently long enough to ensure the complete mixing of the gas with the air. The Reynolds number should be greater than 4000 to ensure the turbulent flow. [20]

Hence the design of the duct system at the available space should be done in a way, the dilution tunnel is a straight horizontal pipe with at least 5m length.

3. All parts of the dilution tunnel and sampling system which are come in contact with the emission particle should be manufactured using electrically conducting and corrosive resistant material. The natural choice is stainless steel. [20]

Hence the design of the chamber, ducts and pipe fittings etc are made from stainless steel (AISI 304/L).

Scheme and Description

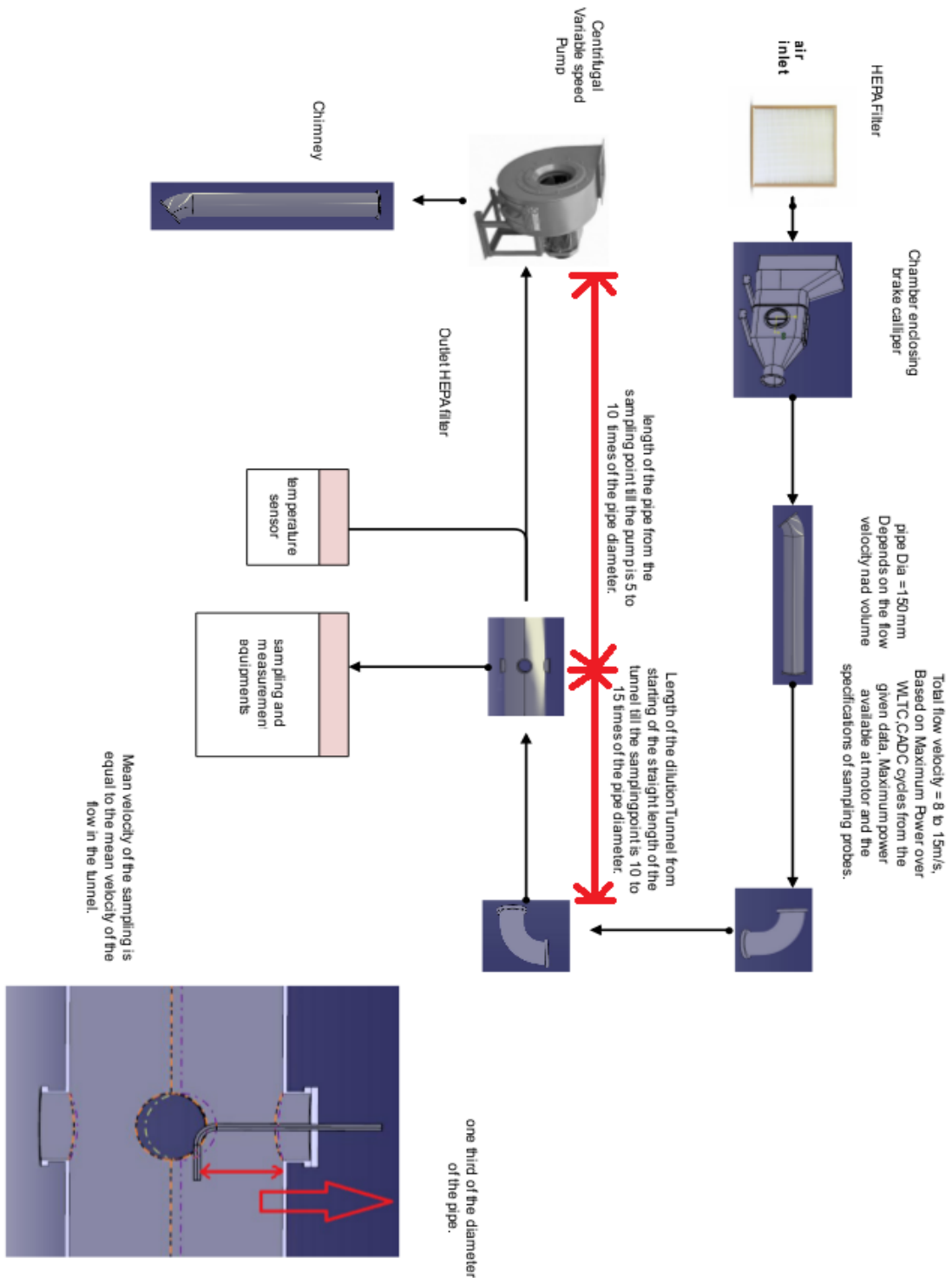


Figure 8 : Scheme of the set up

HEPA Filter

HEPA is an acronym that stands for High-Efficiency Particulate Air. These filters are used for an air purifier or other implementation, come with many benefits and claims. The Institute of Environmental Sciences and Technology dictates that a HEPA filter must trap 99.97% of particulates 0.3 microns or larger. [21] The air contaminations are trapped inside the web structure of the HEPA filter and hence purifies the air. Depending on the size of the particle, this can happen in four different ways: Inertial Impaction, Diffusion, Interception, or Sieving. Larger contaminants are trapped by inertial impaction, Medium-sized particles move through the filter and trapped by the fibre by interception. Smaller particles are dissipated as they travel through the filter and eventually collide with fibre and are trapped. [21]

In this experiment, we are using HEPA E10 from Ekofiltr which is complying ČSN EN 1822 And can be used for installation in all types of air conditioning equipment with temperature resistance up to 100 °C. The filter is made of glass fibre with an aluminium frame. The frame of the filter is equipped with a flat seal. Specifications of the filter are given in table 5. [22]

HEPA E10 EN 779:2012	
Size (mm)	305x610x150
Volume Flow rate (m ³ /h)	1160
Pressure drop (Pa)	130
Area (m ²)	4,5

Table 5: HEPA Filter specifications



Figure 9: HEPA Filter

Chamber enclosing the Brake disc

An airtight metallic enclosure is one of the major element of this sampling system. This chamber encloses the brake rotor, calliper and related sensors in an airtight manner. Also, this chamber is designed with an opening for the intake of the ambient air, where the filter is mounted. The chamber is followed by the duct system.

Duct system

The duct system starts from the airtight enclosure. The ducts to ensure the smooth and leak-proof transportation of the air with wear particulate matter to the dilution tunnel.

Dilution Tunnel

Dilution tunnel is the major element of the system from where the isokinetic sampling is taking place. The condition for locating the sampling point is that the straight length before sampling point must be greater than 15 times of the diameter of the dilution tunnel and the straight length after the sampling point must be greater than 5 times of the diameter of the dilution tunnel. Generally, in practice, the length before sampling point provided is 15 to 20 times of the diameter of the dilution tunnel and the length after the sampling point till the fan 5 to 10 times of the diameter of the tunnel

Sampling probe

Sampling probes are the pipe with a small diameter in order to perform the isokinetic sampling from the dilution tunnel. Inlet of the sampling probe should be at one-third of the depth from the inner diameter of the dilution tunnel.

Temperature sensor

In order to ensure and measure the temperature of the fluid flowing through the dilution tunnel, a temperature sensor is provided.

Centrifugal blower

The working principle of the centrifugal fan is the air enters the spinning impeller through the inlet located at the centre of the fan. As the impeller rotates it accelerates the air outward using the centrifugal force This high-velocity air then diffused and slowed down in the surrounding blower housing to create pressure. The flow rate required, and the pressure drop at the entire dilution tunnel set up is used to determine the basic specification of the centrifugal fan.[23]

Chimney

A chimney is to allow the flow of the mixture of air and emission particles to the atmosphere after the sampling process.

Chapter 5; Calculations

Determination of Total Energy Dissipated in Selected Cycles

Once the vehicle starts moving, it gains speed and the kinetic energy of the vehicle increases, a vehicle can only stop when the kinetic energy is lowered down to zero. A braking system helps reduce the kinetic energy in the vehicle by converting kinetic energy into heat energy and dissipating it to the atmosphere. The heat energy is generated by the friction force acting between the disc brakes and the disc pads. This law of conservation of energy is used for the analysis of heat dissipated in the braking system and hence it is used to determine the diameter of the entire dilution tunnel set up and the required flow rate to cool the disc brake. [24]

$$\text{Change in Kinetic energy} = \text{Heat Energy dissipated at the brake} \quad (1)$$

$$KE = \frac{1}{2} M v_0^2 \quad (2)$$

Change in KE during braking

$$\Delta KE = \frac{1}{2} M (v_0^2 - v_1^2) \quad (3)$$

In the current experimental setup, we are simulating one by third of the mass of a light-duty vehicle. Hence the value of mass $m=505$ kg which is one-third of the mass of Skoda Fabia.

The data from a standard chassis dynamometer experiment for the required cycles are available as the table between vehicle velocity in Km/h and the cycle time in seconds. This data is available for WLTC and ARTEMIS driving cycles. Using this data and the law of conservation of energy I have found the change in kinetic energy during the entire cycle of operation

WLTC

We have chosen WLTC CLASS B cycle for the experiment and it has 4 phases, Low, Middle, High and Extra high phases respectively. The energy dissipated in each phase calculated from the available data is given below in the table 6.

PHASE	ENERGY DISSIPATED (KJ)
LOW	316.6
MIDDLE	472
HIGH	490
EXTRA HIGH	517
TOTOAL	1796

Table 6: WLTC, Energy dissipated in different phases.

ARTEMIS

In this driving cycle, we have three subclasses, Urban, Rural and Motorway. The energy dissipated in each subclass is calculated and represented in table 7.

CLASS	ENERGY DISSIPATED (KJ)
URBAN	763
RURAL	1523
MOTOR WAY	1936
TOTAL	4222

Table 7: ARTEMIS, Energy dissipated in different classes

From the above calculations, it is understood that more energy is dissipated in the ARTEMIS cycle. Therefore, I have chosen the total energy dissipated in ARTEMIS driving condition for finding the diameter of the dilution tunnel since it will satisfy the WLTC condition also.

$$\text{The total power dissipated in the Artemis cycle} = \frac{4222 \text{ kJ}}{1082 \text{ s}} = 3.9 \text{ KW} \quad (4)$$

This value is further used for finding the diameter of the pipe.

Calculation of Diameter of The Pipe

For the calculation, we assume the condition that the total heat dissipated at brake disc is carried away by air flowing through the system.

$$\text{Heat dissipated} = \text{Heat carried away by airflow.} \quad (5)$$

$$\text{Heat carried away by air} = \rho_{\text{air}} A V_{\text{air}} C \Delta T \quad (6)$$

Where,

The density of the air at 20°C $\rho_{\text{air}} = 1.205 \text{ kg/m}^3$

Velocity of air $V_{\text{air}} = 10 \text{ m/s}, 8 \text{ m/s}$

Specific Heat capacity of air $C = 1.006 \text{ kJ/kg-k}$

From the literature and from the other experimental data I have come to the conclusion that the air temperature rises to 55°C approximately. [20]

Therefore, the temperature difference between inlet and exit air temperature can be calculated.

$$\text{Temperature difference} = T_{\text{out}} - T_{\text{in}} = 55 \text{ °C} - 20 \text{ °C} = 30 \text{ °C} \quad (7)$$

Equate equation (4) with (6) and substitute the velocity values to obtain the unknown cross-sectional area of the pipe and then the diameter of the pipe.

For velocity 10m/s

$$\text{Area of the cross-section of the pipe } A=0.010724 \text{ m}^2 \quad (8)$$

$$\text{The diameter of the pipe} = 117\text{mm} \quad (9)$$

For velocity 8m/s

$$\text{Area of the cross-section of the pipe } A=0.0134 \text{ m}^2 \quad (10)$$

$$\text{The diameter of the pipe} = 131\text{mm} \quad (11)$$

Here the highest value of the diameter is 131mm. Apart from that, there are several approximations are done based on the future scope of the experiment.

- The experiment also should be able to conduct in future with an air velocity less than 8m/s
- The standard diameter of the dilution tunnel in practice is between 100 mm to 200mm.
- In this experiment, I must compromise between the space constraint and the possibility to choose a bigger diameter for the future purpose.

Hence considering the above factors I have concluded to a pipe with **diameter 150mm**, which is within the range and available in the market for purchase.

$$\text{The inner diameter of the pipe} =150\text{mm} \quad (12)$$

Calculation of Flow Rate.

Using the continuity equation

$$\text{Flow rate} = \rho_{\text{air}} A V_{\text{air}} \quad (13)$$

Substituting the values of ρ_{air} , V_{air} and Area using the value from the result (12) table 8 is obtained.

Velocity (m/s)	Flowrate(m ³ /Min)
8	10.24
10	12.81
12	15.37

Table 8: Flow Rates

3D models and Design description

There are two design variants based on the availability of the chimney connecting point and other space constraints in the room.

Design Variant 1

The 3D assembly of the design is shown below. The assembly is made with considering the room dimensions where most of the duct system and the blower located. The Duct is entering this room through one of the rectangular hole available near the experimental setup. The assembly included the electric box and the cable tray which are already in the available space to show that the pipe system is not colliding with any of these structures.

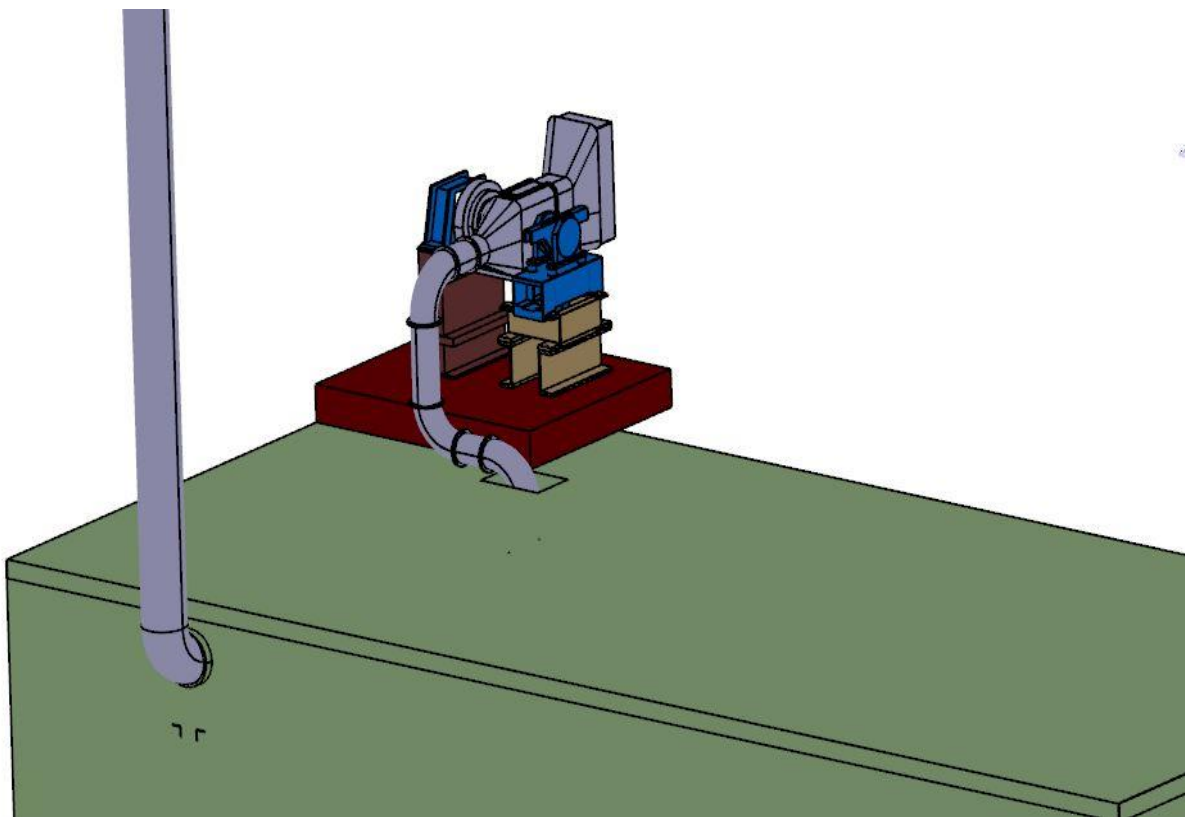


Figure 10 : 3D model of the design variant 1

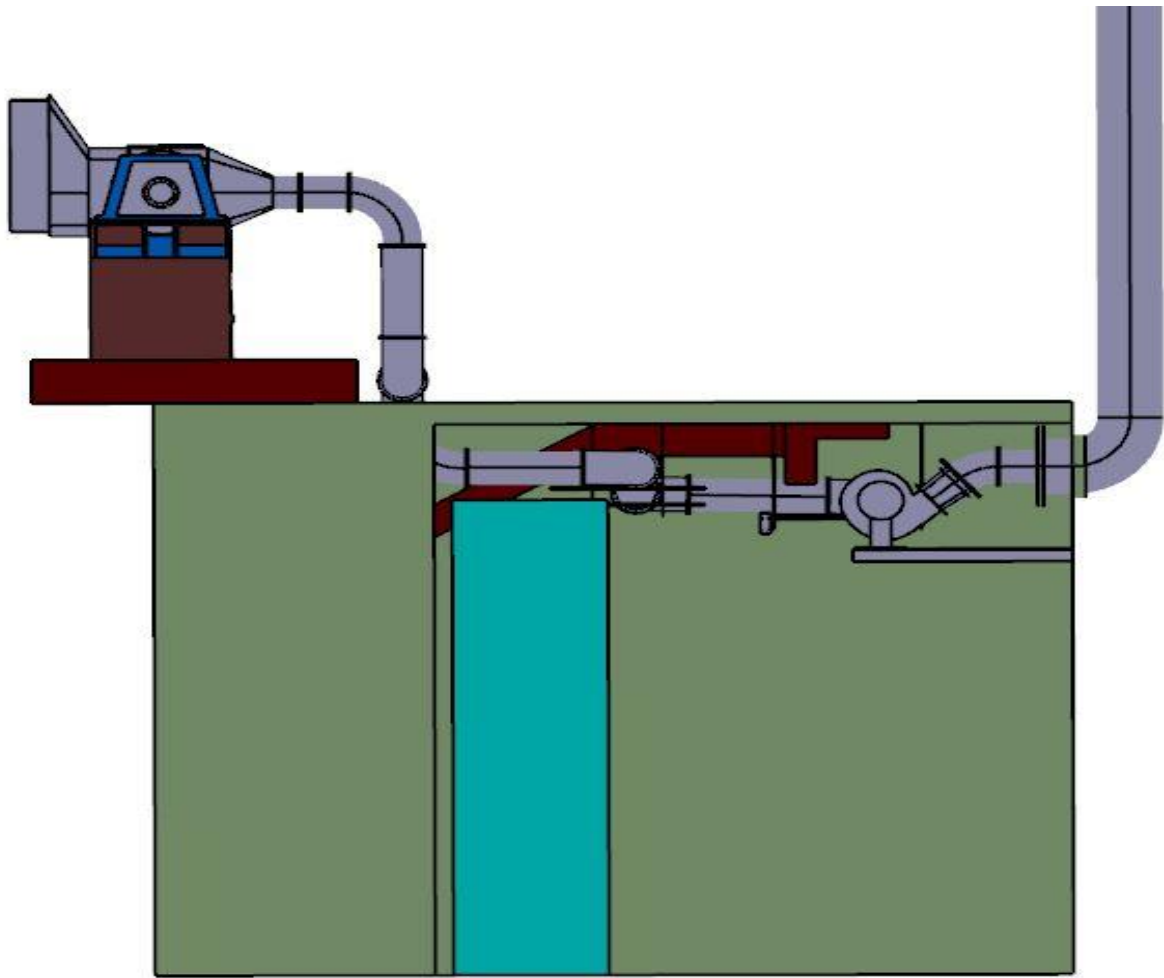


Figure 11: 3D model of the design variant 1 -side view

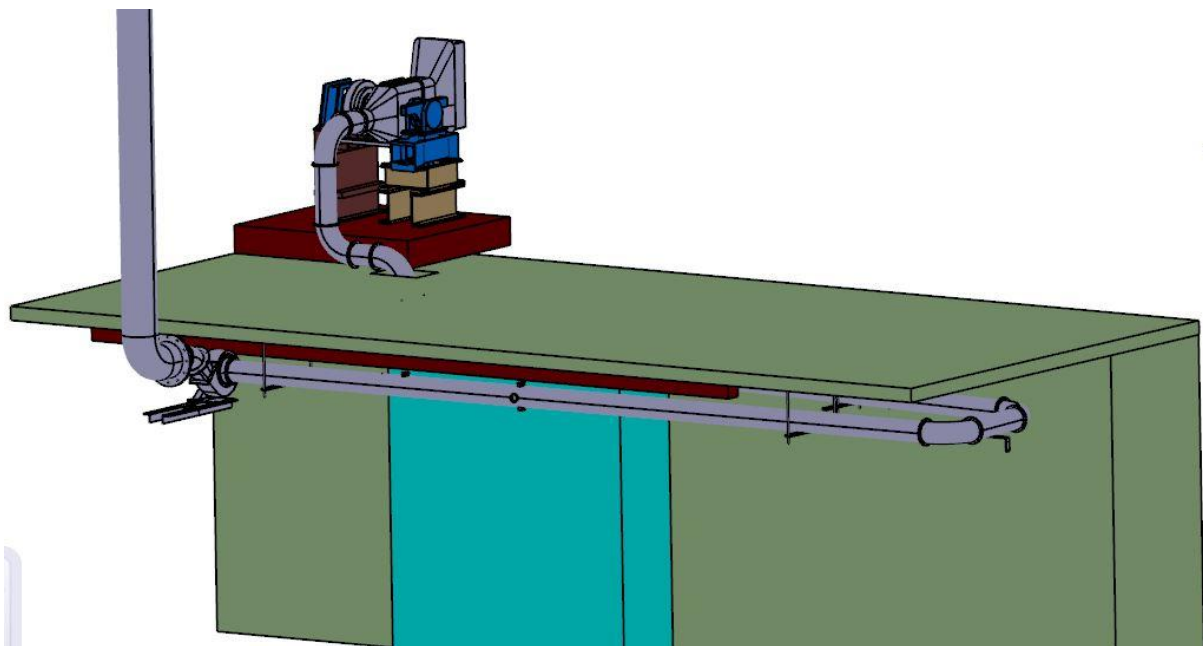


Figure 12: : 3D model of the design variant 1 view 2

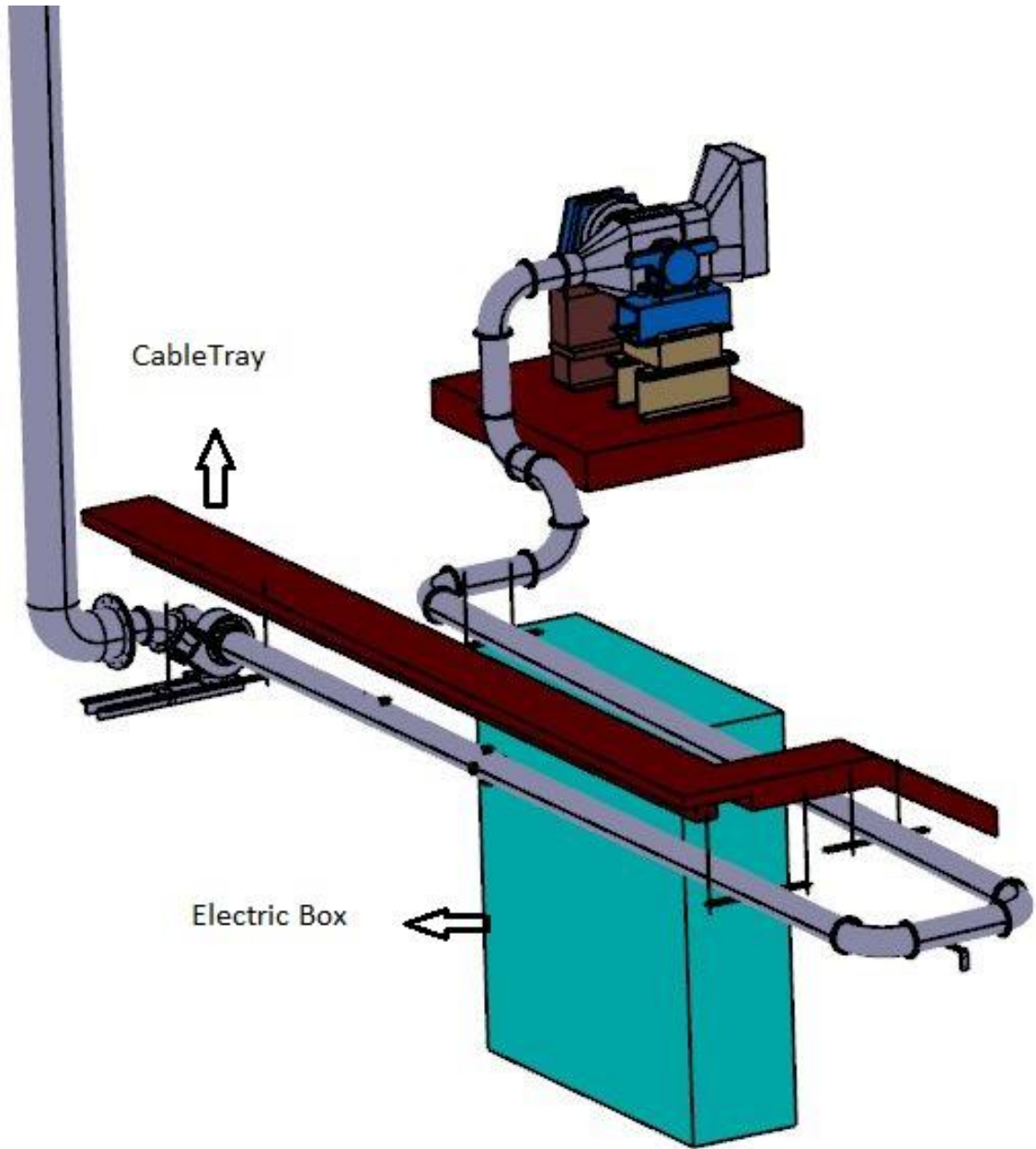


Figure13: 3D model of the design variant 1 View 3

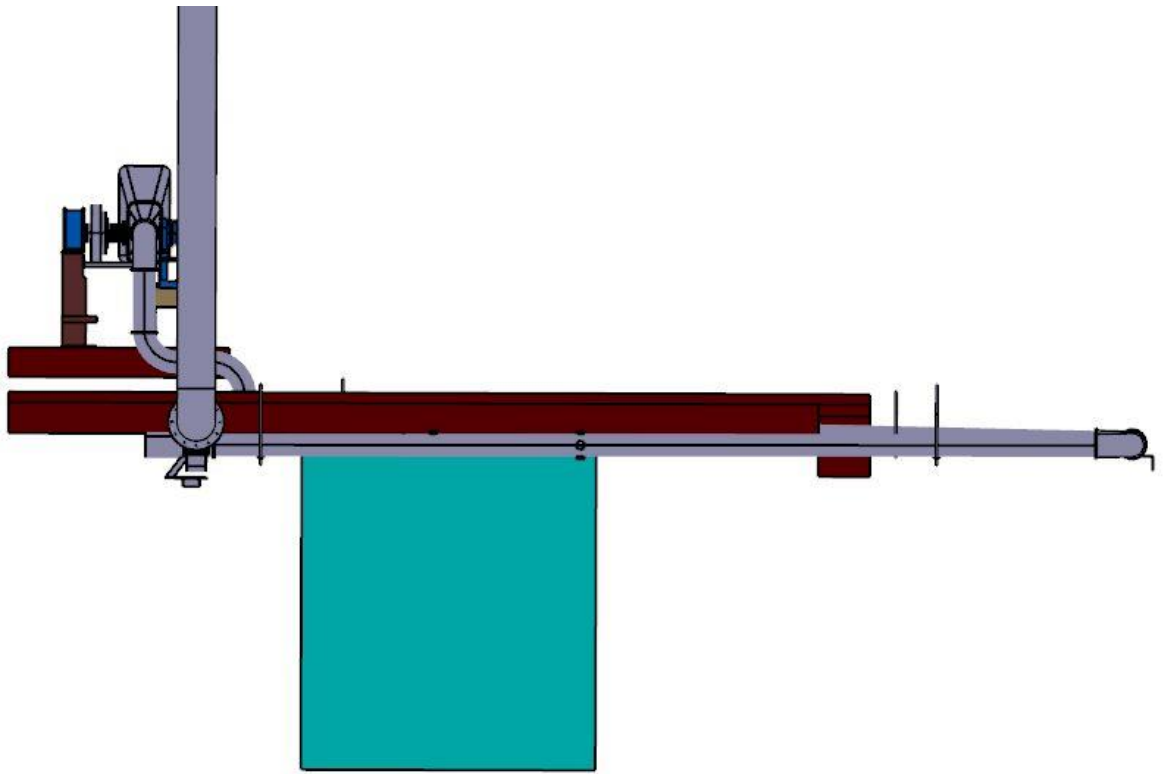


Figure 14: 3D model of the design variant 1 view 4

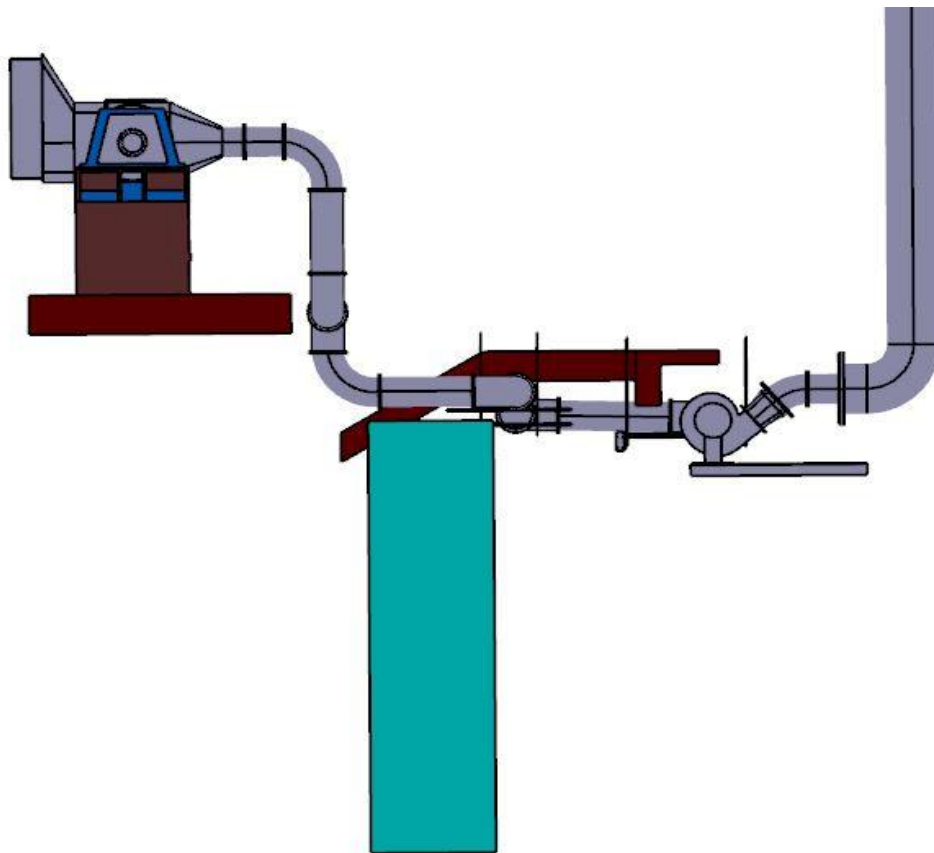


Figure 15 : 3D model of the design variant 1 view 5

The 2D drafts of the assembly are attached to the thesis.

Chamber

The material selected for chamber design is stainless steel (AISI 304/L). Since steel is electrically conducting which is the major requirement for the selection of the material. Apart from that AISI 304/L is austenitic steel with low carbon content, high corrosion resistance, formability and weldability which are good for the purpose and production of the chamber. The low carbon content minimizes the carbide precipitation during high heat input situations like welding. The production method of this stainless steel is cold rolling, hence the surface finish obtained is comparatively good. Despite the above, the material is undergoing surface treatment processes like annealing and pickling. Annealing makes the steel more ductile which is good for the sheet metal bending process and pickling will remove the surface impurities.[25]

Chemical composition	
C	0.02
Cr	18.1
Ni	8.1
Mo	0
N	0

Table 9 : Chemical composition

Mechanical properties	
Yield strength Rp0.2 (MPa)	220
Yield strength Rp1.0 (MPa)	250
Tensile strength Rm (MPa)	520–700
Elongation A (%)	45
Elongation A80 (%)	45

Table10: Mechanical Properties

Physical properties	
Density [kg/dm ³]	7.9
Modulus of elasticity at 20 °C [GPa]	200
Coefficient of thermal expansion 20–100 °C [10 ⁻⁶ / K]	16.0
Thermal conductivity at 20 °C [W/(m x K)]	15
Thermal capacity at 20 °C [J/(kg x K)]	500
Electrical resistivity at 20 °C [Ω x mm ² / m]	0.73

Table11: Physical properties

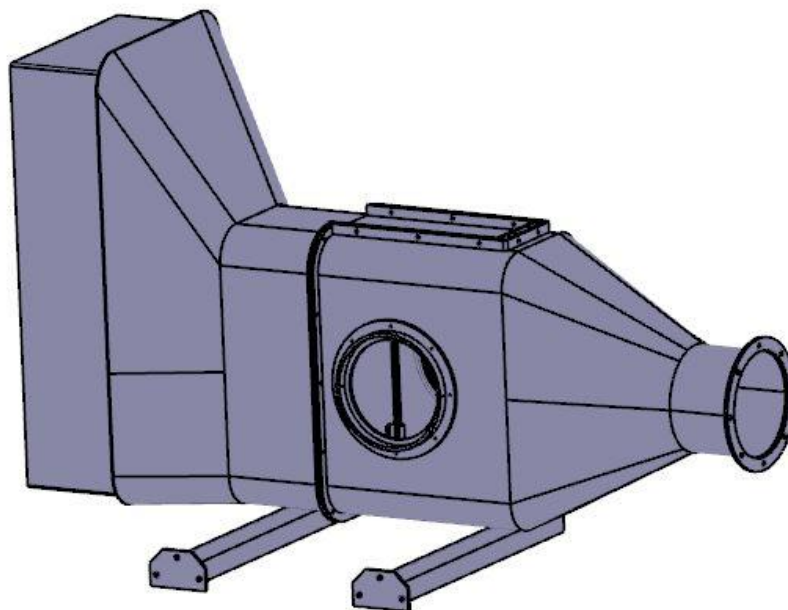


Figure 16 : Chamber assembly view 1

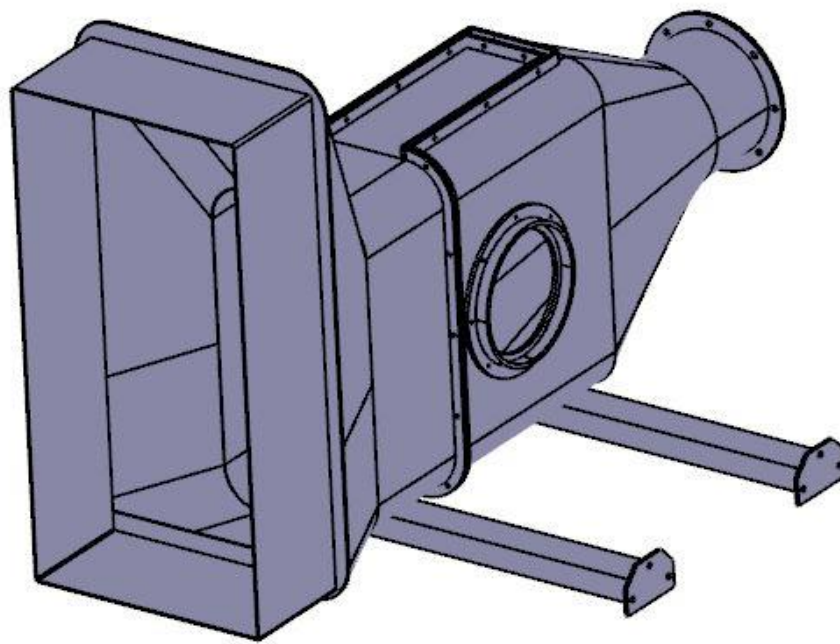


Figure 17 : Chamber assembly view 2

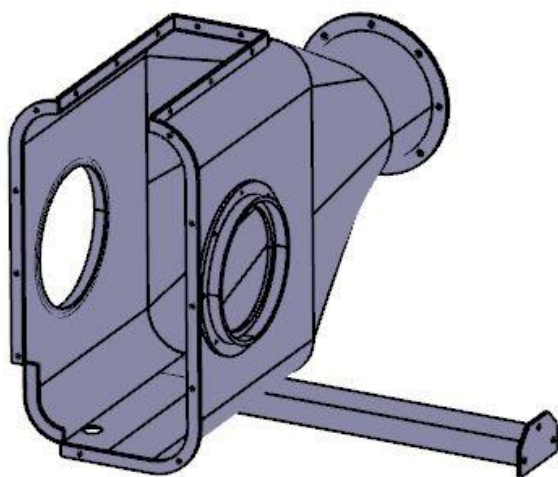


Figure 18 : Chamber part 1 view 1

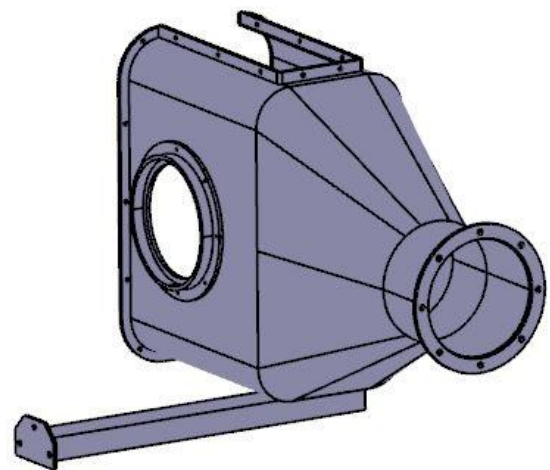


Figure 19 : Chamber part 1 view 2

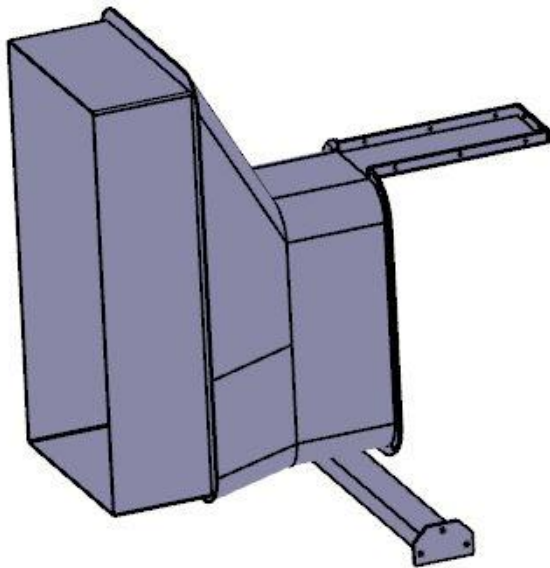


Figure 20 : Chamber part 2 view 1

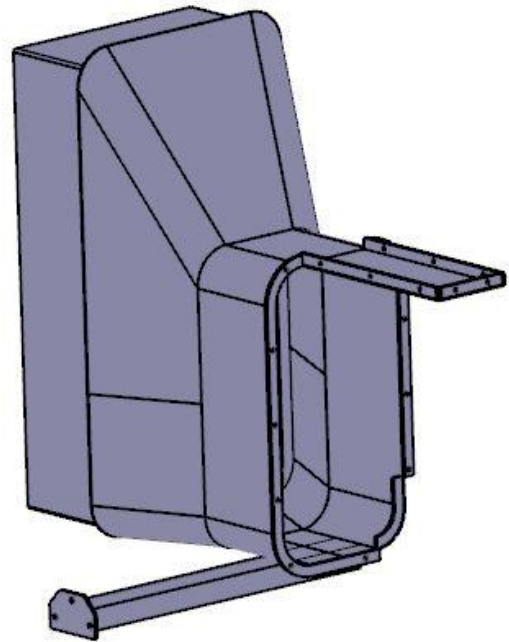


Figure 21 : Chamber part 2 view 2

The chamber is made from the stainless-steel sheet metal by sheet metal operations and welding. There are different parts of the chamber and these parts are welded according to the design. The welding specifications are explained later. At one of the sides, the chamber has support at the stationary end of the test rig (Figure 21)(Part no 7) and the other end is supported by two 'U' profiles which are welded to the bottom of the chamber as shown in the technical drawing. These

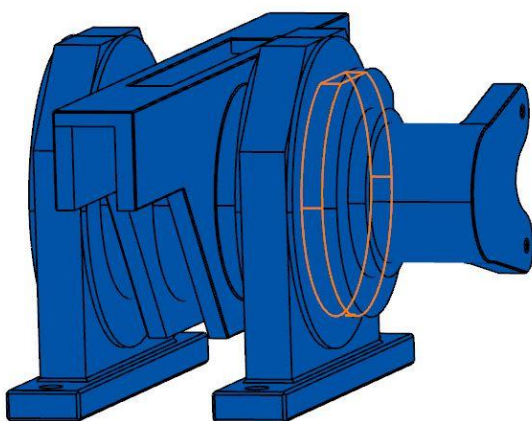


Figure 22: Chamber mounting location on part 7

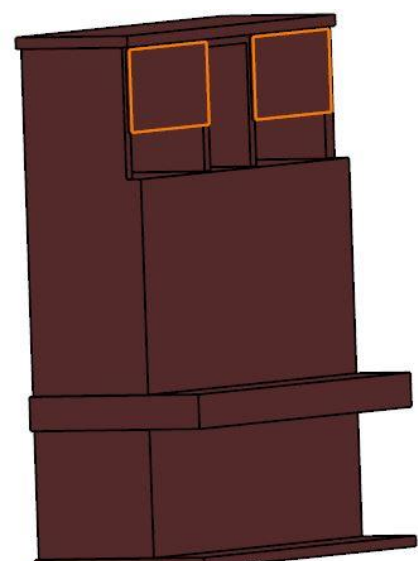


Figure 23: Chamber mounting location on part no 2

'U' profile supporting arms are then bolted to the nearest stationary part (Figure 23)(Part number 2)of the test rig. The specifications of the 'U' profile is given below [26]

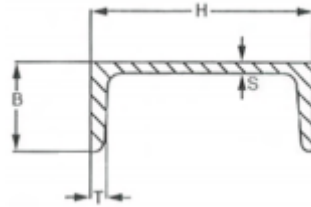


Figure 24: U profile cross-section

Material	AISI 304/L (DIN 1.4301/7)
H	50mm
B	30mm
S	4mm
T	4mm

Table12: U profile dimensions

Disc Set Up to Eliminate Axial Misalignment

Since the chances of the occurrence of the axial misalignment between the mounting axis of the chamber and the axis of the rotating shaft, it is necessary to design a setup which can eliminate very small axial alignment problem. To solve this a disc with a Gufero ring is designed. This set up will be bolted to the side of the chamber with a rubber bushing. Hence the small amount of axial misalignment can be eliminated by adjusting the bolts. Apart from this gufero rings will provide sealing for the chamber at the hole for the rotating shaft. The disc with a sleeve for the installation of the gufero ring is shown in figure 13. The sleeve is welded to the disc coaxially. It can be mounted to the chamber with M4 bolts.

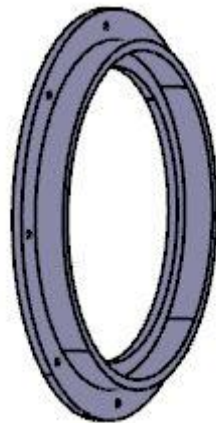


Figure 25 :Disc with sleeve

Gufero Ring

Gufero ring is a radial shaft seal used for providing sealing around the rotating shaft.

A gufero ring with shown specifications is used in this design to provide sealing around the rotating axis of disc brake and flywheel.[27]. For this project, I have used the gufero ring with the following specifications(Table 13) from the manufacturer GUFERO Rubber Production, Ltd

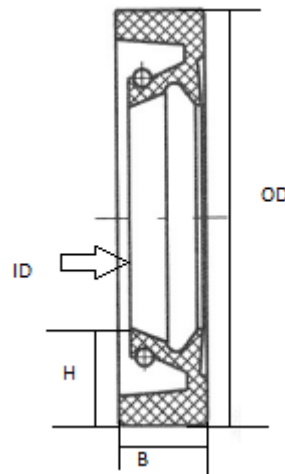


Figure 26 : Gufero cross section

Code	123098
Type	G
Material	NBR
Inner Diameter (ID)	138
Outer Diameter (OD)	160
Height (H)	15

Table 13: Gufero specifications

Pipe Design

The pipe diameter is selected as a result of energy balance calculation and the design is done to reduce the bends and achieve maximum length to the dilution tunnel. Apart from these several factors are considered for the designing of the pipe system.

- The pit dimension which connects the test rig floor to the basement where the dilution tunnel exists.
- Position of the existing pipe and cable system for water, power supply and other purposes.
- Position of the exhaust vent which is connected to the chimney system of the entire building.
- Accessibility of the sampling and auxiliary equipment like sampling probe.

Pipe Specifications

Based on the calculations and final approximation I have selected the pipe of inner diameter 150mm. Welded pipe (DIN 17457 / DIN 11850 / EN 10217-7 / DIN 2463 / ASTM A-312) of material AISI 304/L (DIN 1.4301/7) is used for the constructions. [28]

]

Outer diameter × Thickness (mm × mm)	Inner diameter (mm)	Weight (Kg/m)
153 × 1.50	150	5.69

Table 14: Pipe Specifications

Dimensional details of the pipe system and the assembly is shown in the assembly drawing. The pipe system is designed in such a way that, it is entering to the basement room through the rectangular hole available to the left side of the experimental set up when facing it from the inlet side of the airtight chamber. The pipe is designed without colliding with the installations in the rooms like electric box and cable tray. In order to achieve that the pipe connection 3 (Part number 17) has a 1.15° inclination with horizontal from the top wall of the room. Similarly, pipe connection 4 (Part number 18) has 1.136 ° inclination with horizontal from the top wall of the room.

Flange

The standard dimensions of flanges available for the pipe of diameter 150mm are very big compared to the requirements. since they are designed for high-pressure pipelines. Considering the space constraints for the assembly, weight reduction and the purpose I decided to machine the flanges of required dimension from stainless steel DIN 1.4301 / 7 (AISI 304 / L). There are 32 flanges of diameter 190mm, one flange of diameter 240mm and one flange of diameter 360 mm used in this design variant For this purpose the stainless steel sheet of 2 m length ×1.5m breadth ×5mm thickness. Is necessary. For the manufacturing of the flanges, The dimensions are represented in technical drawing.

Elbow

Elbows of inner diameter of 150mm with standard dimensions are available in the market.[29] Hence for the designing of the pipe system, it is required to construct elbows of unconventional angles and lengths. This is obtained by cutting 90° elbow at required angles and then the flange is welded at the end. The material used is AISI 304/L (DIN 1.4301/7). The specification of the standard 90° elbow given in Table 15. Dimensions of elbows of unconventional angles are given in technical drawing.

Elbow 90° DIN row 1
for welding
AISI 304/L, AISI 316/L

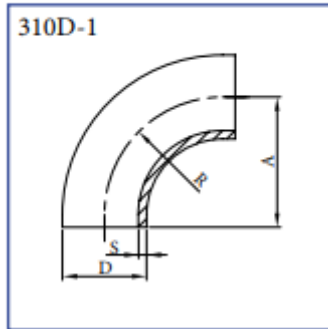


Figure 27 : Standard 90°
elbow

Dn	150mm
D	154mm
S	2mm
A	225mm
R	225
Weight	2.27Kg

Table 15: Elbow specifications

Tunnel

The dilution tunnel is a straight pipe of diameter 150mm and of a length of 5989mm without any bends, till the inlet of the centrifugal fan. The isokinetic sampling is done at this part of the pipe system. Generally, in practice the length before sampling point provided is 15 to 20 times of the diameter of the dilution tunnel and the length after the sampling point till the fan 5 to 10 times of the diameter of the tunnel. In the current design the sampling point is provided at a length of 3500mm from the beginning of the straight 5989mm pipe hence it satisfies both the conditions.

Sampling Point

The sampling points are designed in such a way that sampling probs of multiple diameters can be mounted without complications and quick. Also, there are four sampling points provided at the same cross-section of the pipe to practice sampling at multiple points. (Figure 27)

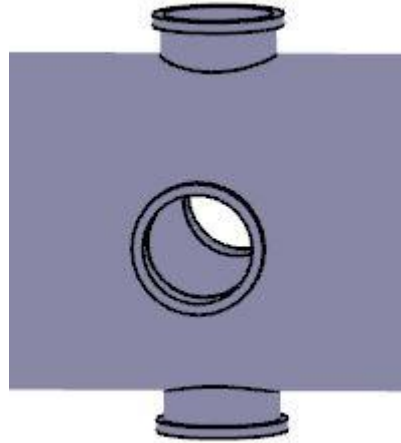


Figure 28 : Sampling points on Tunnel

Sampling Probe

The sampling probs available for the sampling purpose are with below specifications. The flow rate specifications are 1L/min,10L/min,30L/min and 500L/min. Since 500L/min is way too higher value than the requirement. Thus, the remaining sampling probs are considered. The diameter of the sampling probes is calculated for different velocity conditions and tabulated below using the continuity equation.

	1L/Min	10L/Min	30L/Min
V = 8m/s	1.6mm	5mm	8.9mm
V= 10m/s	1.45mm	4.5mm	7.9mm
V=12m/s	1.33mm	4.9mm	7.2mm

Table16: Probable diameters of sampling prob for different velocity conditions.

The sampling point is designed in such a way that the even maximum possible diameter for the given range of velocity can be mounted properly. The model and drawing of the sampling probe of inner diameter 4.5mm welded with the covering lid are shown in figure 28.

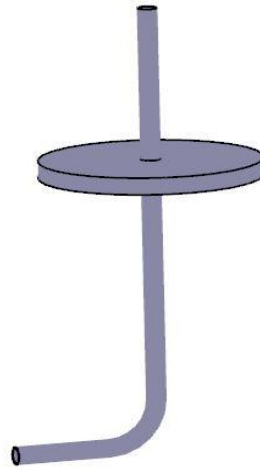


Figure 29: sampling probe

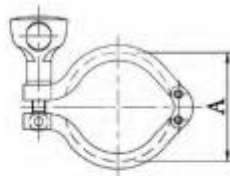
Clamp Connection for Sampling probe

The clamp used between the sampling point and sampling probe is cod K12 clamps. from the manufacturer Armat spol s.r.o The main advantage of this clamp is the easy and quick mounting mechanism. The specifications of the clamp are given in table 17. [30]

Cod. K12

Heavy duty Clamp

Materiál: AISI 304



DIN 32676	DN		Ø diameter of plate	A	kg
	ISO 1127	ASME BPE			
	8-10	¼"-¾"	25,0	28,0	0,15
10-15-20			34,0	37,0	0,17
25-32-40	15-32	1"-1½"	50,5	53,0	0,22
50	40	2"	64,0	67,0	0,30

Table 17 :Clamp specifications



Figure 30 : Cod K12 clamp

Pitot Tube

In order to measure the flow, rate a provision for the mounting of the pitot tube is provided at a distance of 1000 mm from the sampling point towards the centrifugal fan. The design is similar to the sampling points also the same clamping method is used.

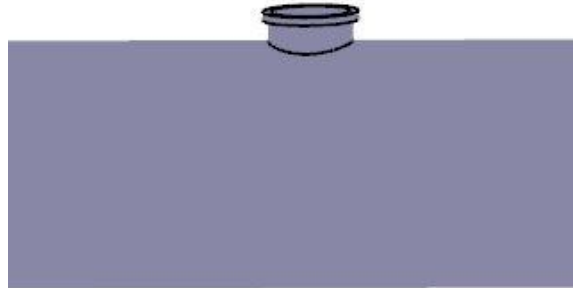


Figure 31 : Connection point for pitot tube

6.3.5 Temperature Sensor

The temperature of the air gas flowing through the tunnel should be measured. A provision for temperature sensor is provided after the 200mm after the position of the pitot tube. The temperature sensor suggested for the purpose is Ultra-precise air and gas measurement RTD temperature sensor. (model P-L-1/3-M30-150-M6-P-1) from the manufacturer omega Engineering Czech Republic. The sensor is equipped with a probe length of 50.8mm and diameter 3mm, together with an M6 mounting thread. Specification of the temperature sensor is given in table 18. [31]

Model	P-L-1/3-M30-150-M6-P-1
Accuracy	1/3 DIN
Sensor diameter	3mm
Mounting Thread	M6
Insulation	PVC

Table 18: Temperature sensor specification

Structure for Mounting Fan

The centrifugal blower is mounted on a structure as shown below in the drawing. The structure is made of L profiles of thickness 5mm by welding. Which can be fixed on the wall as a permanent installation. The fan can be mounted on the grooves provided on the structure using M12 bolts.

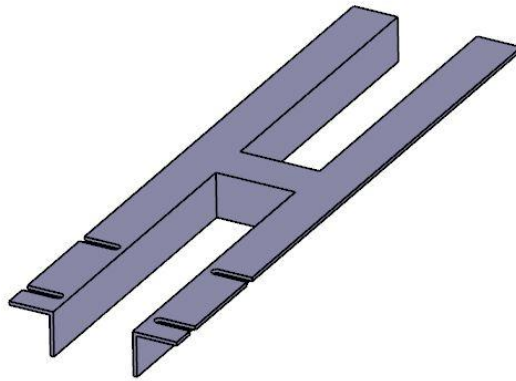


Figure 32 : Bracket for mounting blower

Pipe Clamp

The clamping of the pipe system is done to the ceiling since the design of the pipe system is overhead type. CADDY ROD LOCK Strut clamping system of model CRLP1M8L550 from the manufacturer Nvent Caddy is selected with a frame thickness of 1.5mm and M8 rod for the clamping purpose. [32]



Figure 33 : Caddy clamp assembly

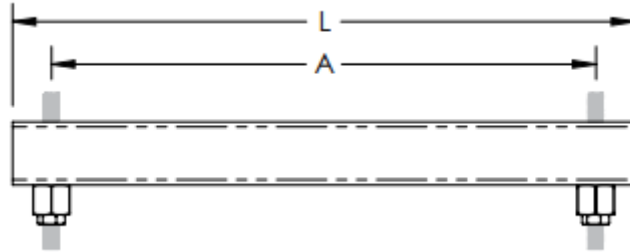


Figure 34 Caddy clamp assembly drawing

Strut Type: C; 21×41 mm; Strut thickness =1.5mm					
Part No	Article-No	Rod Size	Max span A(mm)	Overall strut length L(mm)	Load capacity (N)
CRLPM8L550	390029	M8	550	600	2306

Table 19: Caddy Strut specification

Threaded Rods DIN 976-8.8	
Identification	M8
Material	Fe
Length	1000mm

Table 20: Threaded rod specification

Gasket Sheet

Gasket sheet of model Klingersil C4265 from the manufacturer Napo Morava s.r.o is used at pipe flange couplings, flanges between chamber parts This variant has a wide range of applications including oil and gas fields. This is suitable for low-pressure applications with lighter pressure. A sheet of length 2m and breadth 1.5m is necessary for the manufacturing of the required number of Gaskets.[33]

Compressibility (ASTM F36J) :	26%
Recovery (ASTM F36J)	>50%
cold compression Decrease in thickness at 23°C :	12%
Hot compression decrease in thickness at 200°C :	15%
Thickness increase after immersion in Oil IRM 903, 5h/150°C	<10%

Thickness increase after immersion in Fuel B, 5h/23°C	<15%
Density	1.6g/cm ³

Table 21: Gasket sheet specifications

Rubber Cable Gland

Rubber glad is used to seal the opening of the brake fluid cable from the calliper to the fluid chamber. This ensures the airtight sealing of the opening which is provided at the bottom of the chamber. The diameter of the hole provided is 23mm. The specifications of the rubber glad selected is given in table 22 [34]

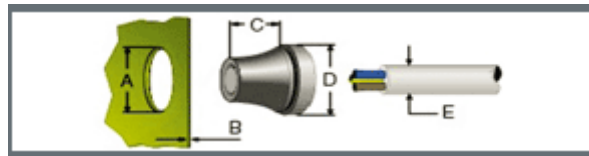


Figure35: Cable gland

Article number	Height(mm)	Hole diameter(mm)	Panel Thickness (mm)	Cable diameter(mm)
GVC-PG16	22.5	23	1.0 4.0	10 - 14

Table22: Cable gland dimensional specifications

6.5 Fasteners

Threaded fasteners of standard dimensions are used for the clamping and mounting purposes. Hexagonal M4, M6 and M8 bolts with full thread zinc-plated DIN 933 - 8.8 from the manufacturer Valenta ZT are used for different mounting situations. The specifications of standard threaded fasteners used for the assembly is given below in table 23,24,25. In this assembly M4 and M6 bolts of length 20mm and M8 bolts of length, 50mm is used together with corresponding standard Hexagonal nuts and washers. [35][36][37]

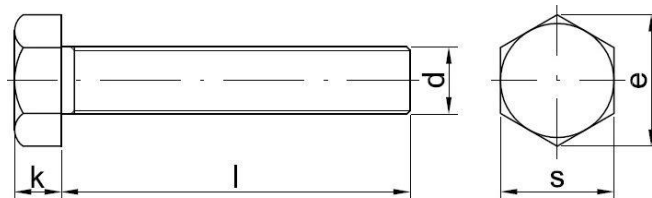


Figure 36: Hexagonal bold dimensions

Hexagonal Bolt DIN 933 -8.8				
Dimension. d×l (mm)	K(mm)	S(mm)	e(mm)	Weight(Kg/100pc)
		M6×20	4	
M8×50	5.3	13	14.32	2.18
M12×	7.5	19	21.9	8.08

Table 23: Hexagonal bolt specifications

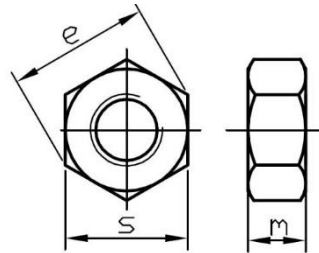


Figure 37 :Hex nut dimensions

Hex nut - DIN 934, ČSN 02 1401					
Identification	Dimension(s×e×m) (mm)	Pitch (mm)	Version	class	Weight(kg/100pc)
M6	10 x 11,1 x 5	1,00	Fe / Zn	8	0.22
M8	13 x 14,4 x 6,5	1.25	Fe / Zn	8 / 10 / 12	0.47
M12	19 x 21,1 x 10	1.75	Fe / Zn	8 / 10 / 12	1.55

Table 24: Hex nut specifications

Flat washers -DIN 125 A, ČSN 02 1702 -STAINLESS					
Identification	Inner diameter(mm)	Outer Diameter(mm)	Thickness(mm)	Version	Weight(Kg/100 pc)
M6	6.4	12	1.6	Stainless steel A2	0.10
M8	8.4	16	1.6	Stainless steel A2/A4	0.18
M12	13	24	2.5	Stainless steel A2/A4	0.63

Table 25: washer specification

Design Variant 2

This design variant differs from the variant 1 only in the designing of the pipe system. Here the pipe from the airtight chamber enters to the basement room through a rectangular hole located at the right side of the experimental set up when facing it from the inlet side of the airtight

chamber. Since the majority of the elements are the same for both the design Variants, here I will be describing only the elements which differ from the design variant 1.

Pipe design

The pipe design of this design variant is different from the initial design. It is because of the different chimney connection, different rectangular opening to the basement room. However, the design includes several bends in order to make a collision-free assembly with the cable tray and Waterpipe installations in the room. Apart from that the second Electric box in the room also considered during the designing.

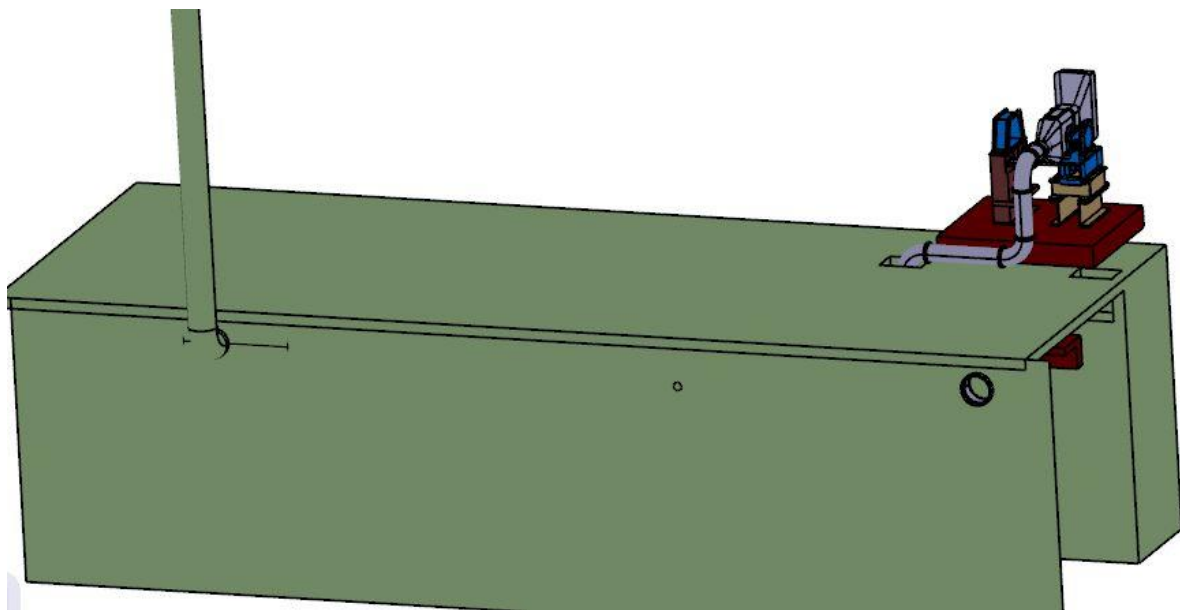


Figure 38 : 3D model of design variant 2 view 1

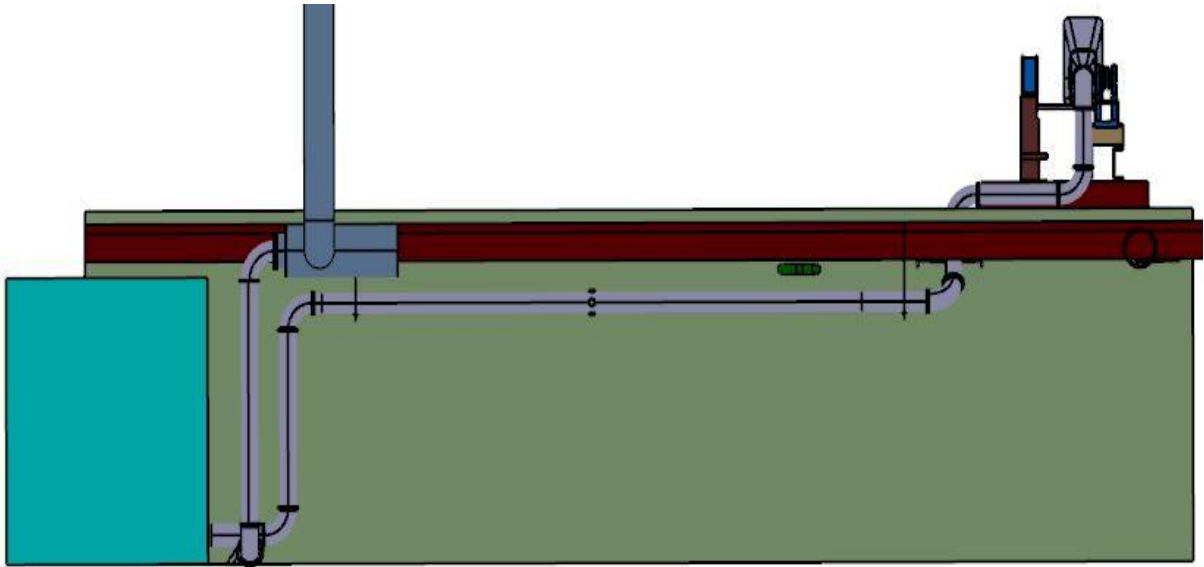


Figure 39 : 3D model of design variant 2 view 2

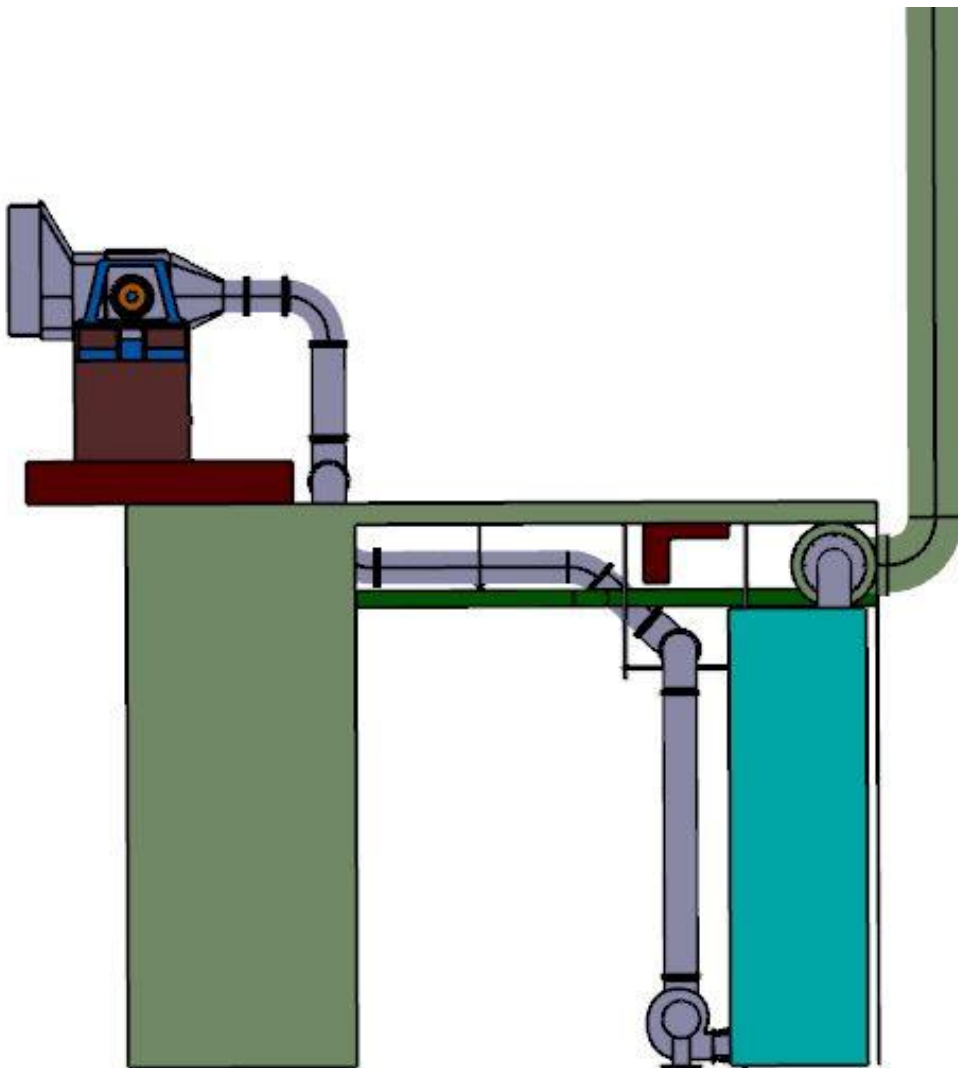


Figure 40: 3D model of design variant 2 view 3

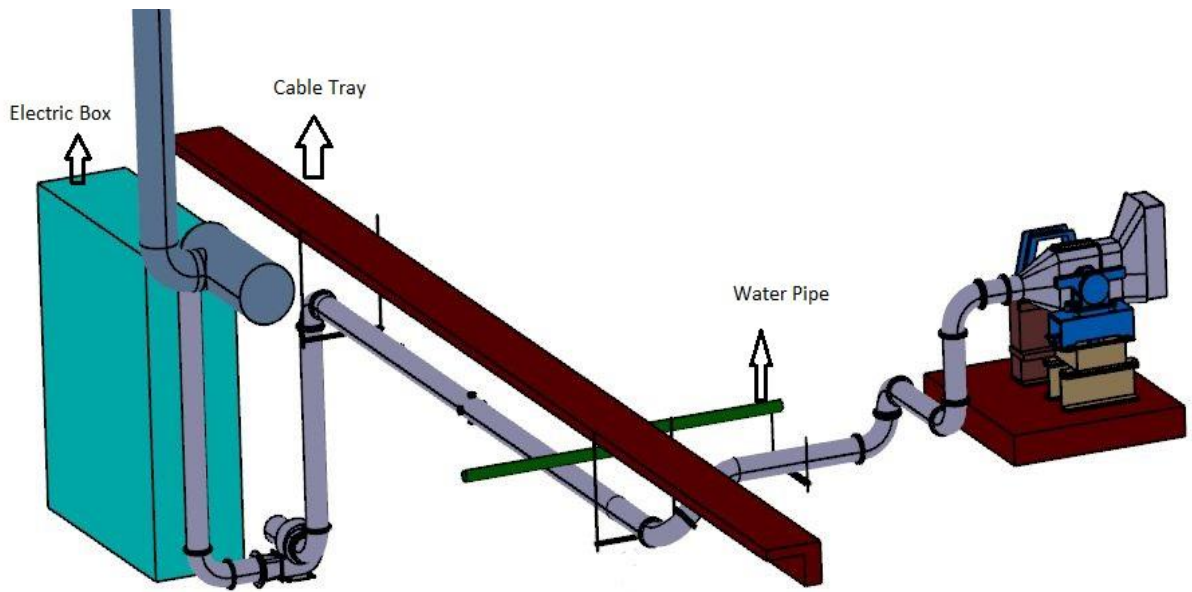


Figure 41 : 3D model of design variant 2 view 3

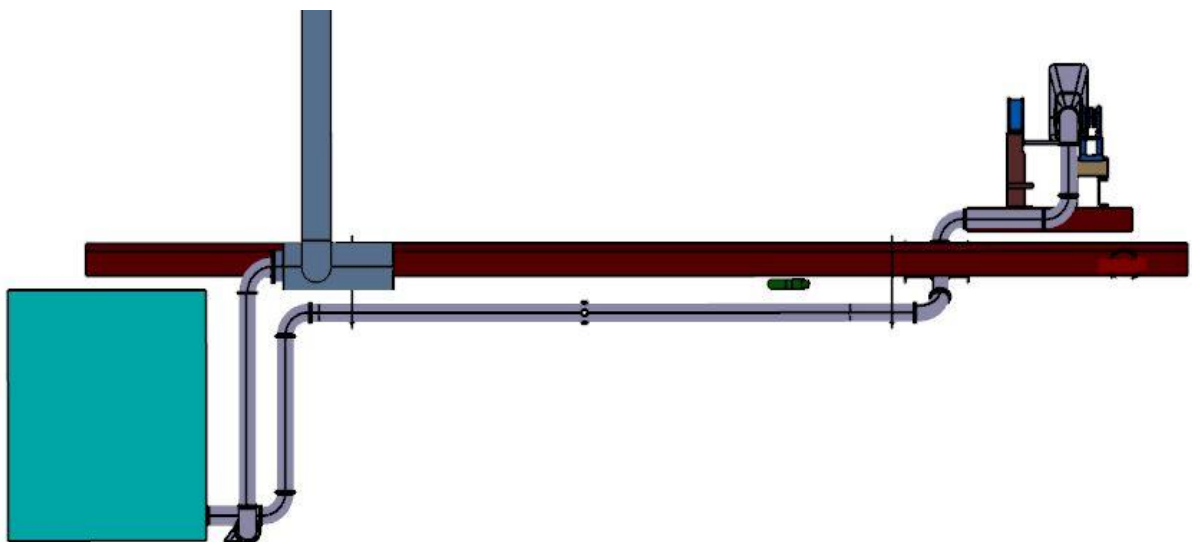


Figure 42: 3D model of design variant 2 view 3

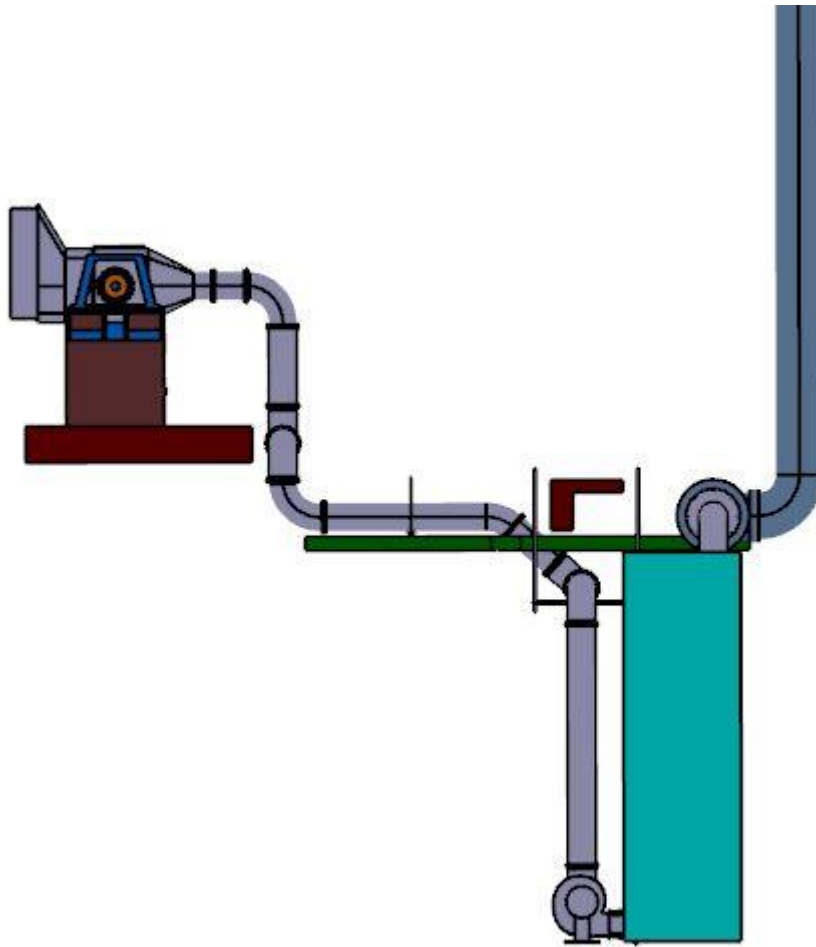


Figure 43: 3D model of design variant 2 view 3

However, the blower is placed at the ground since the position of the tunnel is too low from the top wall and also too large from the side of the wall where the chimney is located. Hence the mounting of the blower on brackets is difficult also dangerous. Because it will be projected to the centre of the room sharp edges in a dangerous manner.

Tunnel

In this design, the sampling tunnel is a straight pipe of length 5490 mm. With sampling points provided at 3000mm from the beginning of the pipe. The opening for the pitot tube is provided at 1377mm from the sampling point towards the blower. Similarly, an M6 hole with thread is provided at 1595mm from the sampling point towards the blower for mounting the temperature sensor.

Mounting of the Blower

Since the blower is placed on the ground there is no need of separate structure for mounting. Since the blower itself is available with a stand to fix the blower to a flat surface with M12 bolts.

5.3 Calculation of Pressure drop

.Pressure Drop at HEPA filter

The pressure drop at given flowrate is obtained from the filter specification (Table 5). Since the pressure drop is a function of velocity, the pressure drop at different flow rates is calculated.

Flow rate(m ³ /Min)	Pressure drop (Pa)
10.24	68.85
12.81	86.13
15.37	103.35

Table26: Pressure drop at HEPA Filter

Pressure drop during the flow through the pipe

Using the energy equation

$$\text{Total pressure drop} = \text{Major losses} + \text{Minor Losses} - \text{Pressure drop due to the difference in elevation btw inlet and outlet} \quad (14)$$

Major losses are the pressure loss due to friction in the pipes. Which can be calculated using the Darcy-Weisbach equation.

$$\text{Head loss over a pipe length } h_L = f_{Re} \cdot \frac{L}{D} \cdot \frac{v^2}{2g} \quad (15)$$

Darcy friction factor (f_{Re}) is a function of Reynolds number and can be calculated using the Swamee Jain equation.

$$f_{Re} = \frac{0.25}{\left(\log\left[\frac{\epsilon/D}{3.7} + \frac{5.74}{Re^{0.9}}\right]\right)^2} \quad (16)$$

$$\text{Reynolds number} = Re = \frac{\rho v D}{\mu} \quad (17)$$

Minor losses are the pressure loss due to components as valves, bends Tees and change in cross-section etc.

$$\text{Head loss due to bends. } h_b = k_l \frac{v^2}{2g} \quad (18)$$

Where $k_l = 0.3$ for 90° elbows.

$$\text{Head loss due to square reduction } h_{rs} = k_s \frac{v^2}{2g} \quad (19)$$

Where

$$K_s = (0.6 + 0.48f_1)(D_1/D_2)^2[(D_1/D_2)^2 - 1] \quad (20)$$

For finding the head loss due to a tapered reduction replace K_s with K_{tap}

$$K_{tap} = K_s \sqrt{\sin\left(\frac{\theta_1}{2}\right)} \quad (21)$$

Where,

θ_1 is the taper angle.

$$\text{Head loss due to the difference in elevation btw inlet and outlet } h_z = \text{Elevation of Inlet} - \text{Elevation of outlet} \quad (22)$$

There are two proposed designs of pipe system considering the collision-free design, the connecting point to the chimney etc. The Pressure drop in each design has calculated manually using the equations as well as the flow analysis using Ansys Fluent.

The manual calculation is done using the average velocity value however the analysis using software has done for all three velocities.

Manual Pressure drop Calculation of design Variant 1

Total pressure drop can be calculated using the equation (14).

Major Losses

Raynolds number can be calculated using equation (17). When substituting the values of parameters

$$\rho = 1.205 \text{ kg/m}^3$$

$$V = 10 \text{ m/s}$$

$$D = 0.15 \text{ m}$$

$$Re = 97914.$$

The value of Reynolds number is above 4000 hence it is satisfying the requirement.

Darcy friction factor (f_{Re}) can be calculated using equation (16).

Where,

$$\varepsilon = 0.015 \text{ mm}$$

$$f_{Re} = 0.01937$$

Head loss due to friction over a pipe length of 14.9m, h_L can be calculated by substituting the obtained values in equation (15).

$$h_L = 9.8 \text{ m}$$

The chimney length is approximated to 10m using the approximate height of the building.

The diameter of the chimney also assumed to be 250mm from observation.

Raynolds number of the flow-through chimney can be calculated using equation (17). When substituting the values of parameters

$$\rho = 1.205 \text{ kg/m}^3$$

$$V = 10 \text{ m/s}$$

$$D = 0.25 \text{ m}$$

$$Re' = 163190.$$

Darcy friction factor for the flow-through chimney (f_{Re})' can be calculated using equation (16).

$$f_{Re} = 0.01619$$

Head loss due to friction over chimney length of 10 m, $h_{L \text{ chimney}}$ can be calculated by substituting the obtained values in equation (15).

$$, h_{L \text{ chimney}} = 3.3 \text{ m}$$

$$\text{Total Major headloss} = 13.1 \text{ m} \quad (23)$$

Minor Losses

Head loss due to bends can be calculated using equation (18).

$$\text{Head loss due to bends. } h_b = 1.53 \text{ m}$$

There are 8 numbers of 90° elbows in the design variant 1.

$$\text{Total Head loss due to bends} = 12.24 \text{ m}$$

Head loss due to the reduction in the chamber can be calculated using equations(19) (20) &(21).

$$h_{rt} = 24.98 \text{ m}$$

$$\text{Total Minor losses} = 37.22\text{m} \quad (24)$$

Head loss due to the difference in elevation btw inlet and outlet h_z can be calculated using equation (22).

$$h_z = -9\text{m}. \quad (25)$$

Total pressure drop due to flow

Total head loss due to flow can be calculated by adding results (23)(24)(25)

$$H_t = 59.32\text{m}$$

$$\text{Total Pressure drop } \Delta P = \rho \text{air } g H_t + \text{Pressure drop at HEPA filter} \quad (26)$$

Where,

Pressure drop at HEPA for flow velocity of 10 m/s = 86.13 Pa

$$\Delta P = 787.13\text{Pa}. \quad (27)$$

Manual Pressure drop Calculation of design Variant 2

Major Losses

Head loss due to friction over a pipe length of 14.6m, h_L can be calculated by equation (15).

Where,

$$f_{Re} = 0.01937$$

$$L = 14.6\text{m}$$

$$h_L = 9.6\text{ m}$$

Head loss due to friction over chimney length of 10 m, $h_{L \text{ chimney}}$ can be calculated by substituting the obtained values in equation (15).

$$h_{L \text{ chimney}} = 3.3\text{m}$$

$$\text{Total Major headloss} = 12.9\text{m} \quad (28)$$

Minor Losses

Head loss due to bends. $h_b = 1.53\text{m}$

There is 10 number of 90° elbows in the design variant 2.

Total Head loss due to bends = 15.3m

Head loss due to the reduction in the enclosing chamber can be calculated using equations(19) (20) &(21).

$h_{rt} = 24.98\text{m}$

$$\text{Total Minor losses} = 40.28\text{m} \quad (29)$$

Total pressure drop due to flow

Total head loss due to flow can be calculated by adding results (28)(29)(25)

$H_t = 65.53\text{m}$

Total Pressure drop ΔP can be obtained by substituting values in equation (26)

$$\Delta P = 860.76 \text{ Pa} \quad (30)$$

Total pressure drop calculation using Ansys

CFD simulation is done to estimate the pressure drop of the entire system. In order to do this, I have modelled the regions before and after the blower, excluding the region of the blower. I obtained two CFD models as a result. The simulation is done separately on each model for the three different flowrates. Ultimately total pressure drop is found out by adding the pressure drop at both regions and pressure drop at the filter.

Design variant 1

The assembly is split into two parts. The region before blower and after blower as shown in the images 43, 44.

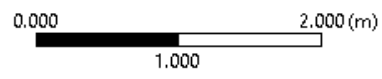


Figure 44: Design 1- region 1

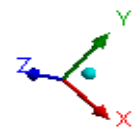
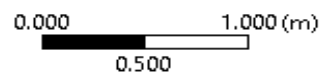
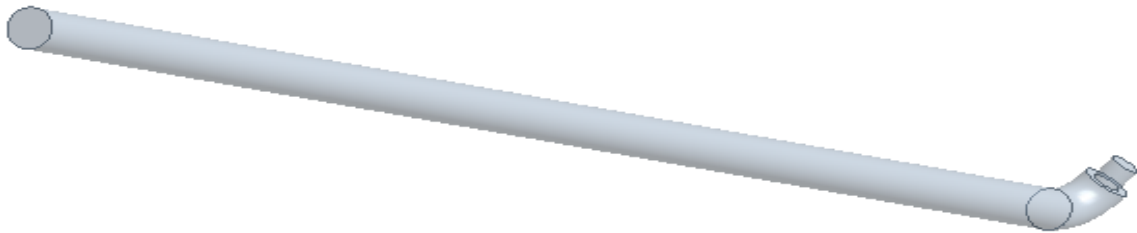


Figure 45: Design 1- region 2

Meshing

	Region 1	Region 2
Mesh Type	Unstructured	Unstructured
Number of elements	464303	67992
Number of nodes	93072	15005

Table 27: Meshing details

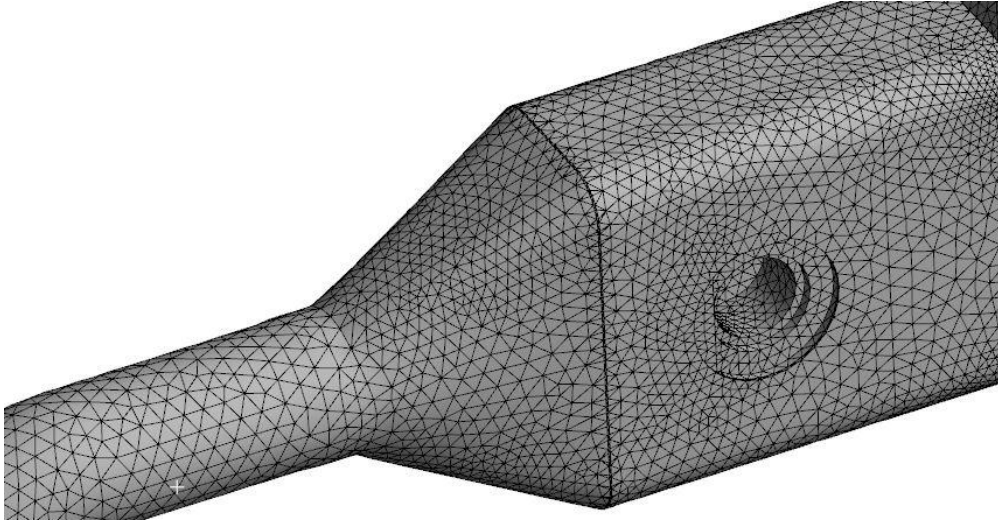


Figure 46: Meshing view 1

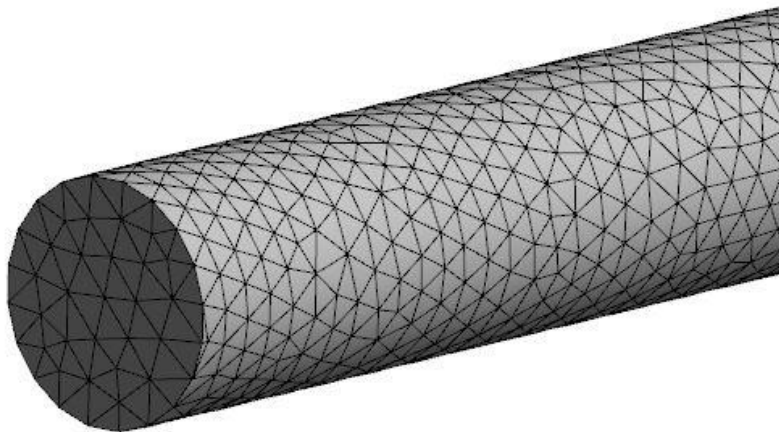


Figure 47: Meshing view 2

Boundary Conditions

There are three cases of flow rates corresponding to three different flow velocities.

Cases	Velocity (m/s)	Flow rate (m ³ /min)
Case 1	8	10.24
Case 2	10	12.81
case 3	12	15.37

Table 28: Flow rates corresponding to velocities

Material of Fluid	Air
Inlet condition	Desired flow rate
Outlet condition	Gauge pressure =0
solver	Steady-state
Viscous model	K-epsilon

Table 29: Boundary conditions

The simulation is done for three different flow rate on each CFD models separately in order to find the pressure drop.

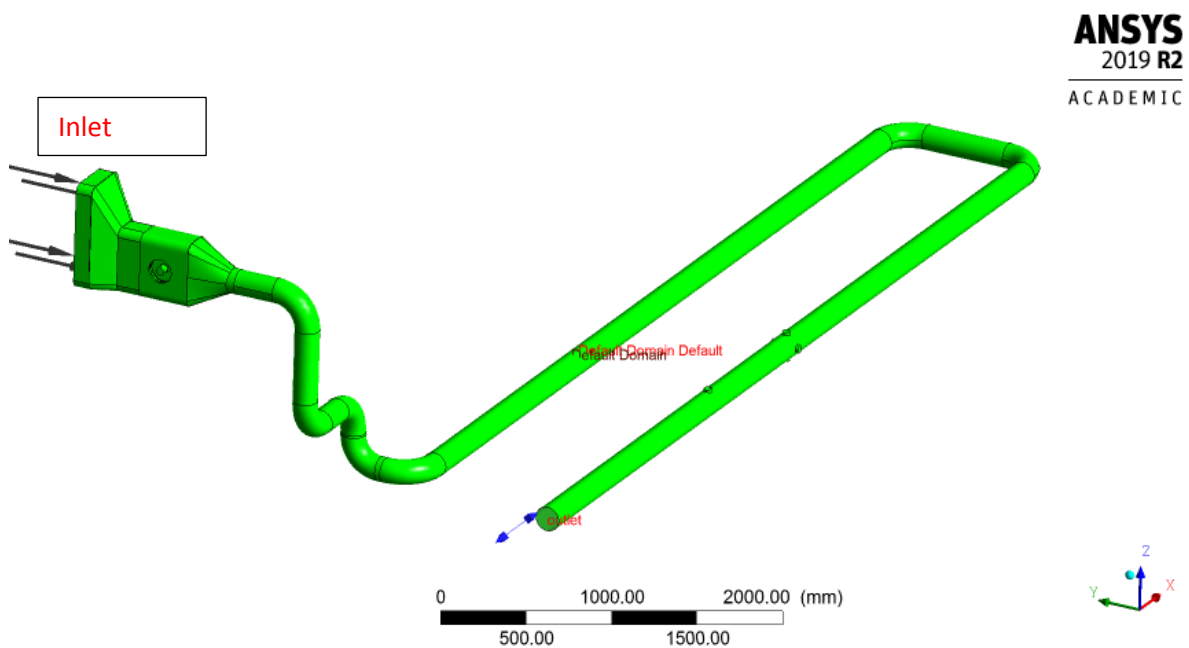


Figure 48: Boundary conition part 1

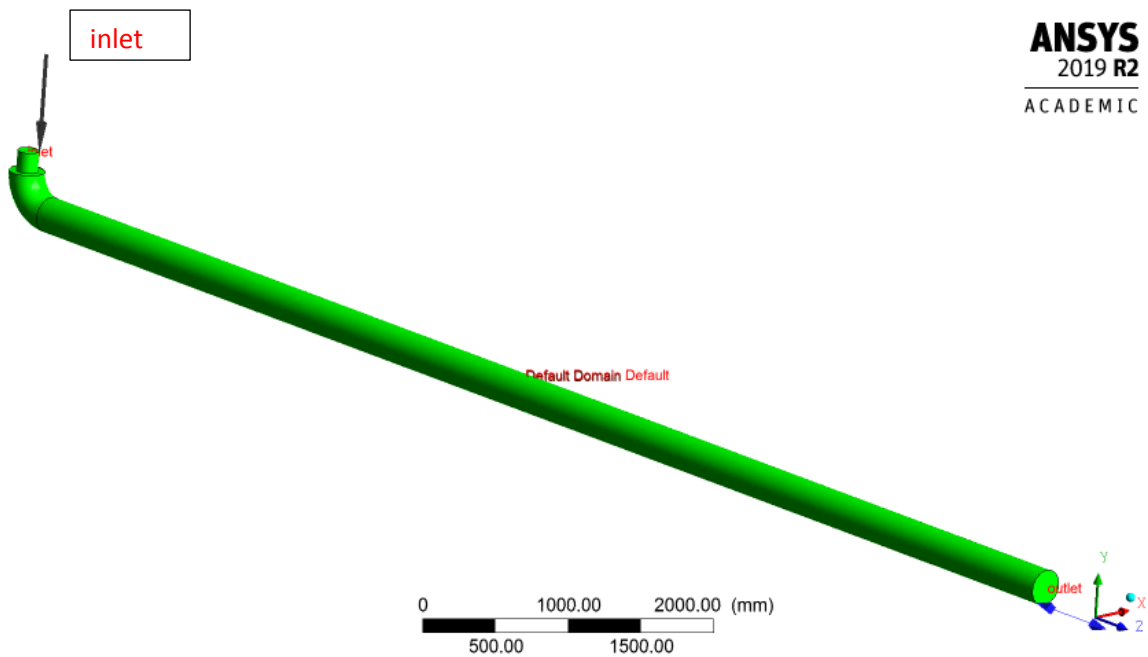


Figure 49: Boundary conition part 1

Result

The pressure loss in each CFD model is calculated by taking the difference between inlet and outlet pressure of the respective models. Pressure drop at the filter is added to the obtained value in order to find the total pressure drop in the system.

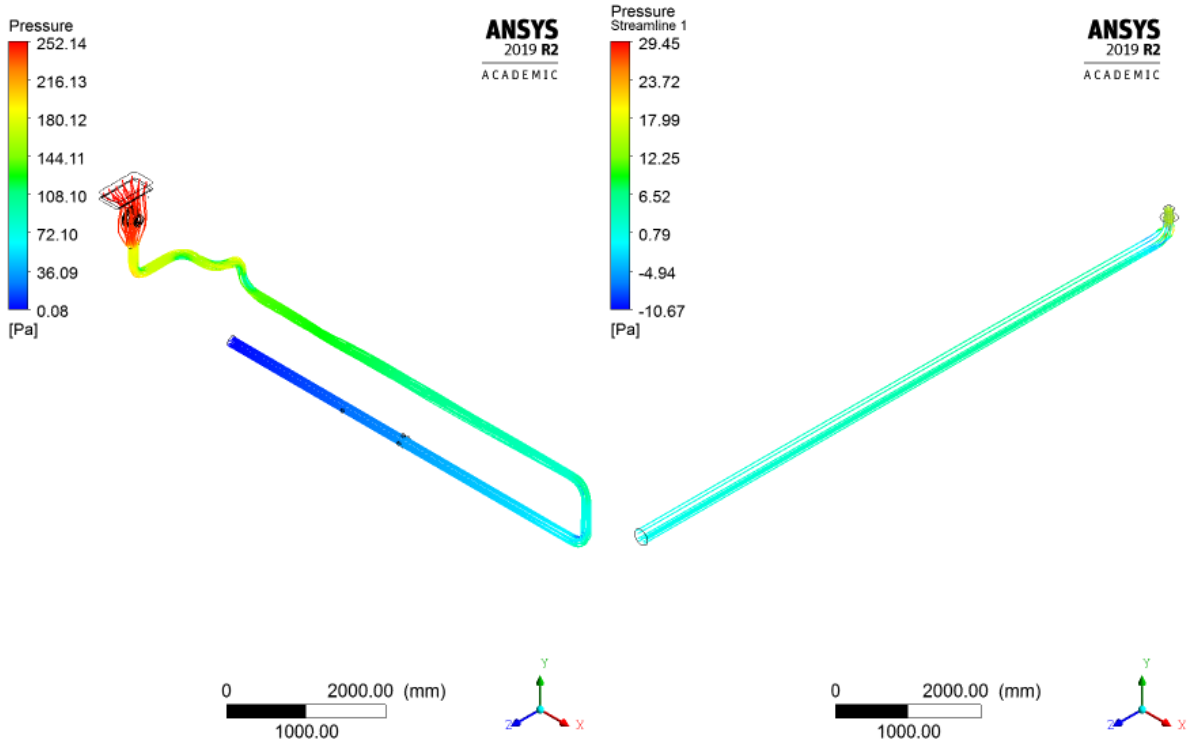


Figure 50: Pressure gradient for flow velocity 8 m/s

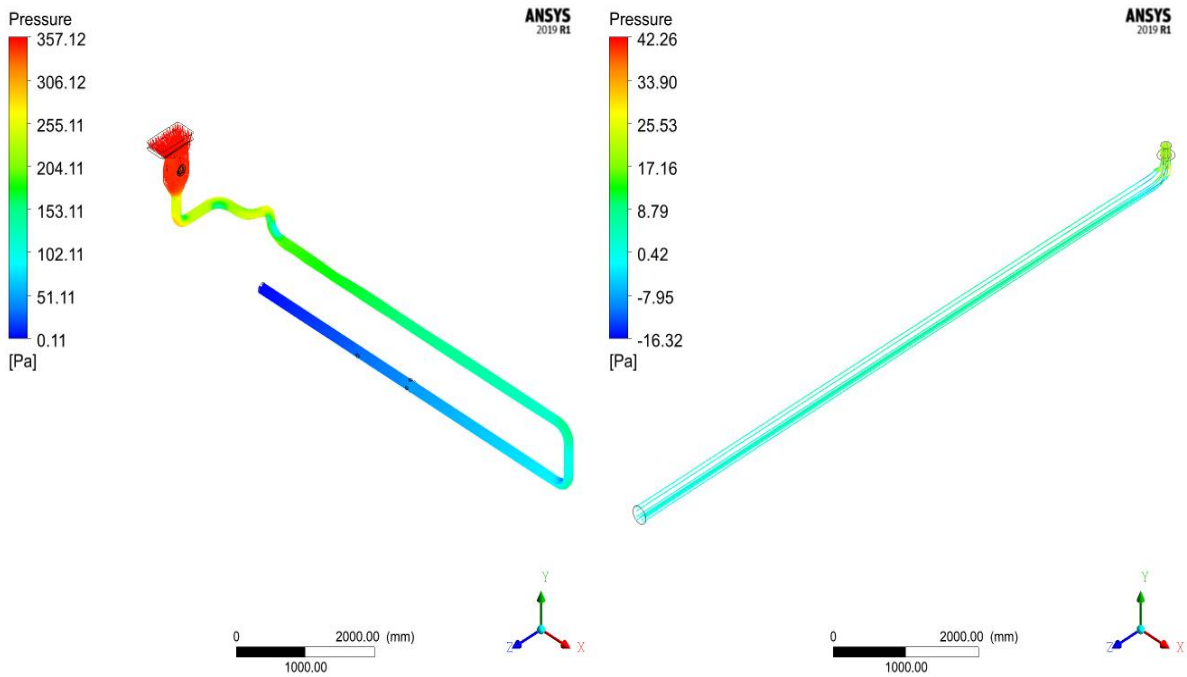


Figure 51: Pressure gradient for flow velocity 10 m/s

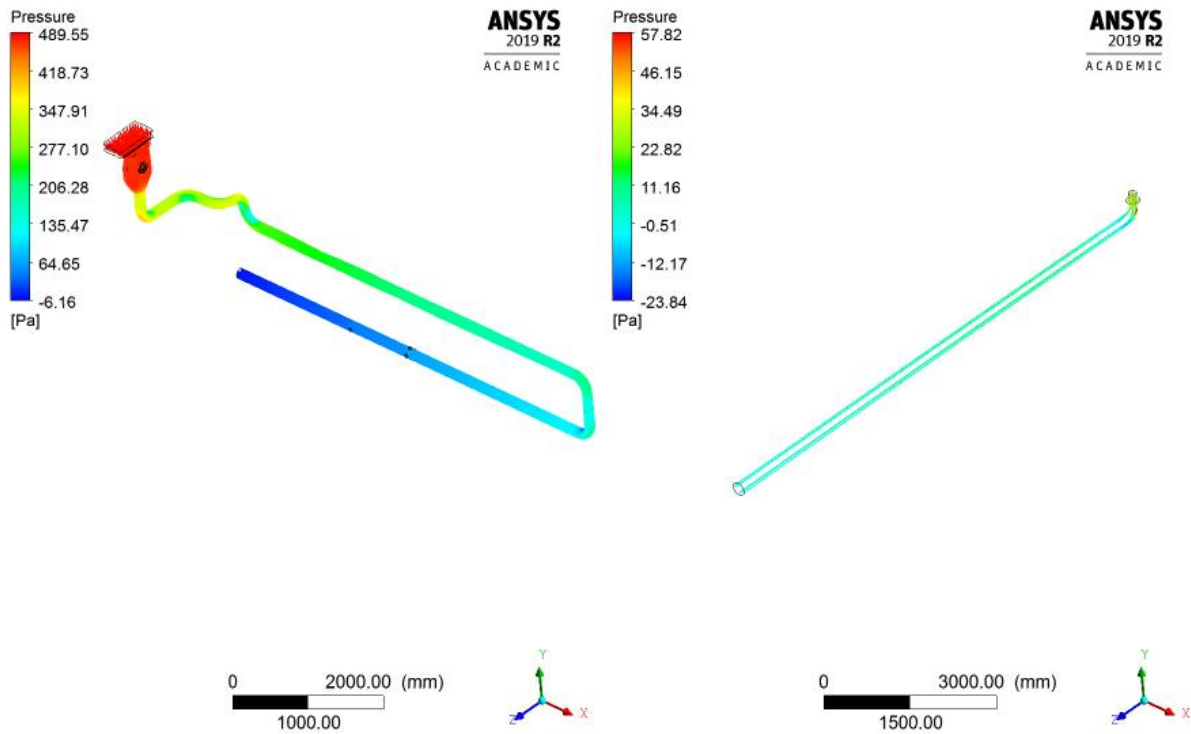


Figure 52: Pressure gradient for flow velocity 12 m/s

Flow rates (m ³ /min)	Gauge pressure (Pa)				Total pressure drop in pipe (Pa)	Pressure drop at HEPA filter	Total pressure drop in the system (Pa)
	Region 1		Region 2				
	inlet	outlet	inlet	outlet			
10.24	250.81	0.48	15.71	0.08	265.96	68.85	334.81
12.81	354.76	0.70	20.03	0.11	373.98	86.13	460.11
15.37	486.22	1.00	32.23	0.16	517.29	103.35	620.64

Table 30 : Design 1 Total pressure drop in the system

Design Variant 2

Similarly, the assembly is divided into two, region before and after blower and two CFD models are obtained.

Meshing

	Region 1	Region 2
Mesh Type	Unstructured	Unstructured
Number of elements	224750	94193
Number of nodes	47936	20950

Table 31: Meshing details – Design variant 2

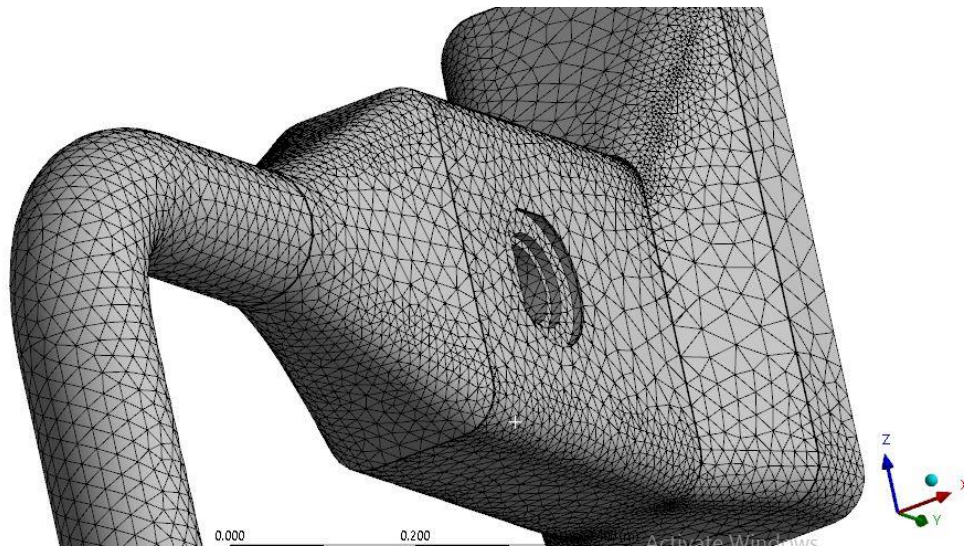


Figure 53: Design 2 , meshing view 1- Part 1



Figure 54: Design 2-meshing view part 2

Boundary Conditions

As described in the previous simulation, the flow rates corresponding to different flow velocities considered from the table. And same boundary conditions are applied as in table 29.

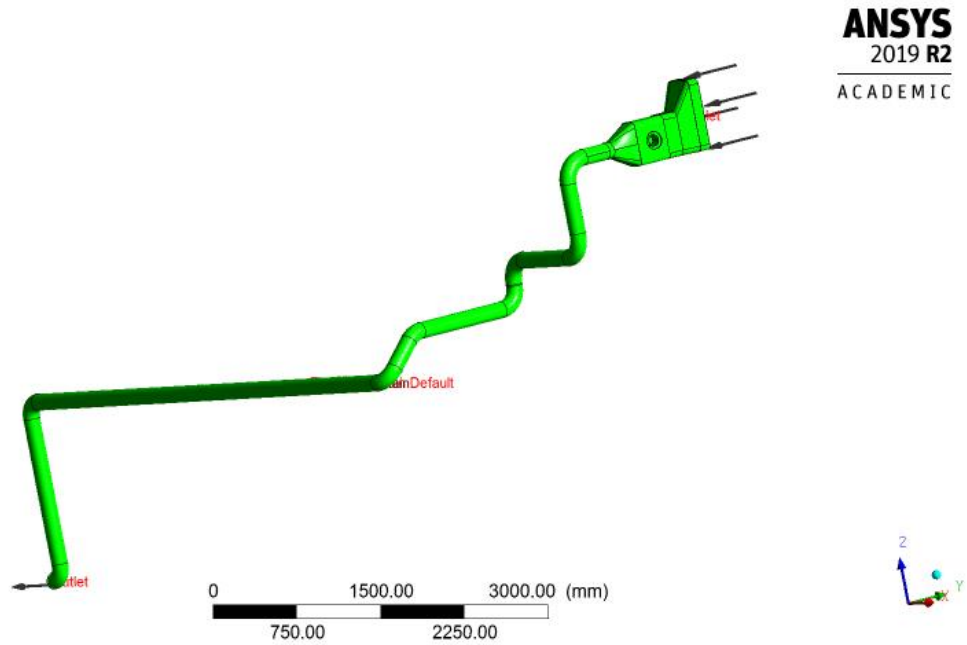


Figure 55: Boundary conditions -design 2-part 1

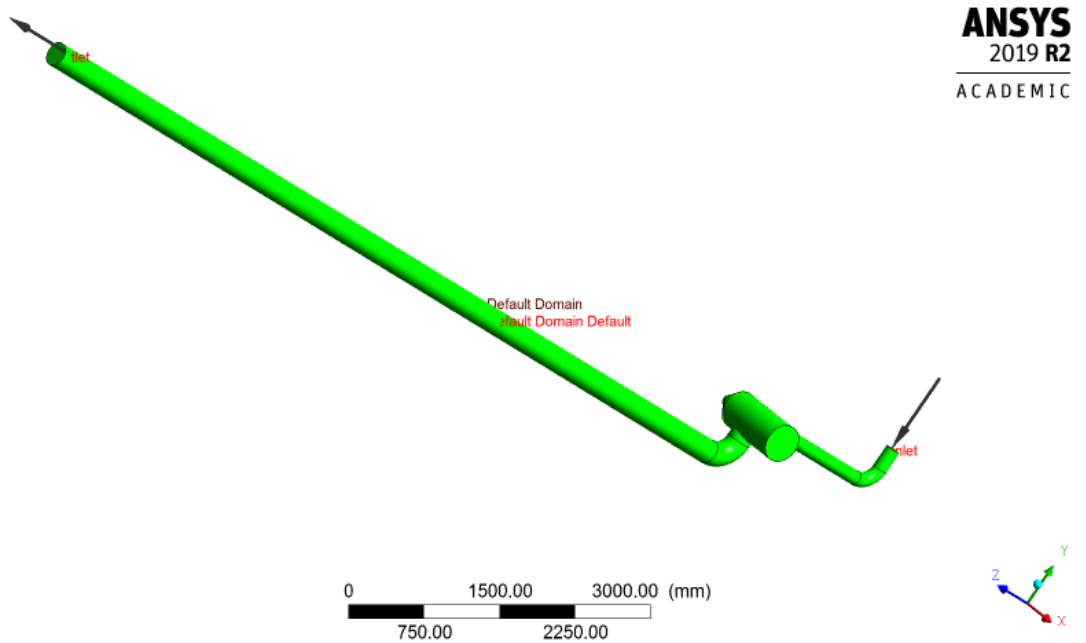


Figure 56: Boundary conditions -design 2-part 2

Result

The simulation results are given below.

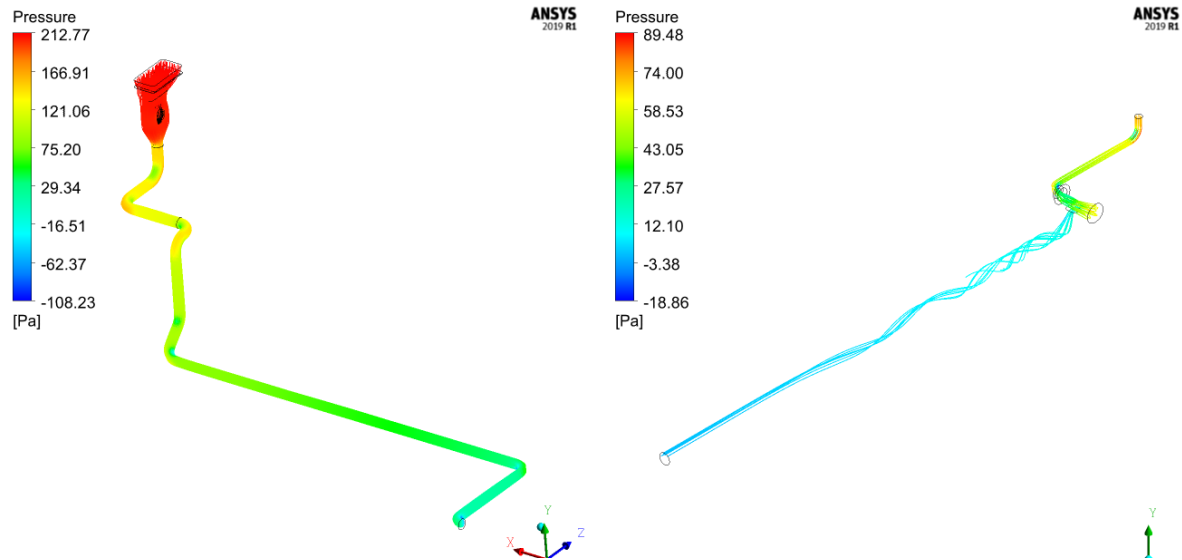


Figure 57: Pressure gradient for flow velocity 8 m/s -Design 2

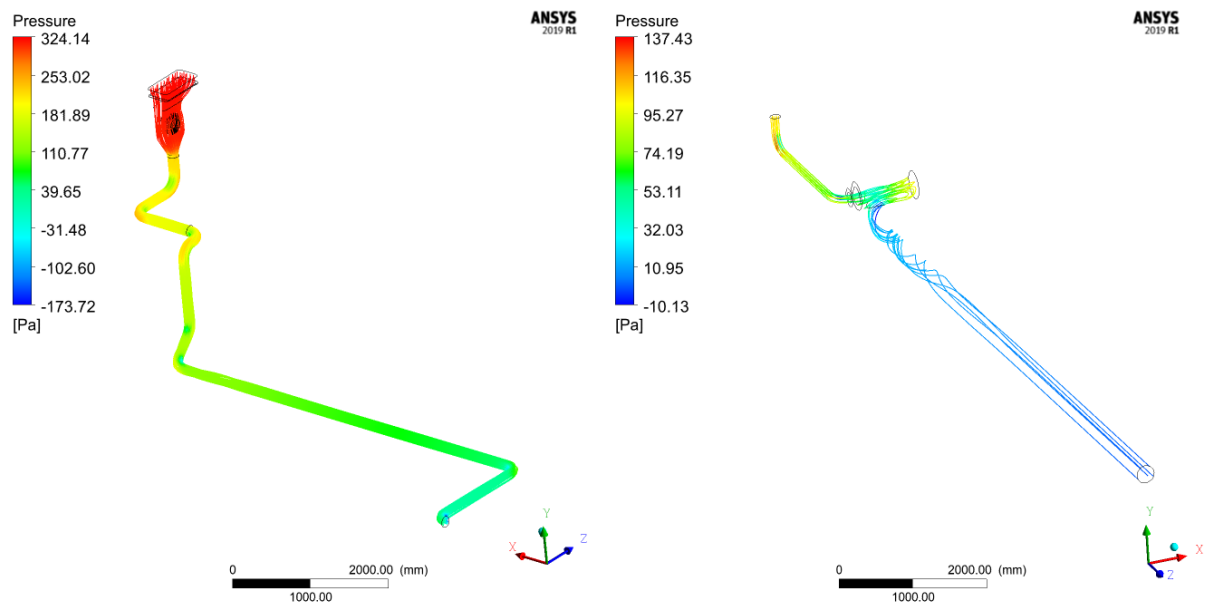


Figure 58: Pressure gradient for flow velocity 10 m/s -Design 2

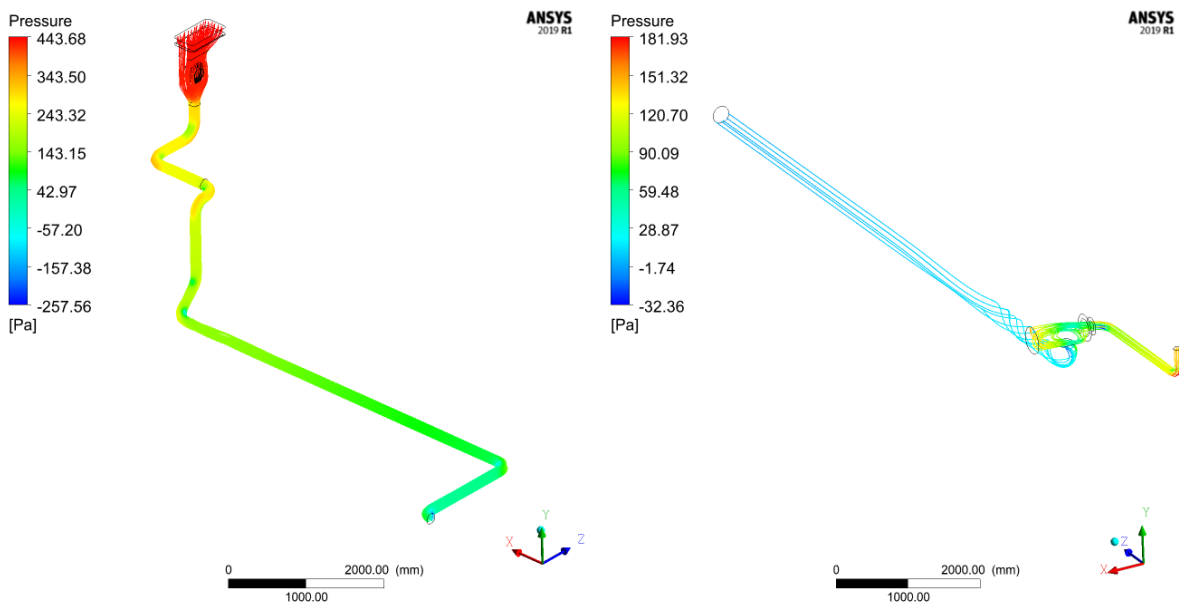


Figure 59: Pressure gradient for flow velocity 12 m/s -Design 2

Flow rates (m ³ /min)	Gauge pressure (Pa)				Total pressure drop in pipe (Pa)	Pressure drop at HEPA filter	pressure drop in the system (Pa)
	Region 1		Region 2				
	inlet	outlet	inlet	outlet			
10.24	211.24	-4.22	70.76	0.90	285.32	68.85	354.17
12.81	321.87	-7.21	104.29	0.13	433.24	86.13	519.37
15.37	440.51	-10.06	142.19	0.18	592.58	103.35	695.93

Table 32: Total pressure drop in the system -Design 2

Pump Selection

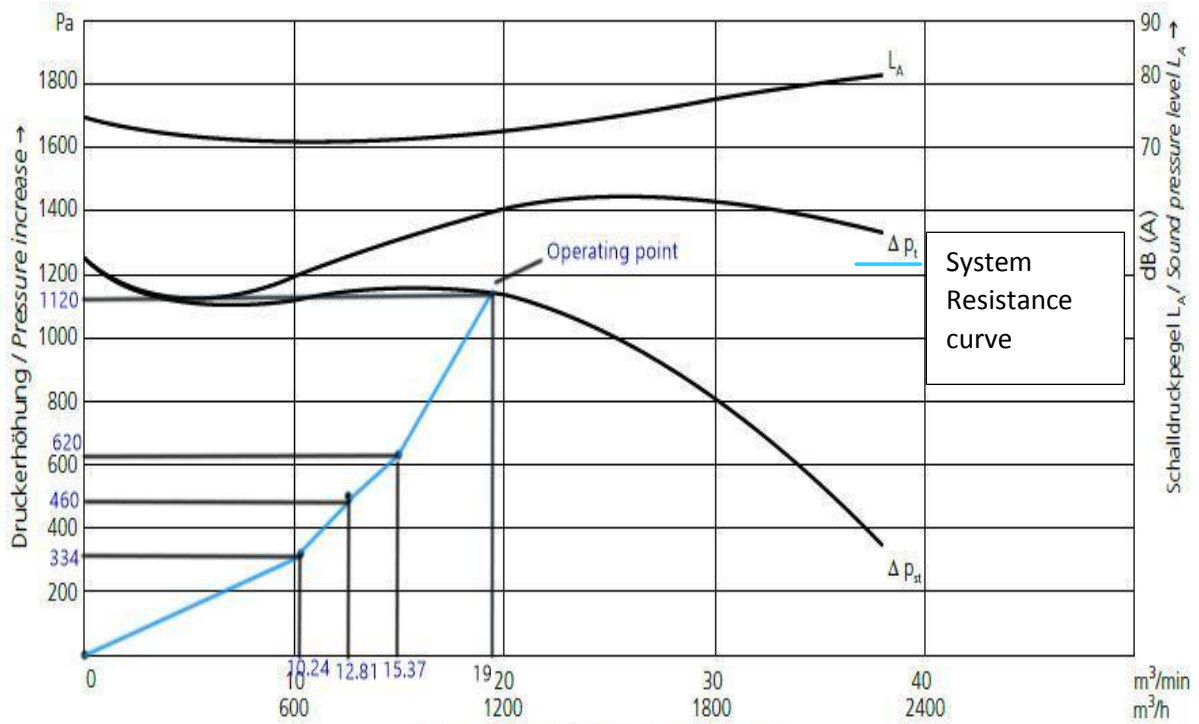
Based on the above calculations I have selected a radial low-pressure centrifugal fan, S-LP 200/77 from the manufacturer Elektor air systems gmbh with below specifications. (Table 33) [38]

S-LP 200/74		
Volumetric flow rate	m ³ /min	38
Total pressure difference	Pa	1260
Voltage	V	230/400
Frequency	Hz	50
Current consumption	A	5.40/3.10
Motor rating	kW	1.5

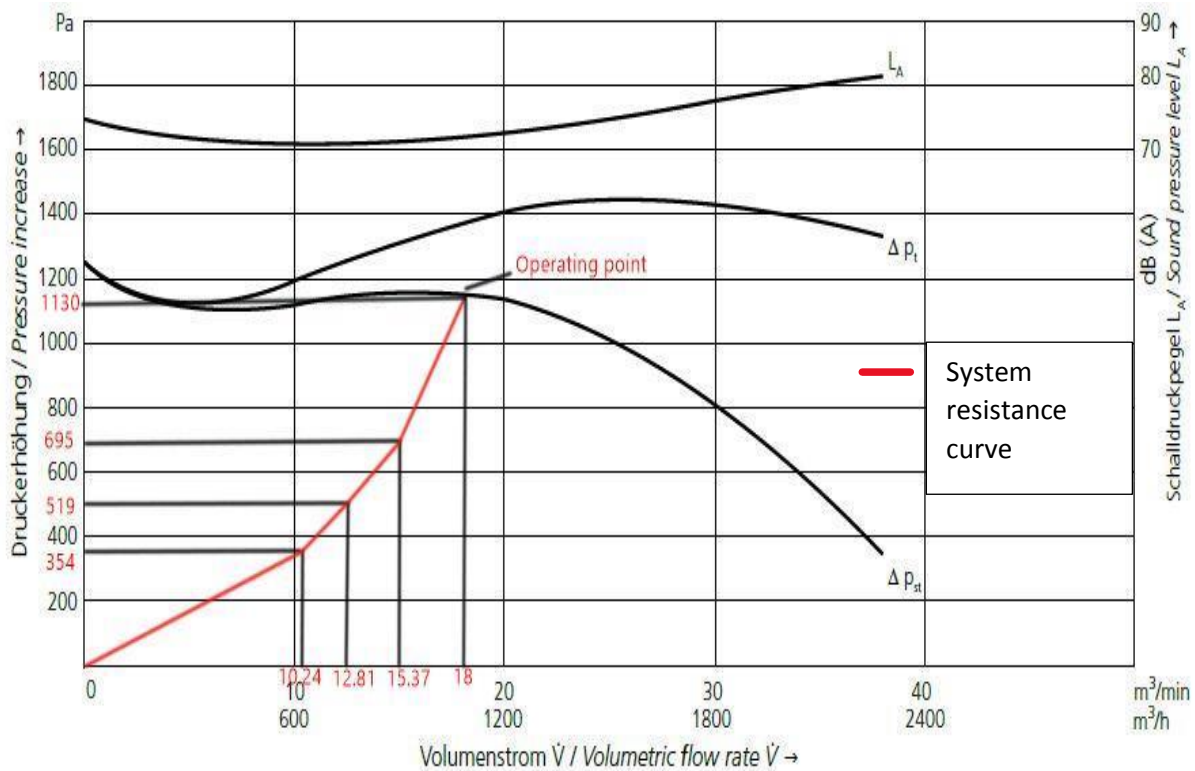
Number of revolutions	min-1	2905
Weight	Kg	22.5

Table 33: Blower Specification

The evaluation of the selected blower is done by comparing the characteristic curve of the blower with the generated system resistance curve. The system resistance curve is generated by plotting the total pressure drop values in the system. System resistance curve is generated for both the design variant based on the total pressure drop values obtained using CFD analysis. [39]



Graph 9: Design 1 System Resistance curve and Blower Characteristic curve



Graph : 10 Design 2 System resistance curve and blower characteristic curve

The system resistance curves are generated by interpolating the pressure drop values. For both the design the pressure drop values lay within the static pressure drop curve of the blower (ΔP_{st}), also operating points are not at the stall region of the static pressure curve. Apart from that, the highest flow rate required is closer to the flow rate of the operating point. Hence it can be concluded that the blower selection is correct. Even though the system resistance curves for both designs are very close to each other in values, design variant 1 showed less total resistance and little better operating point. [40]

Frequency converter

A frequency converter is used for regulating the rotational speed of the centrifugal fan

The model of the frequency converter is Kostal INVEOR (EMC-category C2, 400 V class) from the manufacturer Kostal Air systems gmbh and it is used with a three-phase supply with 50Hz (Table 34). It can be mounted on the motor and also mounted on the wall at a maximum distance of 3m from the motor.

Hence for design variant 1, the Frequency converter can be mounted on the nearest wall since the blower is placed too high from the ground. Whereas in the second variant the frequency controller can be placed on the motor itself since the blower is placed on the ground.

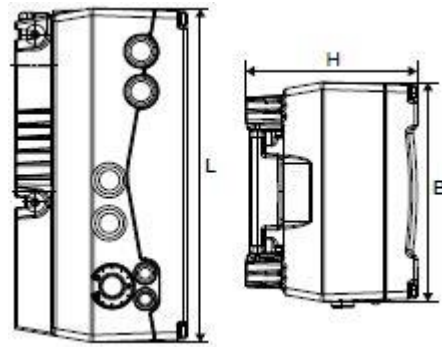


Figure 60: Frequency converter

L	233mm
B	153mm
H	120mm
Rated Power	1.5KW
Weight	3.9Kg
Article Number	020744

Table34: Specifications of the frequency converter

SUMMARY AND CONCLUSION

Literature studies were conducted on non-exhaust emission and the relevance of the particular topic in the present days, various emission test cycles used for chassis dynamometer test, several non-exhaust measurement methods which are usually using in practices. As a result of these studies and the analysis of WLTC and ARTEMIS, driving cycles are selected for running the experiment. A detailed inspection is done on the brake inertia measurement apparatus available at the laboratory and two 3D models are made for the designing of the sampling chamber. The sampling chamber is designed considering the installation space, mounting facilities and production method. 3D models and the 2D drafts of the chamber parts are made for the production purpose. Selection of HEPA filter and centrifugal blower are done based on the requirements and specifications which are obtained from the calculations, CFD analysis and literature studies. Based on the results obtained from the calculations and future scope of the experiment, the diameter of the dilution tunnel has decided. The dilution tunnel including the couplings are designed and 3D models of the overall duct system and assembly has done for both design variants. The blower selection is verified by comparing the system resistance curve and the blower characteristic curve. Detailed 2D draft of the pipes, couplings and clamps are made for the production. Design of auxiliary elements like blower mount, provision for flow measurement is made along with the 3D model and 2D draft.

Some key conclusions are given below

- Non-exhaust emissions are as important as the exhaust emissions and they cause numerous physiological and ecological problems.
- Brake emission is one of the major contributors towards the automotive non-exhaust emission.
- The available experimental set up with the motor can simulate the WLTC, ARTEMIS driving cycles.
- The actual value of the inner diameter of the tunnel required for the sampling process considering standard sampling parameters is 131mm. However considering the following situations like simulating various driving conditions with different parameters in future, the availability of the pipe dimension in the market, space constraint for the installation at the laboratory, the value of the inner diameter is then approximated to 150mm

- The design of the chamber is complying with space and installation constraints and material requirement. Also, it is compatible with the possibility to eliminate small axial misalignment during the installation.
- The dilution tunnel with the sampling points is designed to perform as isokinetic sampling with multiple sampling points.
- Design variant 1 gives slightly better result in the sense of compactness of the design of the pipe system, better space utilization of the room available and total pressure drop in the system.

THESIS CONTRIBUTION

Contribution of this thesis

- Assembly drawing of two design variants with BOM
- List of components for the manufacturing of the sampling chamber with Technical drawing.
- 3D Model of the sampling chamber with 2D draft and weld specifications.
- 3D Model of the Stainless-steel elbow, Pipes and flanges with 2D draft and material, dimensional specification along with the supplier details.
- Details of the clamping techniques, fasteners used for the pipes with technical specification.
- 3D model of the dilution tunnel with sampling points, sampling probe
- Details of Centrifugal blower, Frequency converter with technical specifications, drawing and manufacturer details.
- Details of the HEPA filter with dimension, specification and supplier details.
- Details of Temperature sensor and compensator connection with technical specifications and supplier details.

Future suggestions

- Modified chamber design to eliminate axial misalignment.
- Modification in duct design to minimise the number of bends and flanges.
- A suggestion of a chamber design with an observation window and removable tray at the bottom with quick accessibility to collect the particle deposited at the bottom of the chamber.

References

- [1] Sawyer R F, 2010. *Vehicle emissions: Progress and challenges* J. Expo. Sci. Environ. Epidemiol. **20** 487–8
- [2] TSI, 2015. *Measurement of Brake Wear Emissions By the Engine Exhaust Particle Sizer (Eps) Spectrometer and Optical Particle Sizer (Ops)*
- [3] Green car congress, *The importance of considering non-exhaust traffic emissions; the role of EVs* .Electr. (Battery), Emiss. Heal. Policy, Regul. <https://www.greencarcongress.com/2016/05/20160502-nonehaust.html>
- [4] Grigoratos T and Martini G, 2014 .*Non-exhaust traffic related emissions. Brake and tyre wear PM* . Science and Policy Report by the Joint Research Centre, the European Commission's in-house science service
- [5] Thorpe A and Harrison R M, 2008. *Sources and properties of non-exhaust particulate matter from road traffic: A review* .Sci. Total Environ.
- [6] Chasapidis L, Grigoratos T, Zygogianni A, Tsakis A and Konstandopoulos A G ,2018. *Study of Brake Wear Particle Emissions of a Minivan on a Chassis Dynamometer* Emiss. Control Sci. Technol. **23** 2–3
- [7] Gadd J and Kennedy P, 2000. *Preliminary Examination of Organic Compounds present in Tyres, Brake Pads and Road Bitumen in New Zealand* .Ministry of Transport.
- [8] Thomas D.Gillespie. *Fundamentals of Vehicle Dynamics* -.SAE.Inc.
- [9] Kennedy PC, Gadd J M I, 2002 .*Emission Factors for Contaminants Released by Motor Vehicles in New Zealand*.Ministry of Transportation.
- [10] Tjälve H and Henriksson J,1999. *Uptake of metals in the brain via olfactory pathways*. Neurotoxicology **20** 181–95
- [11] Sydbom A, Blomberg A, Parnia S, Stenfors N, Sandström T and Dahlén S E, 2001. *Health effects of diesel exhaust emissions*. Eur. Respir. J. **17** 733–46.
- [12] Wolff R K, Henderson R F, Snipes M B, Griffith W C, Mauderly J L, Cuddihy R G and McClellan R O ,1987. *Alterations in particle accumulation and clearance in lungs of rats chronically exposed to diesel exhaust*. Fundam. Appl. Toxicol. **9** 154–66.
- [13] Dieselnet,2013. *Emission Test Cycles*. <http://www.dieselnet.com/standards/cycles/>
- [14] Tzirakis E, Technical N, Kyriakidis A and Zannikos F ,2008. *Methodologies for driving cycle development , using on-Road data from Methodology*. Researchgate e.net/publication/258256299
- [15] Lawrence S,2009. *Non-exhaust emission sources*.RST INTEREST GROUP ENVIRONMENTAL CHEMISTRY. <https://www.envchemgroup.com/non-exhaust-emission-sources.html>
- [16] Fung Y S and Wong L W Y, 1995. *Apportionment of air pollution sources by receptor models in Hong Kong*. Atmos. Environ.
- [17] Hujňák V Měření,2015. *kotoučových brzd na setrvačnickovém stanovišti*. <https://dspace.cvut.cz/handle/10467/63387?show=full>
- [18] Hagino H, Oyama M and Sasaki S, 2016. *Laboratory testing of airborne brake wear*

particle emissions using a dynamometer system under urban city driving cycles Atmos. Environ.131 (2016)269 278

- [19] Burtscher H and Majewski W A, 2012. *Exhaust Gas Sampling and Conditioning*. DieselNet.com. https://www.dieselnet.com/tech/measure_sample.php
- [20] Petrović V, Bracanović Z, Grozdanić B, Petrović S, Sazhin S and Knežević D, 2015. *The design of a full flow dilution tunnel with a critical flow venturi for the measurement of diesel engine particulate emission* FME Trans. **43** 99–106
- [21] First.M,2016. *HEPA Filters*. American Biological Safety Association (2016) 3(1) 33-42
- [22] Ekofilter.cz,2012. *EPA Filter E10*. <https://www.ekofiltr.cz/produkt/hepa-filtr-e10>
- [23] Augusto Bianchini,2005.. *Fans and Blowers*. Bureau of Energy Efficiency
- [24] Tyler Cunningham, James Jenden, Kai, Ellen Lloyd, Kailyn Stenhouse, Matthew Tierney J D , *Braking*. Energy education. <https://energyeducation.ca/encyclopedia/Braking>
- [25] ARMAT spol, *Stainless steel catalogue -Metal Plates*, <https://armat.cz/nerezove-plechy/>
- [26] ARMAT spol, *Stainless steel catalogue -Bars ,Profiles*. <https://armat.cz/pdf/nerezovy-u-profil.pdf>,
- [27] Gufero Rubber production ltd, *NBR G/WA*. <https://www.gufero.com/eshop-kategorie-gufera-nbr-g-wa-a.html?strana=55>
- [28] ARMAT spol, *Stainless steel catalogue -Welded Pipes...* <https://www.armat.cz/pdf/nerezove-trubky-svarovane.pdf>
- [29] ARMAT spol, *Stainless steel catalogue -Elbow 90°* . <https://armat.cz/pdf/nerezova-kolena-90.pdf>
- [30] ARMAT spol, *Stainless steel catalogue-clamp connection-Heavy duty clam*. <https://armat.cz/pdf/spojeni-clamp-objimky.pdf>
- [31] Omega ,*Ultra Precise Immersion RTD Sensors*. https://br.omega.com/omegaFiles/temperature/pdf/P-ULTRA_RTd.pdf
- [32] Nvent CADDY, *Fixing, Fastening, and Support Products*. <https://www.erico.com/catalog/literature/FM1296C-EUEN.pdf>
- [33] Klinger ,*Product catalogue,Industrial Sealing Division*. <http://www.klinger.co.uk/assets/files/Klinger%20Catalogue%202014.pdf>
- [34] Wapro Wiring and clamping experts, *2004-2006. Special rubber cable grommets for conductor tension reduction* <http://www.wapro.cz/Product.aspx?lang=en&pid=3255&sid=410>
- [35] Valenta, 2016. *Hex bolts DIN 931 and screws DIN 933*. <https://www.valentazt.com/hex-bolts-and-screws.html>
- [36] Valenta ,2016. *Hex, self-locking, coupling and other nuts*. <https://www.valentazt.com/nuts.html>
- [37] Valenta ,2016. *Flat, large-area, locking, spring and other washers*, <https://www.valentazt.com/washers.html#din-125-stainless-steel>

- [38] Elektror airsystem gmbh, 2019, *S-LP 200/74 Radial Low Pressure Blower* .
https://www.elektor.de/en/product/S-LP200_74
- [39] The Engineering Toolbox, 2004 .*Utilize the system curve and the pump performance curve to select the proper pump for a particular application.*
https://www.engineeringtoolbox.com/pump-system-curves-d_635.html
- [40] Twin City Fan, Fan Engineering. *Understanding Fan Curves.* <https://www.tcf.com/wp-content/uploads/2018/06/Understanding-Fan-Curves-FE-2000.pdf>

List of Figures

<i>The penetration ability of particulate matter</i>	12
The brake inertia measurement test bench	18
Arrangement of individual fly wheels	19
Brake disc dimensions currently available on the test rig	20
Basic dimensions of currently using brake pad.	21
Infrared sensor set up.	21
Speed sensor set	22
Scheme of the set up	24
HEPA Filter	25
3D model of the design variant 1	30
3D model of the design variant 1 -side view	31
3D model of the design variant 1 view 2	31
3D model of the design variant 1 View 3	32
3D model of the design variant 1 view 4	33
3D model of the design variant 1 view 5	33
Chamber assembly view 1	35
Chamber assembly view 2	36
Chamber part 1 view 1	36
Chamber part 1 view 2	36
Chamber part 2 view 1	37
Chamber part 2 view 2	37
Chamber mounting location on part 7	37
Chamber mounting location on part no 2	37
U profile cross-section	38
Disc with sleeve	38
Gufero cross section	39
Standard 90° elbow	41
Sampling points on Tunnel	42
sampling probe	43

Cod K12 clamp	43
Connection point for pitot tube	44
Bracket for mounting blower	45
Caddy clamp ssembly	45
Caddy clamp assembly drawing	46
Cable gland	47
Hexagonal bold dimensions	47
Hex nut dimensions	48
3D model of design variant 2 view 1	49
3D model of design variant 2 view 2	50
3D model of design variant 2 view 3	50
3D model of design variant 2 view 3	51
3D model of design variant 2 view 3	51
3D model of design variant 2 view 3	52
Design 1- region 1	58
Design 1- region 2	58
Meshing view 1	59
Meshing view 2	59
Boundary conition part 1	60
Boundary conition part 1	61
Pressure gradient for flow velocity 8 m/s	62
Pressure gradient for flow velocity 10 m/s	62
Pressure gradient for flow velocity 12 m/s	63
Design 2 , meshing view 1- Part 1	64
Design 2-meshing view part 2	64
Boundary conditions -design 2-part 1	65
Boundary conditions -design 2-part 2	65
Pressure gradient for flow velocity 8 m/s -Design 2	66
Pressure gradient for flow velocity 10 m/s -Design 2	66
Pressure gradient for flow velocity 12 m/s -Design 2	67

Design 1 System Resistance curve and Blower Characteristic curve	68
Design 2 System resistance curve and blower characteristic curve	69
Frequency converter	70

List of Tables

Motor specifications	19
Transmission Specification	19
Parameters of individual flywheels	20
Speed sensor Specification	22
HEPA Filter specifications	25
WLTC, Energy dissipated in different phases.	28
ARTEMIS, Energy dissipated in different classes	28
Flow Rates	29
Chemical composition	34
Mechanical Properties	34
Physical properties	35
U profile dimensions	38
Gufero specifications	39
Pipe Specifications	40
Elbow specifications	41
Probable diameters of sampling prob for different velocity conditions.	42
Clamp specifications	43
Temperature sensor specification	44
Caddy Strut specification	46
Threaded rod specification	46
Gasket sheet specifications	47
Cable gland dimensional specifications	47
Hexagonal bolt specifications	48
Hex nut specifications	48
washer specification	48
Pressure drop at HEPA Filter	53
Meshing details	59

Flow rates corresponding to velocities	60
Boundary conditions	60
Design 1 Total pressure drop in the system	63
Meshing details – Design variant 2	63
Total pressure drop in the system -Design 2	67
Blower Specification	68
Specifications of the frequency converter	70

List of Graphs

NEDC-Urban Driving Cycle	13
NEDC -Extra Urban Driving Cycle	14
Artemis Urban cycle	14
Artemis Rural roads	15
Artemis Motorways	15
WLTC Class3a	16
WLTC Class 3b	17
WLTC class 1	17
Design 1 System Resistance curve and Blower Characteristic curve	68
10 Design 2 System resistance curve and blower characteristic curve	69

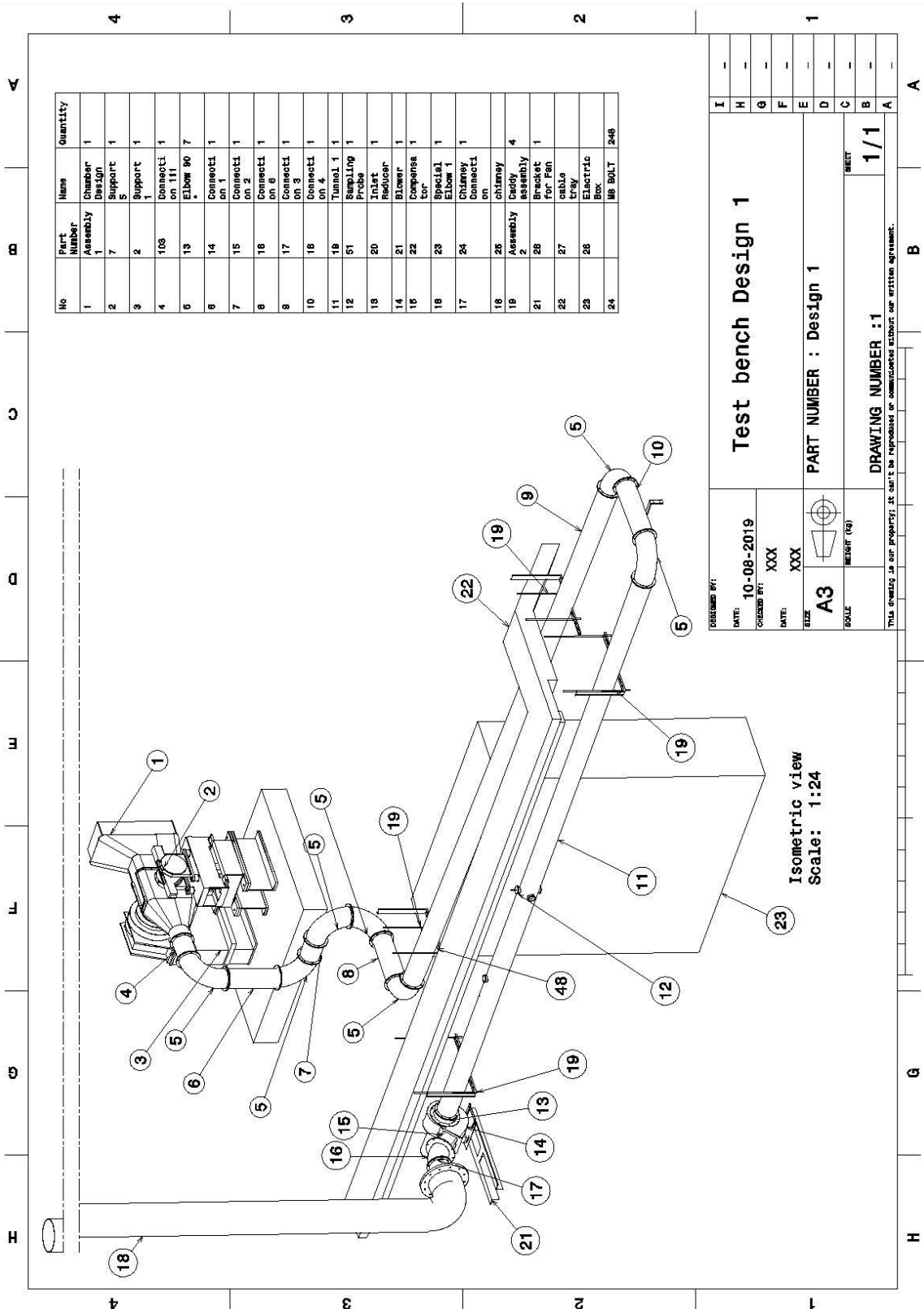
List of Attachments

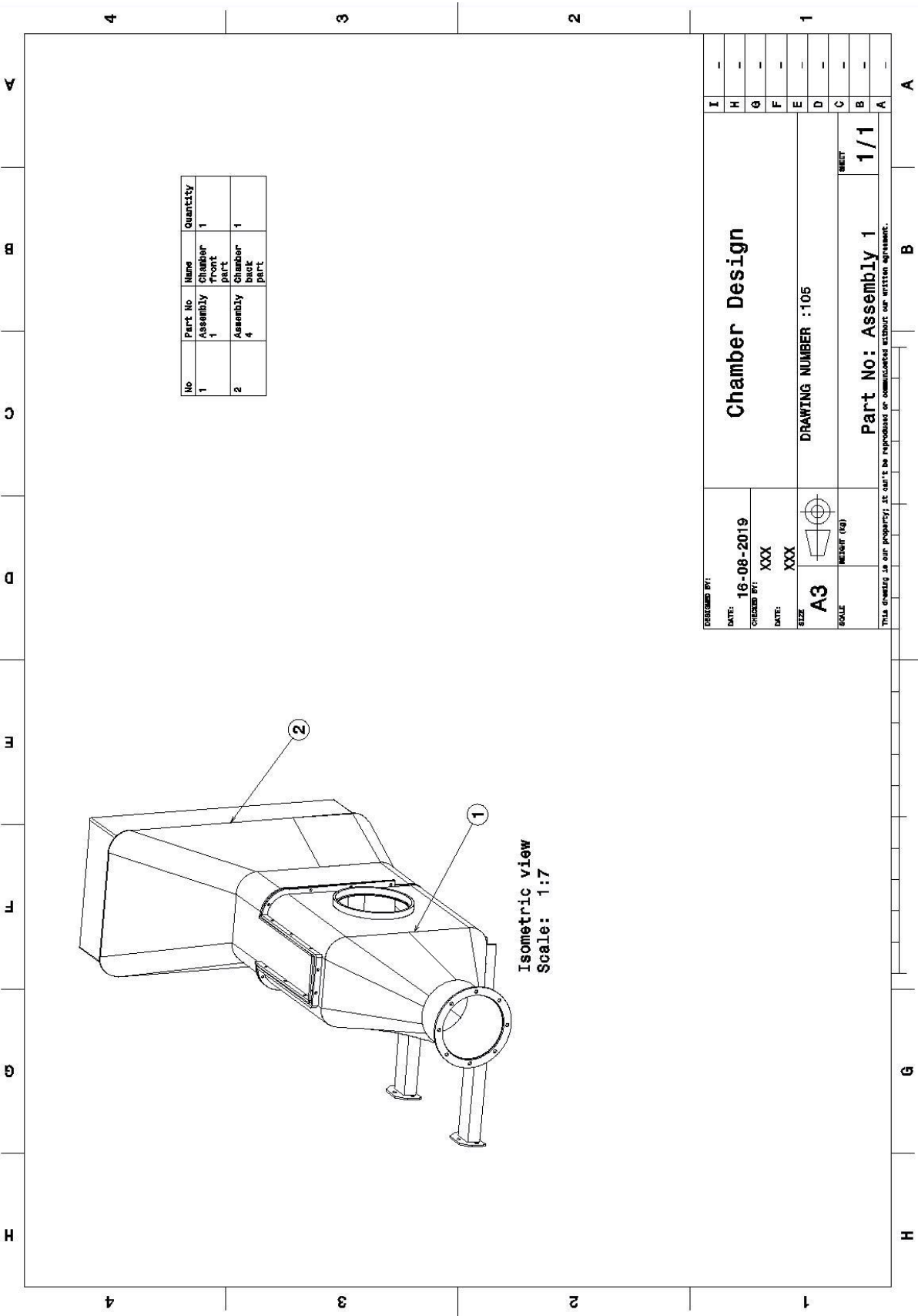
Attachment 1	87
Attachment 2	88
Attachment 3	89
Attachment 4	90
Attachment 5	91
Attachment 6	92
Attachment 7	93
Attachment 8	94
Attachment 9	95
Attachment 10	96
Attachment 11	97
Attachment 12	98
Attachment 13	99
Attachment 14	100
Attachment 15	101
Attachment 16	101
Attachment 17	102
Attachment 18	104
Attachment 19	105
Attachment 20	106
Attachment 21	107
Attachment 22	108
Attachment 23	109
Attachment 24	110
Attachment 25	111
Attachment 26	112
Attachment 27	113
Attachment 28	114
Attachment 29	115
Attachment 30	116
Attachment 31	117
Attachment 32	118
Attachment 33	119
Attachment 34	120
Attachment 35	121
Attachment 36	122
Attachment 37	123
Attachment 38	124
Attachment 39	125
Attachment 40	126
Attachment 41	127
Attachment 42	128
Attachment 43	129
Attachment 44	130

Attachment 45	131
Attachment 46	132
Attachment 47	133
Attachment 48	134
Attachment 49	135
Attachment 50	136
Attachment 51	137
Attachment 52	138
Attachment 53	139
Attachment 54	140
Attachment 55	141

Attachments

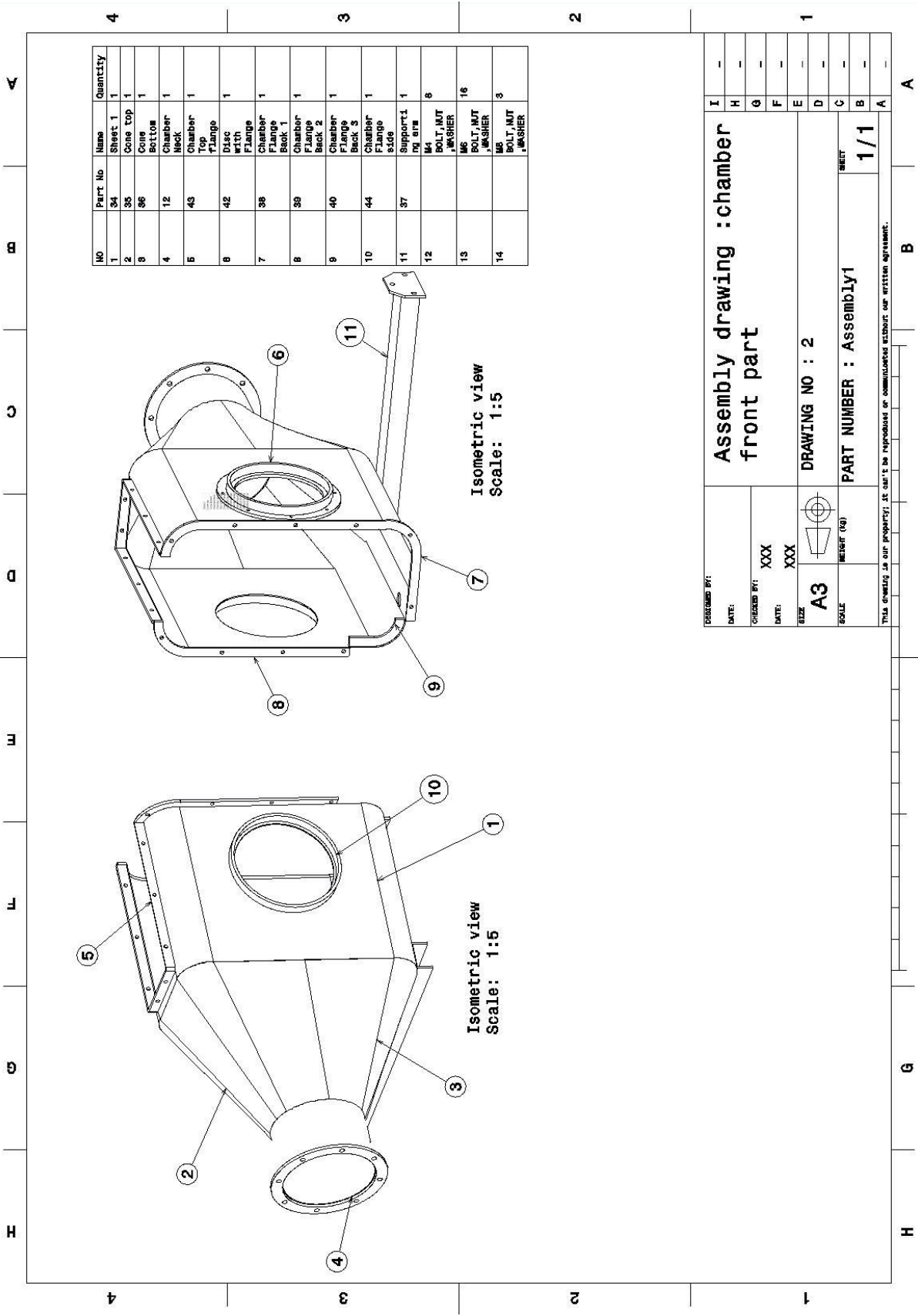
Attachment 1



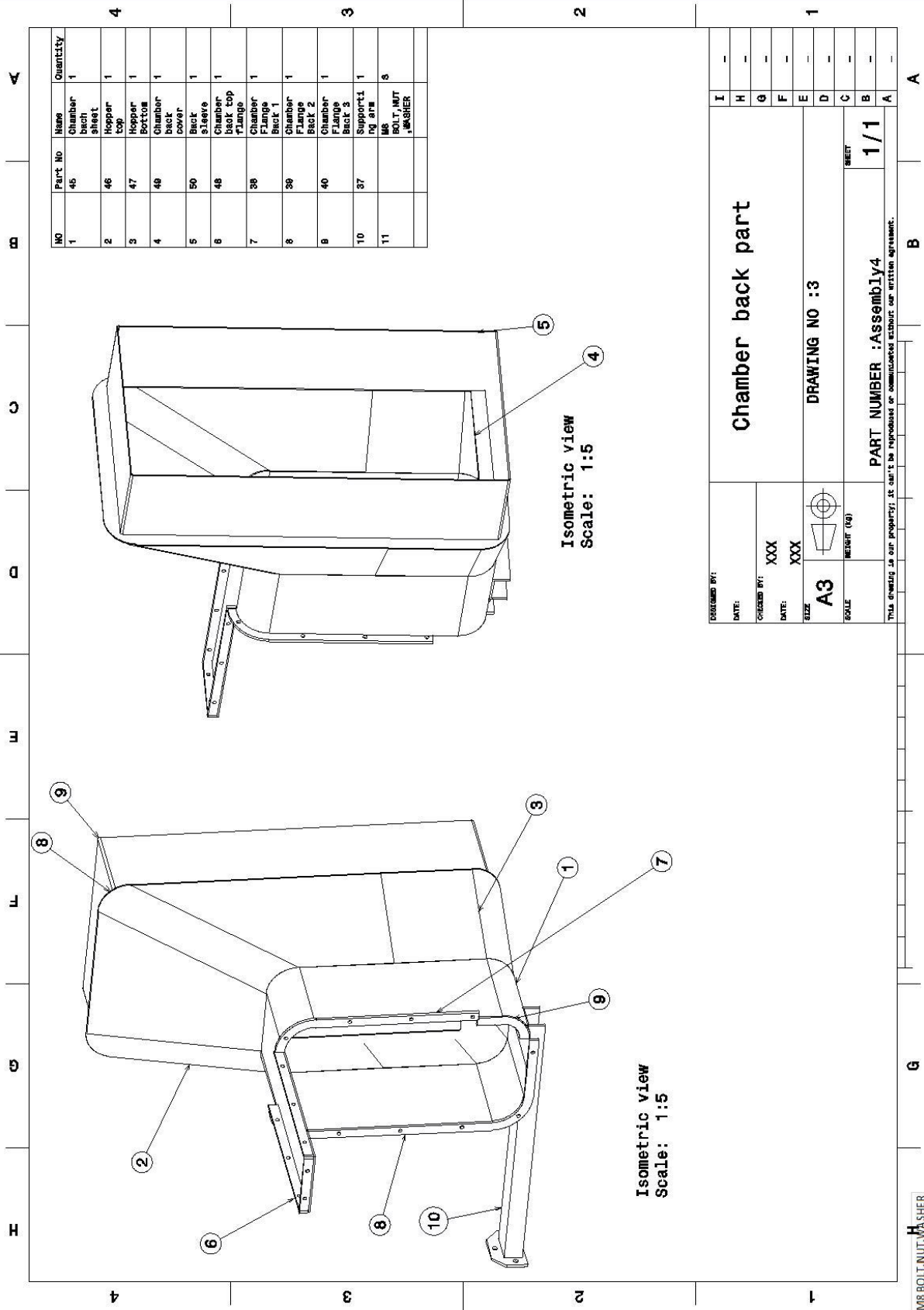


No	Part No	Name	Quantity
1	Assembly 1	Chamber front part	1
2	Assembly 4	Chamber back part	1

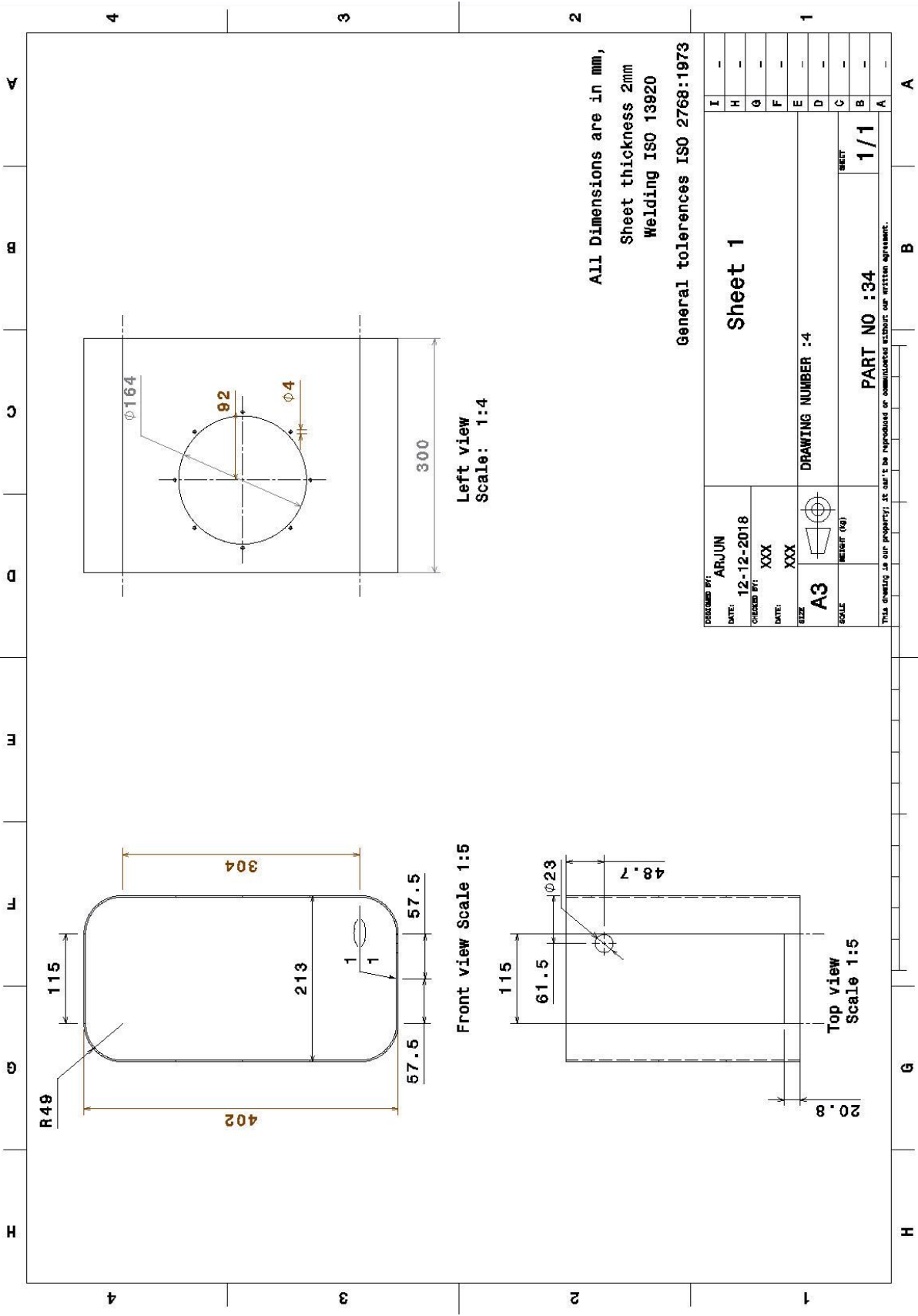
DESIGNED BY:		DATE: 16-08-2019	
DRAWN BY: XXX		DATE: XXX	
SIZE: A3		SCALE: METRIC (kg)	
DRAWING NUMBER : 105		SHEET: 1/1	
Part No: Assembly 1		1/1	
THIS DRAWING IS OUR PROPERTY. IT CAN'T BE REPRODUCED OR COMMUNICATED WITHOUT OUR WRITTEN AGREEMENT.			

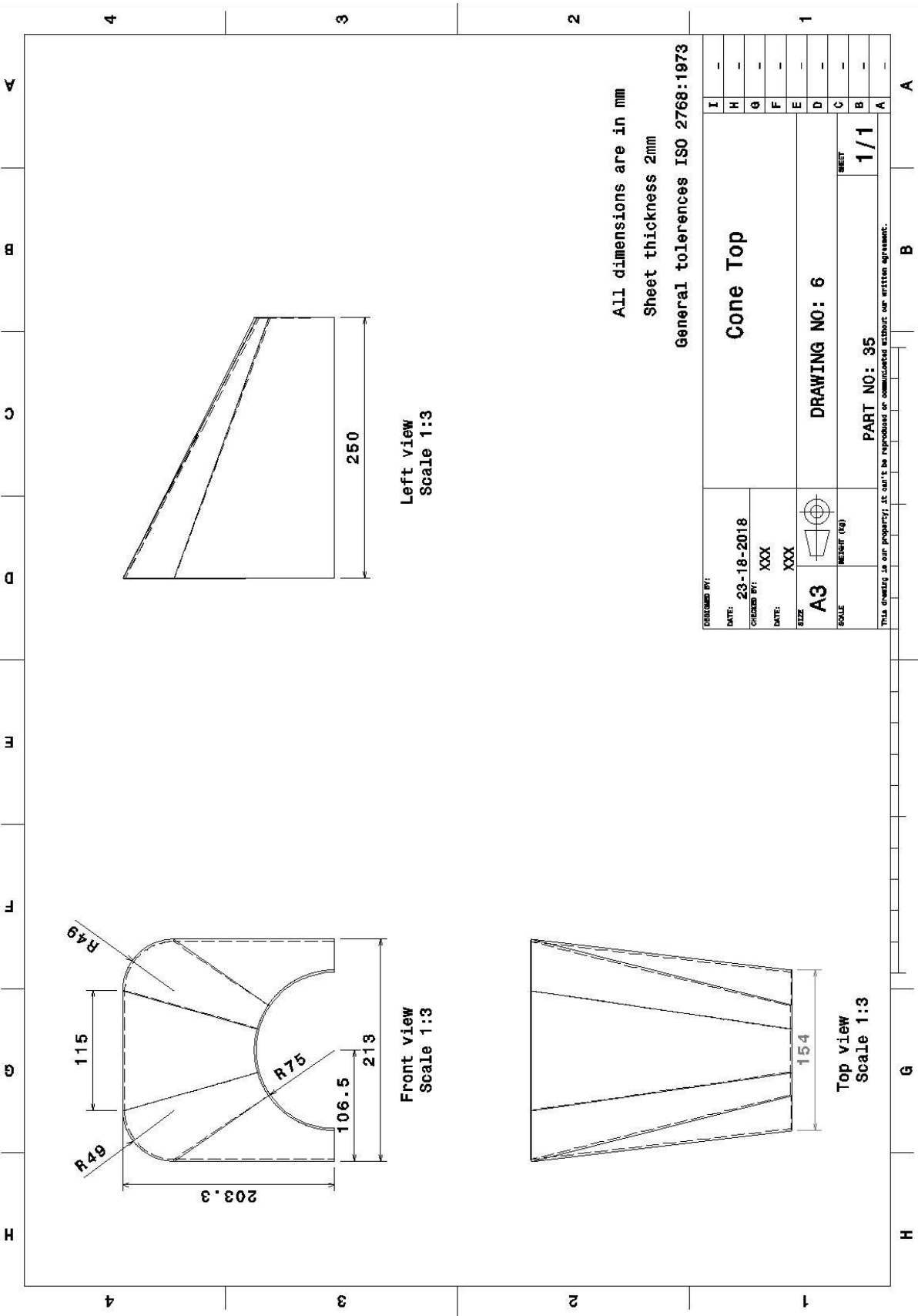


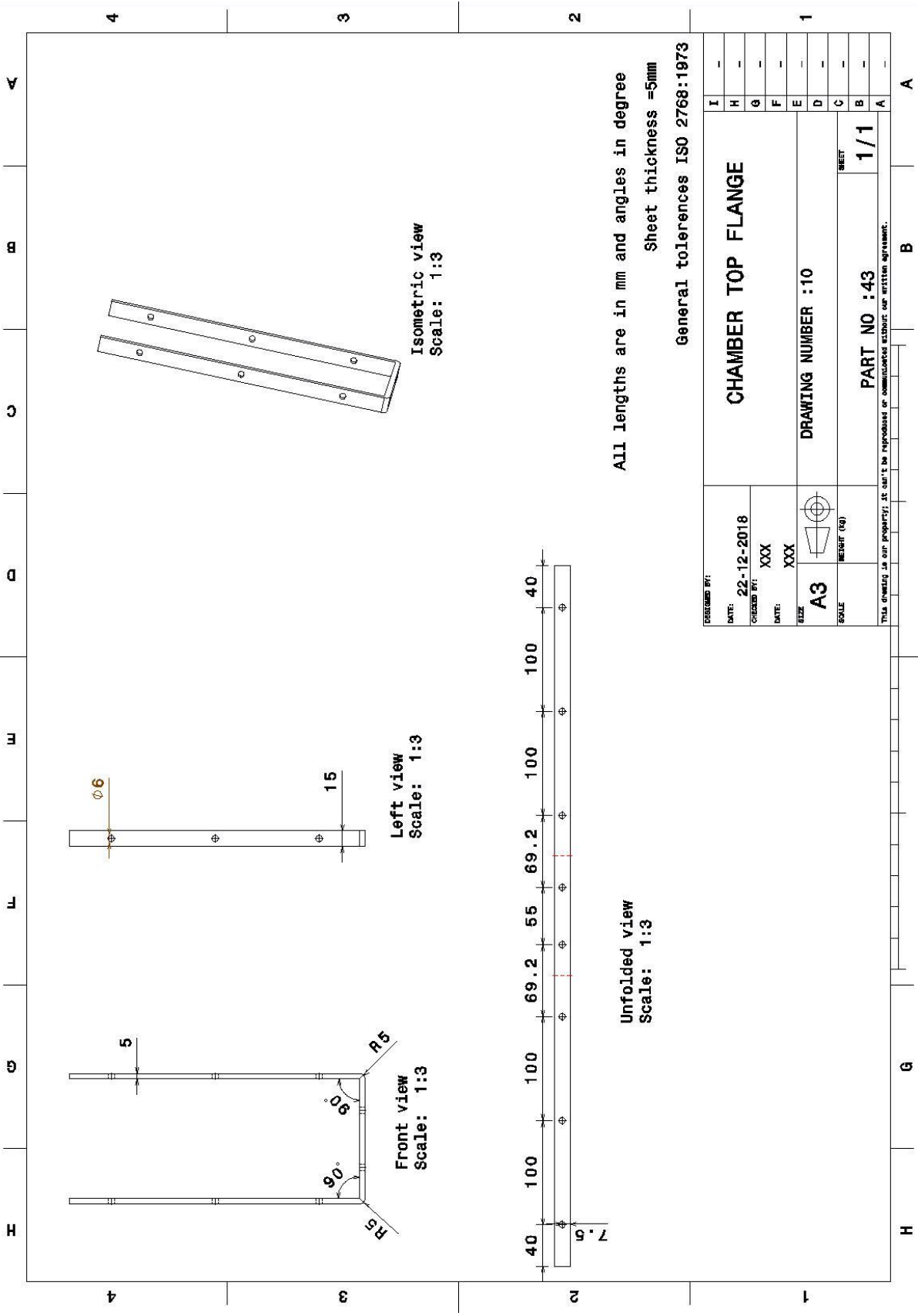
DESIGNED BY:		DATE:		CHECKED BY: XXX		DATE: XXX		SIZE: A3		SCALE: METRIC (KG)	
Assembled by: chamber		front part		DRAWING NO : 2		PART NUMBER : Assembly1		SHEET		1/1	
<small>THIS DRAWING IS OUR PROPERTY. IT CAN'T BE REPRODUCED OR COMMUNICATED WITHOUT OUR WRITTEN AGREEMENT.</small>											

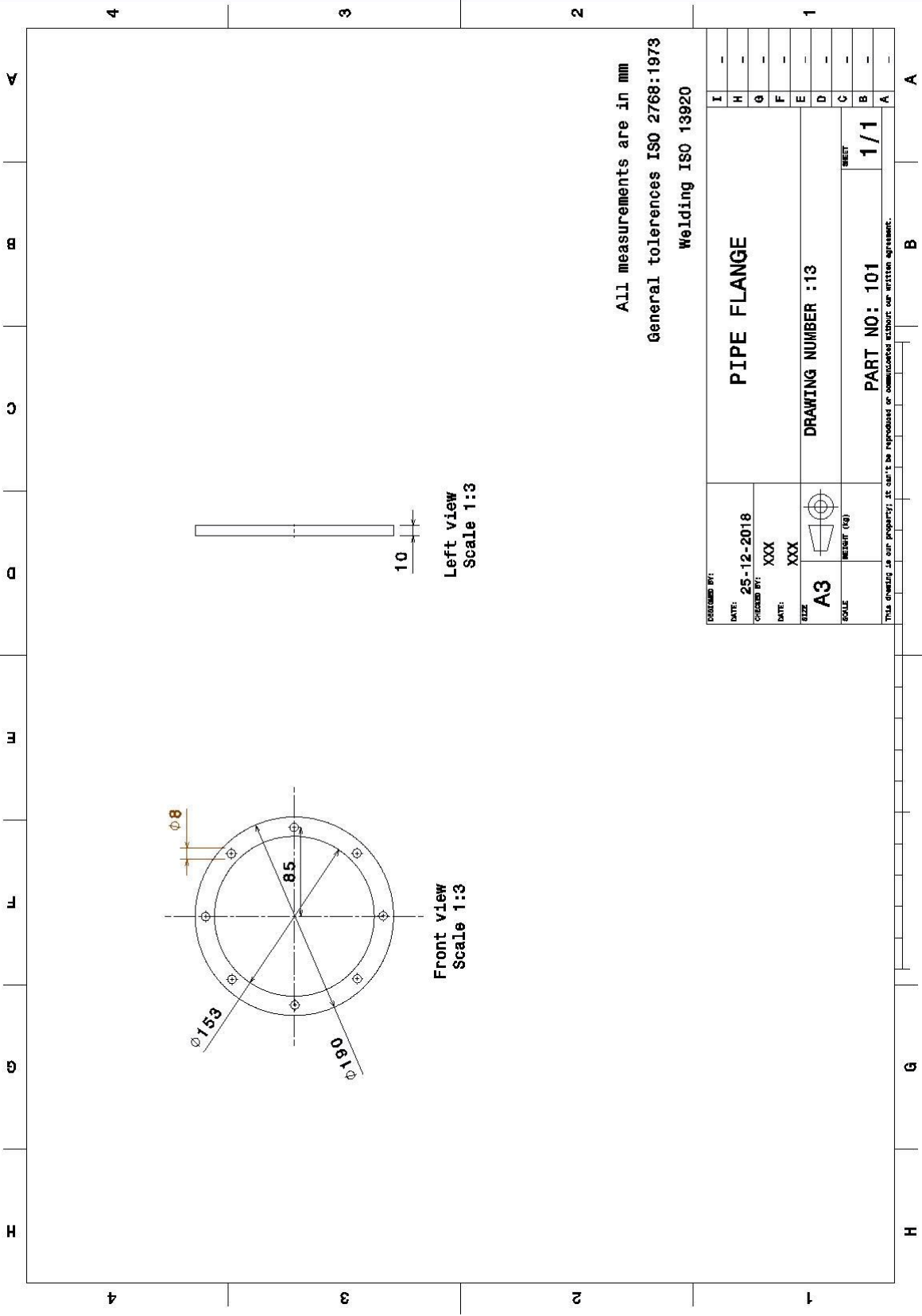


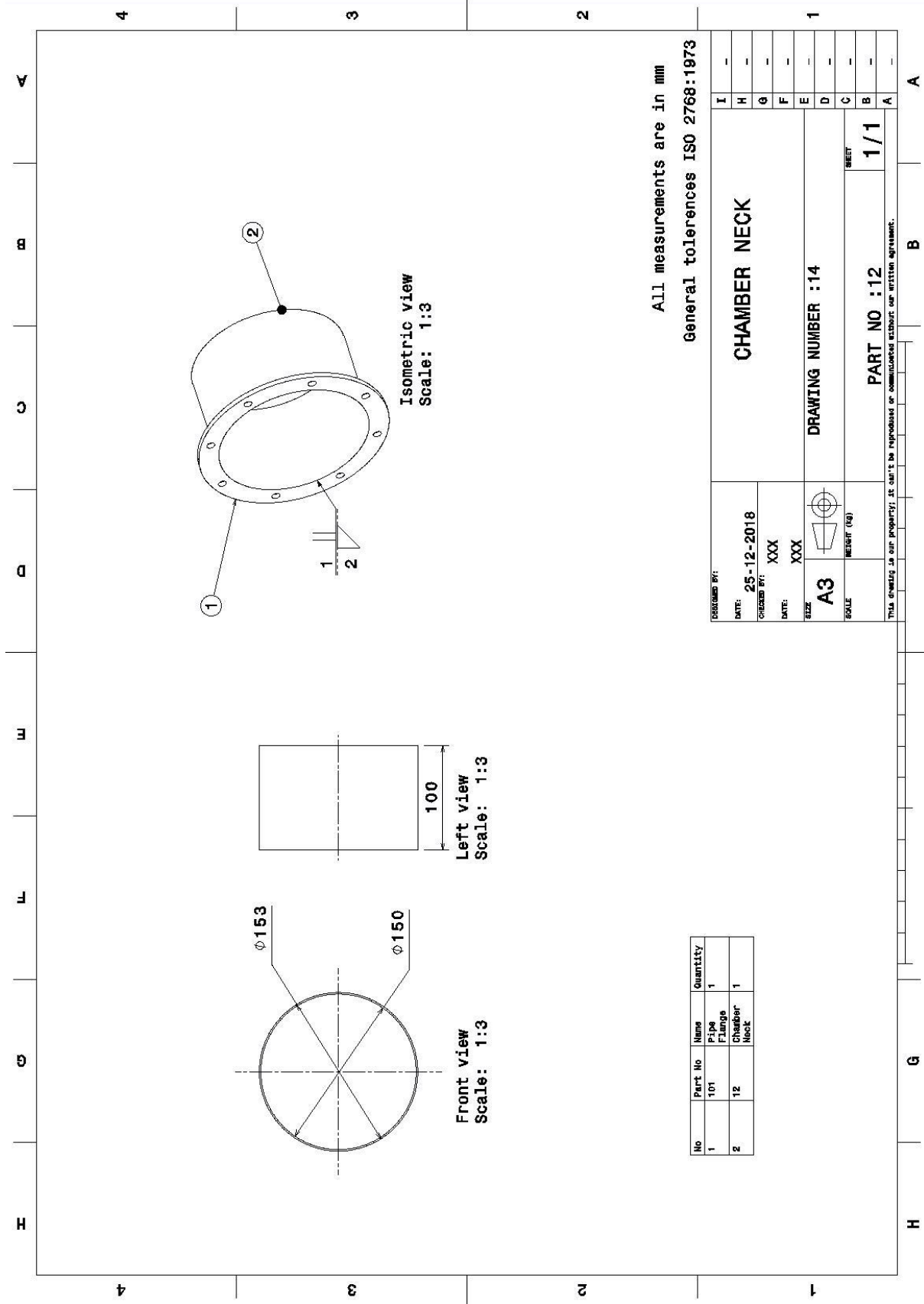
M8 BOLT, NUT, WASHER









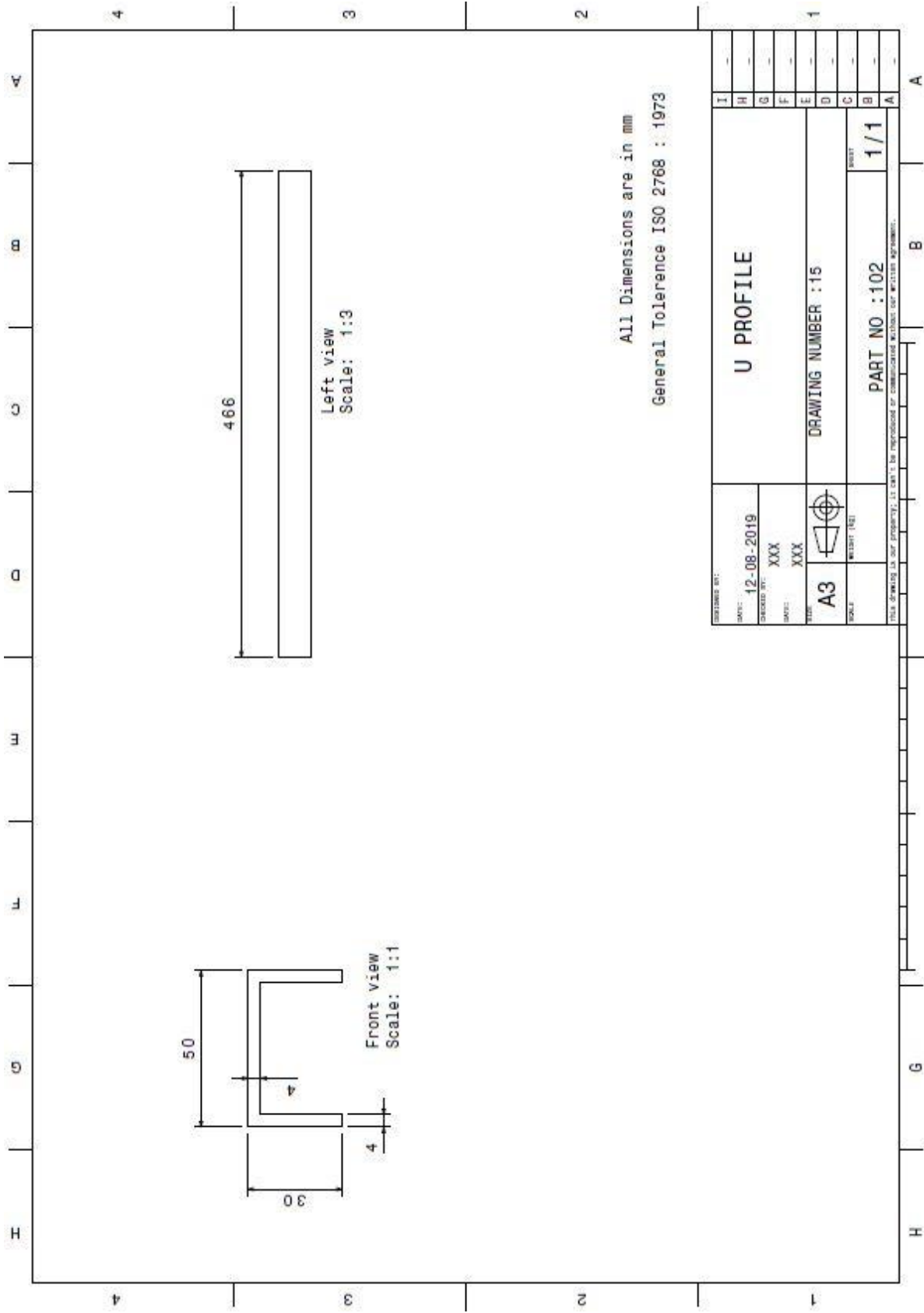


No	Part No	Name	Quantity
1	101	FLANGE	1
2	12	CHAMBER NECK	1

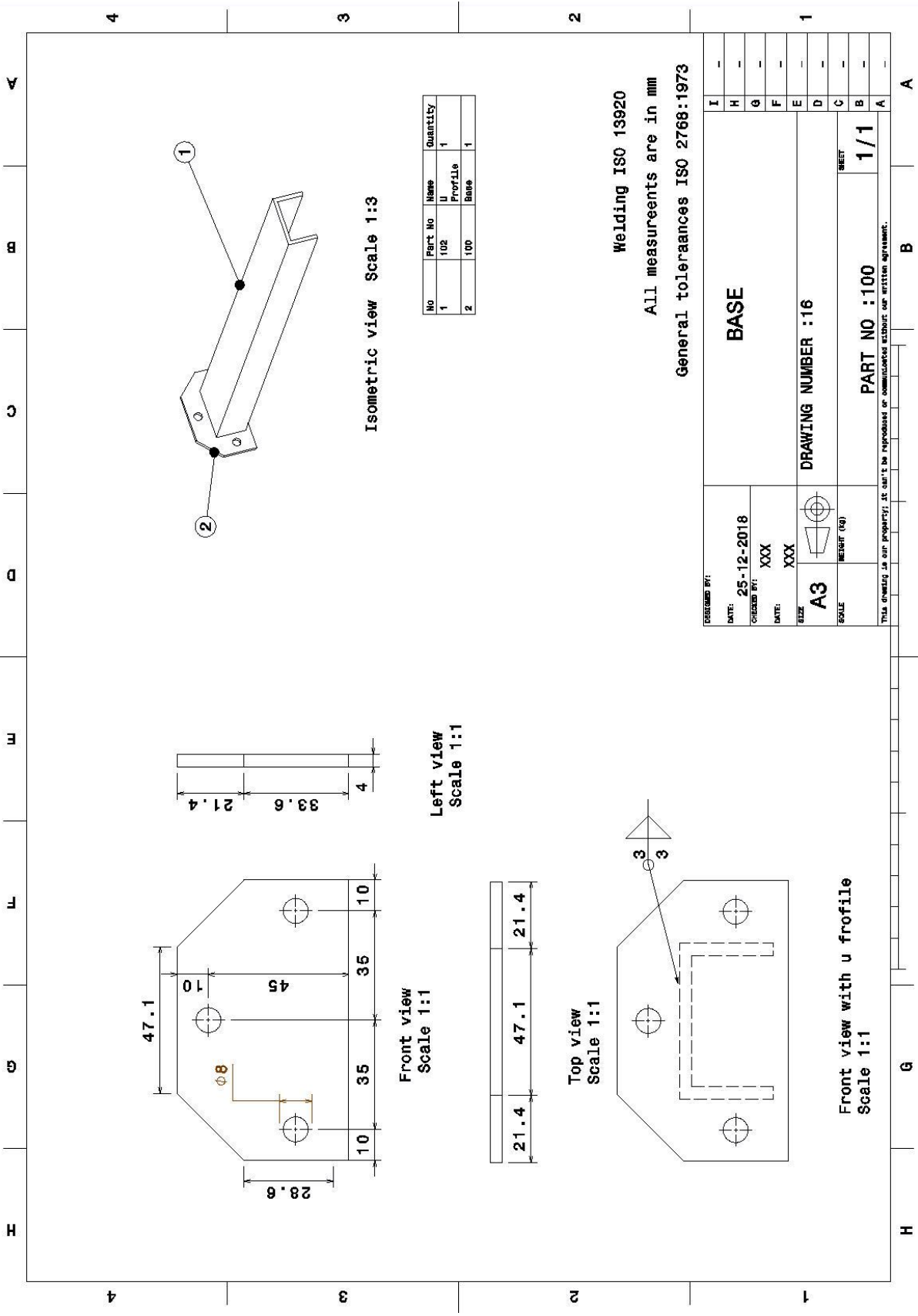
All measurements are in mm
 General tolerances ISO 2768:1973

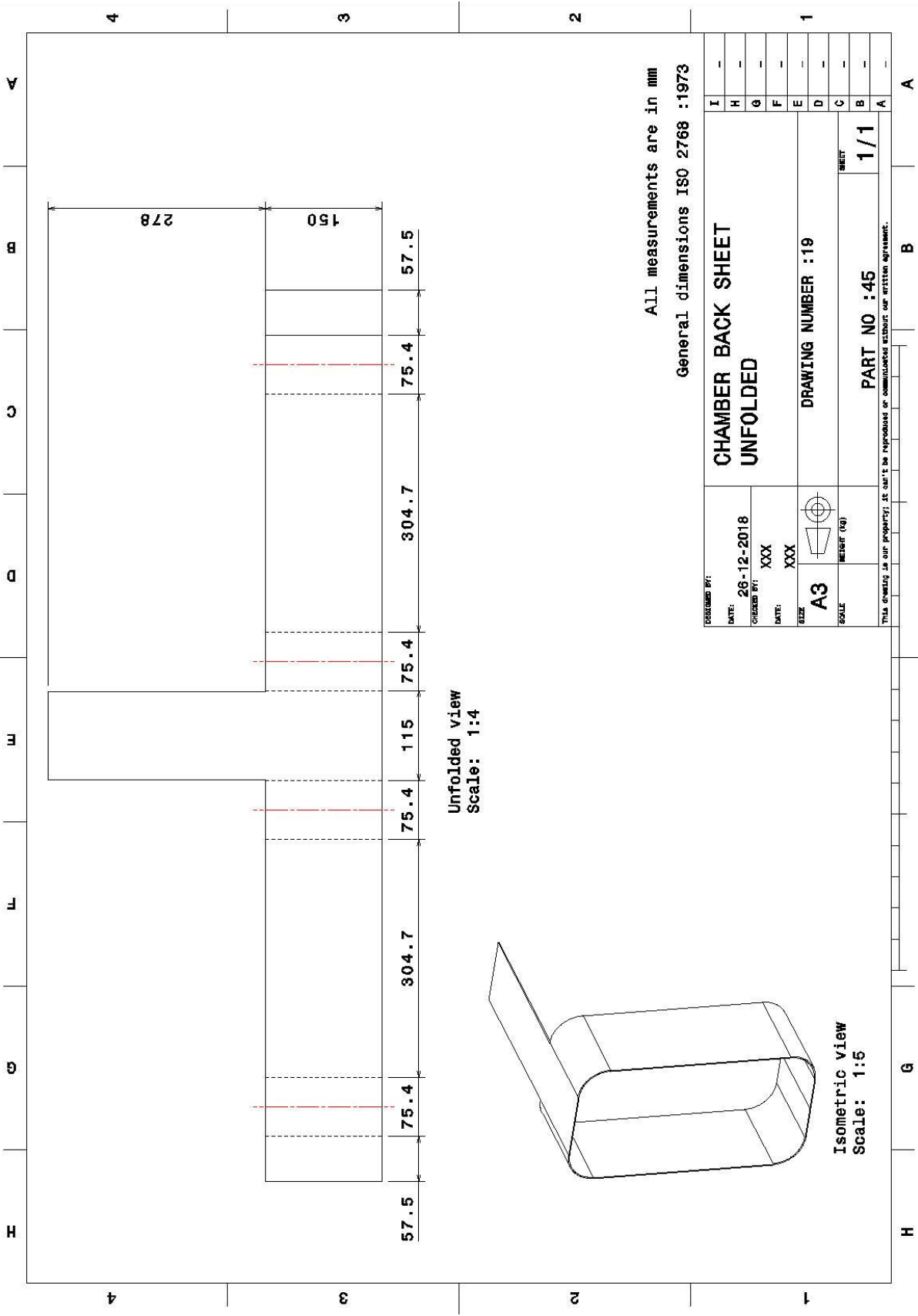
DESIGNED BY:		DATE: 25-12-2018	
DRAWN BY:		DATE: XXX	
CHECKED BY:		DATE: XXX	
SIZE: A3	SCALE: METRIC (kg)	DRAWING NUMBER : 14	
SHEET: 1/1		PART NO : 12	

THIS DRAWING IS OUR PROPERTY. IT CAN'T BE REPRODUCED OR COMMUNICATED WITHOUT OUR WRITTEN AGREEMENT.



Attachment 16

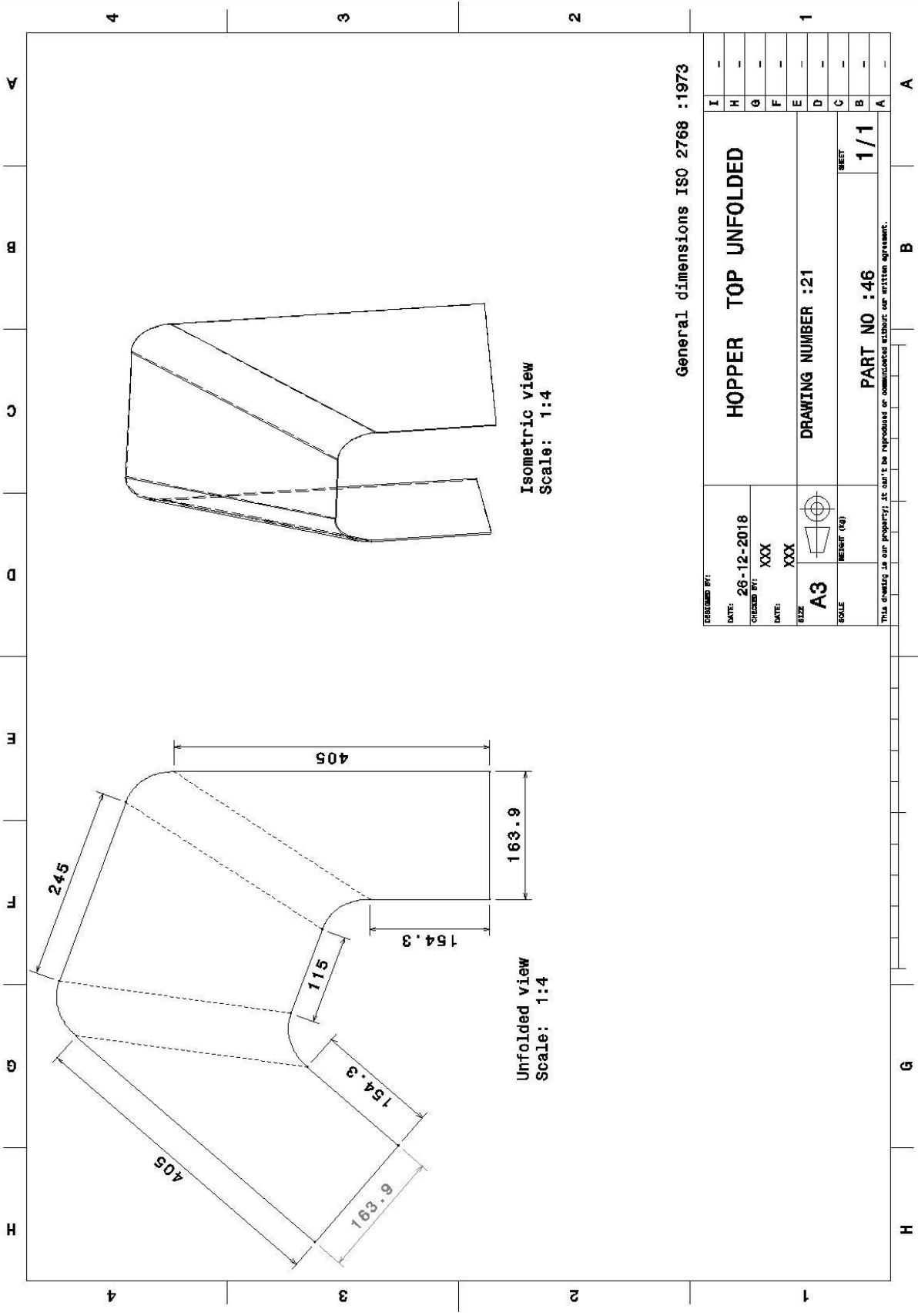


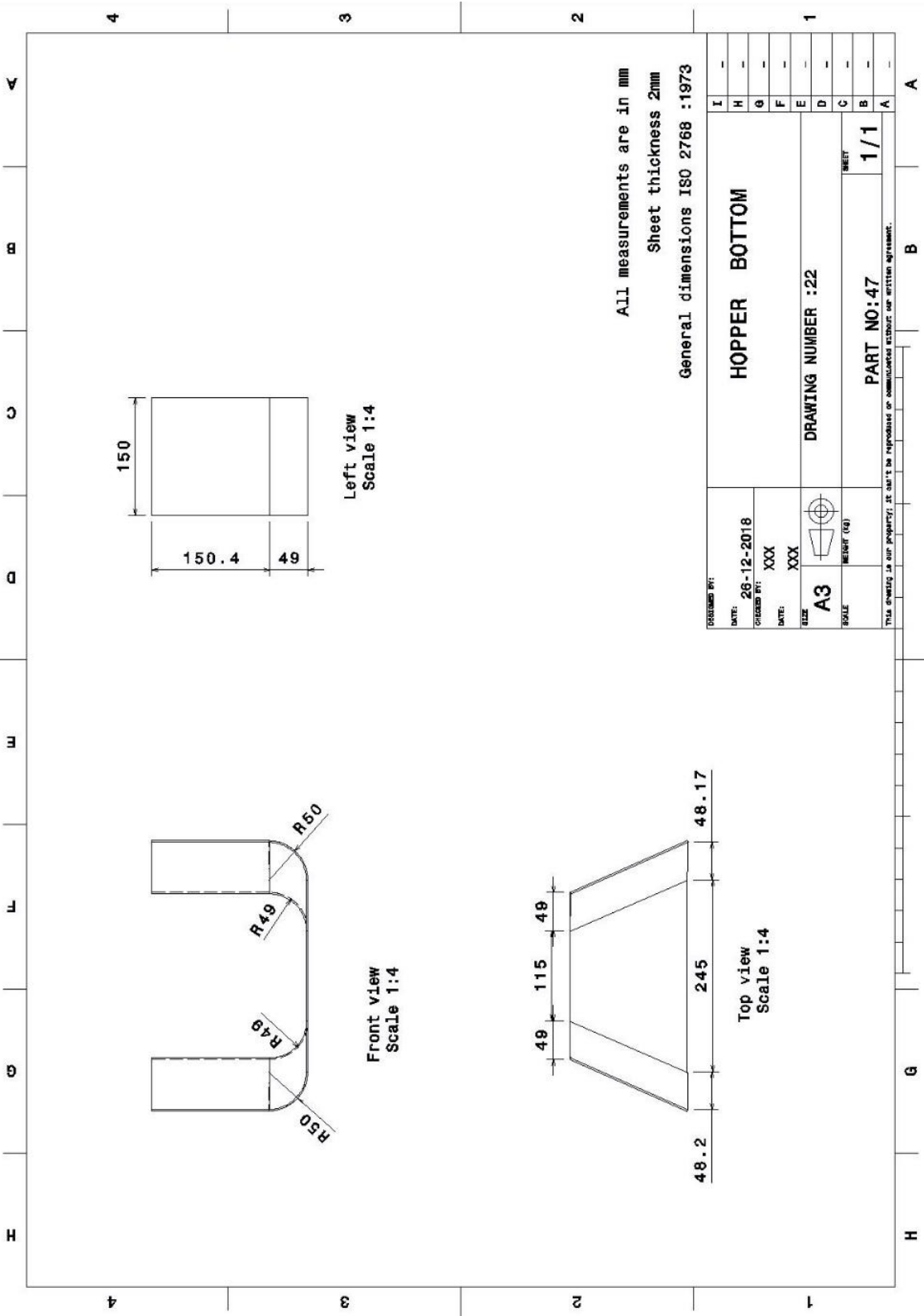


All measurements are in mm
General dimensions ISO 2768 : 1973

DESIGNED BY:		DATE: 20-12-2018	
CHECKED BY: XXX		DATE: XXX	
SIZE: A3		DRAWING NUMBER : 19	
SCALE: METRIC (M)		PART NO : 45	
SHEET		1/1	

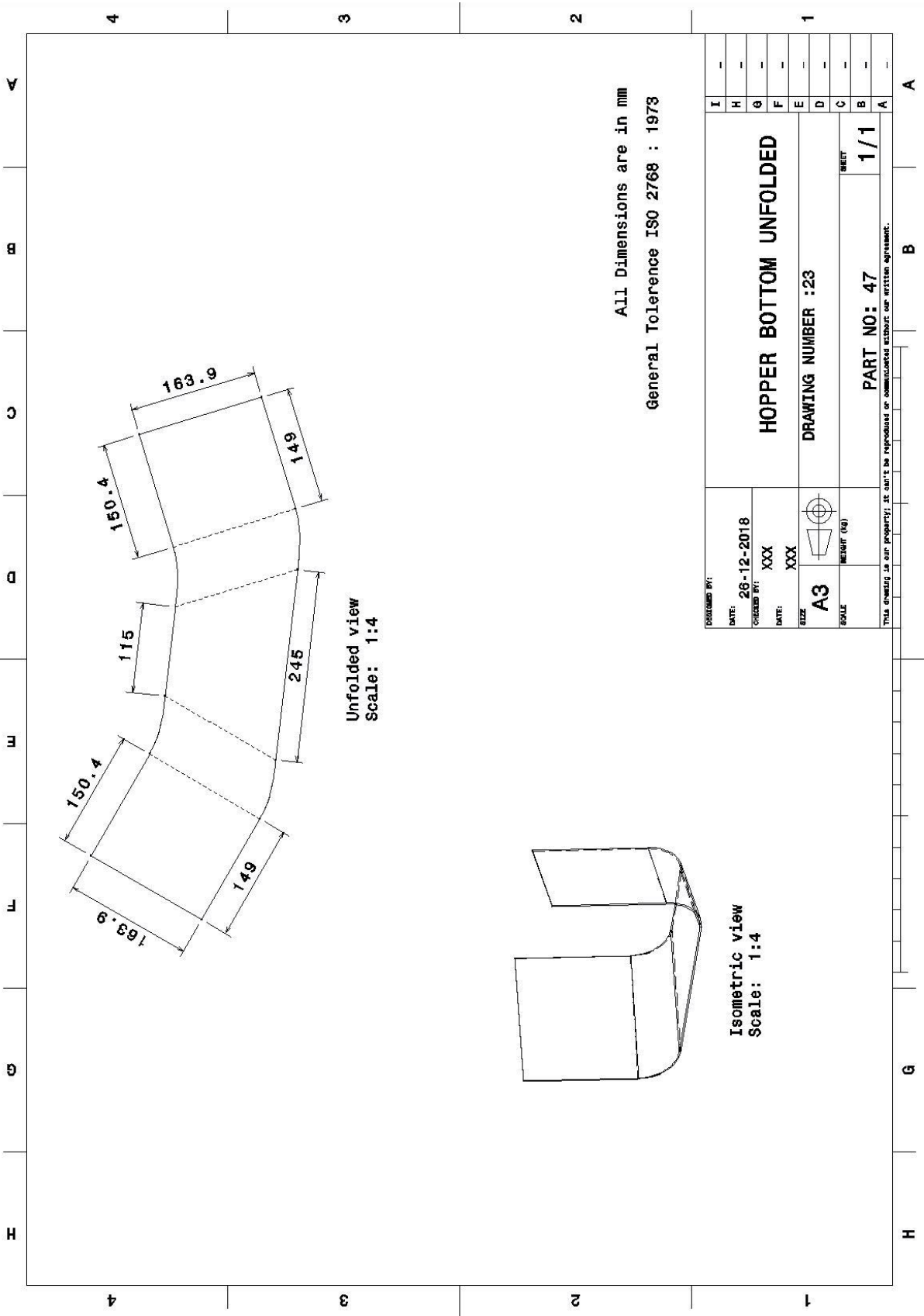
THIS DRAWING IS OUR PROPERTY, IT CAN'T BE REPRODUCED OR COMMERCIALIZED WITHOUT OUR WRITTEN AGREEMENT.

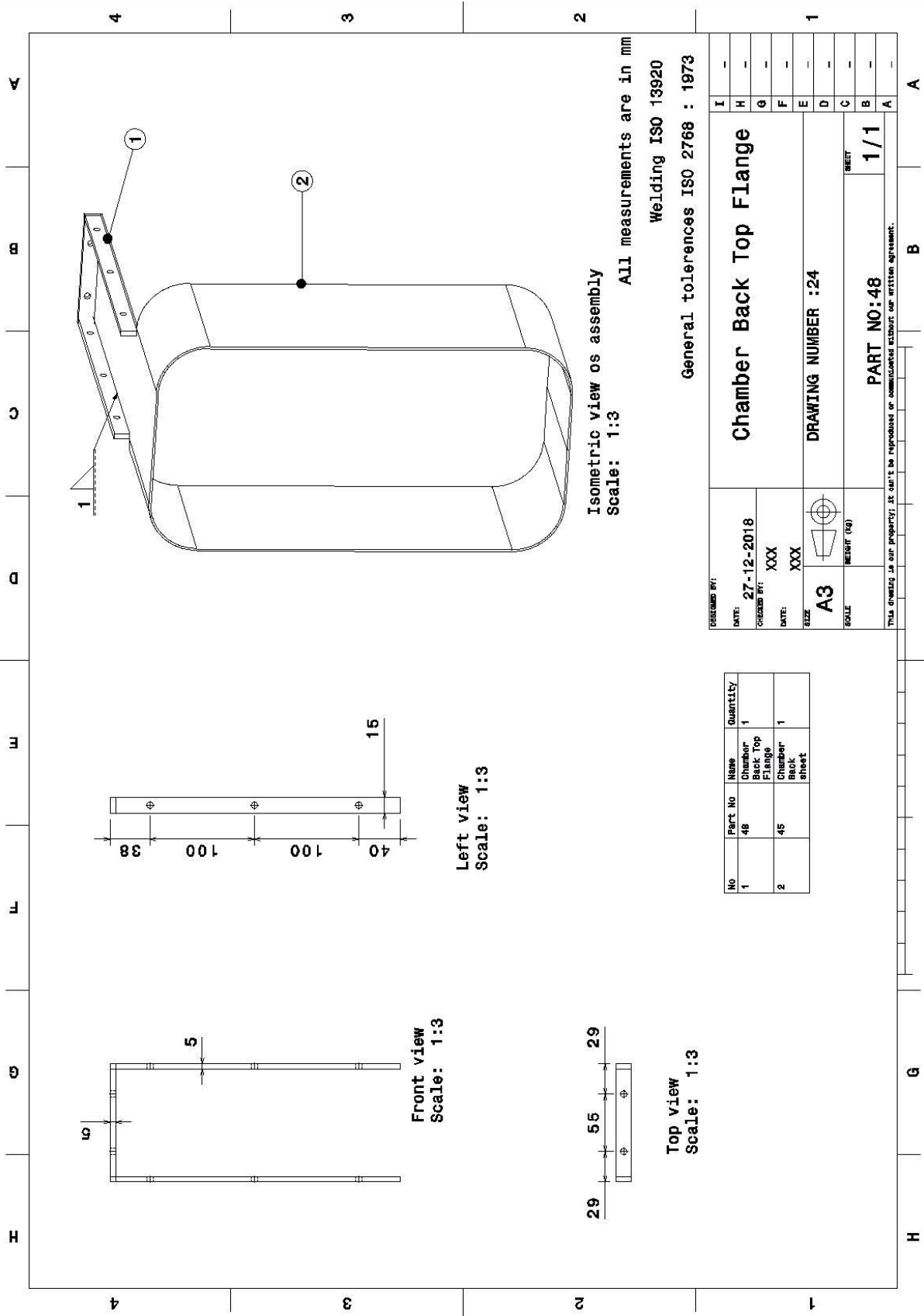




All measurements are in mm
 Sheet thickness 2mm
 General dimensions ISO 2768 :1973

DATE: 26-12-2018	DRAWING NUMBER :22	DRAWING NUMBER :22	PART NO:47	SHEET 1/1
CREATED BY: XXX				
DATE: XXX				
SIZE: A3				
SCALE: 1:1				
THIS DRAWING IS OUR PROPERTY; IT CAN'T BE REPRODUCED OR COMMUNICATED WITHOUT OUR WRITTEN AGREEMENT.				

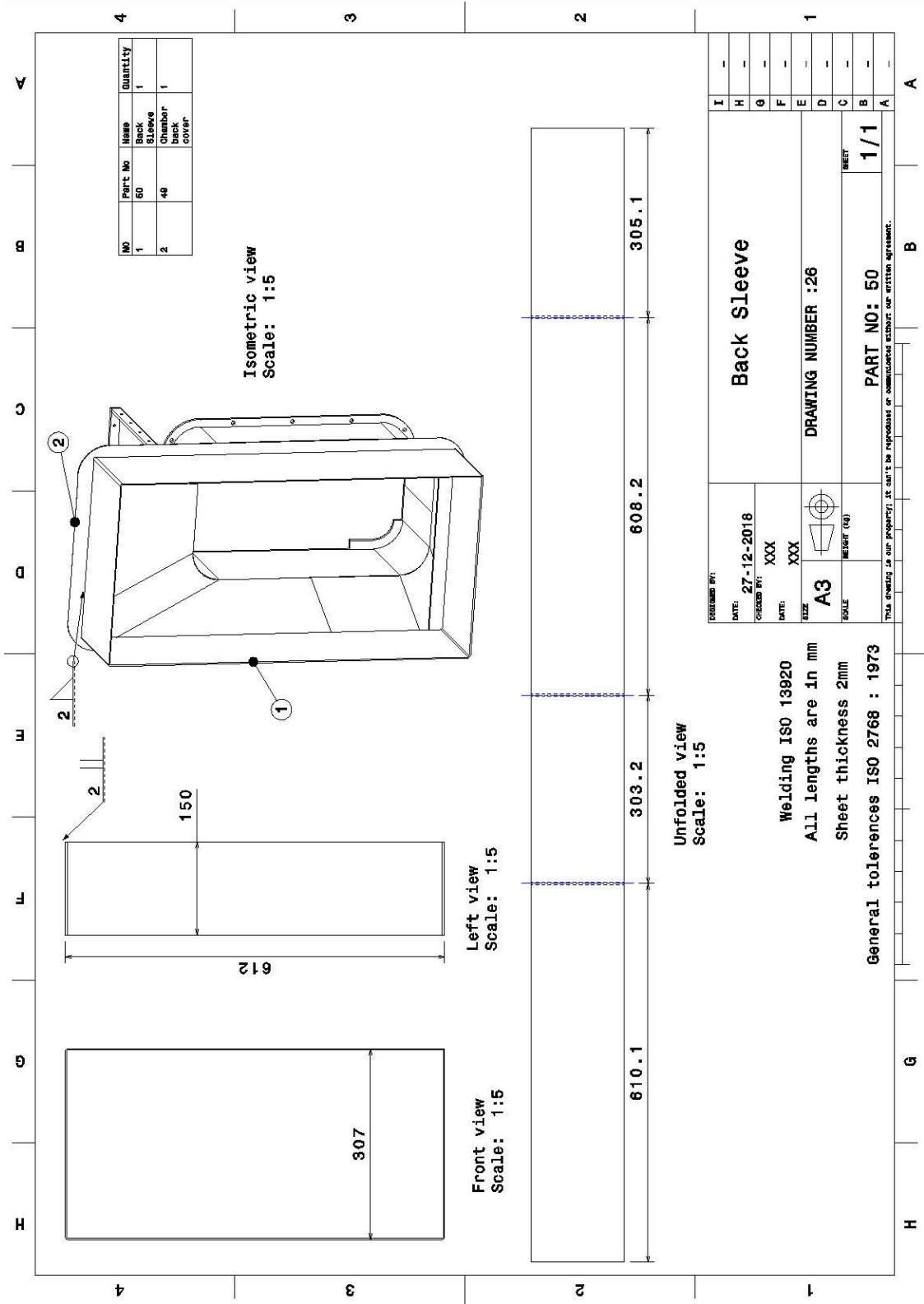


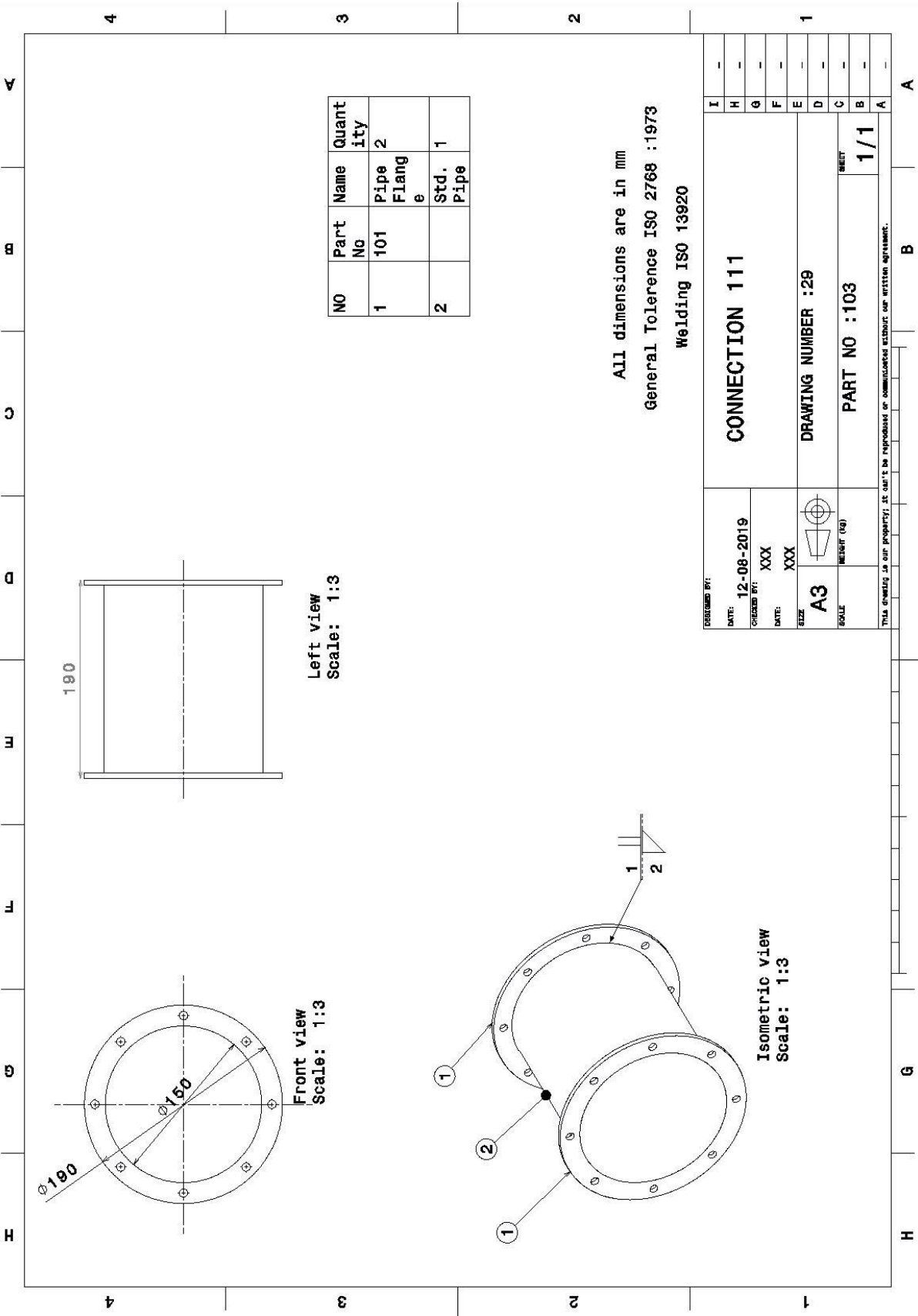


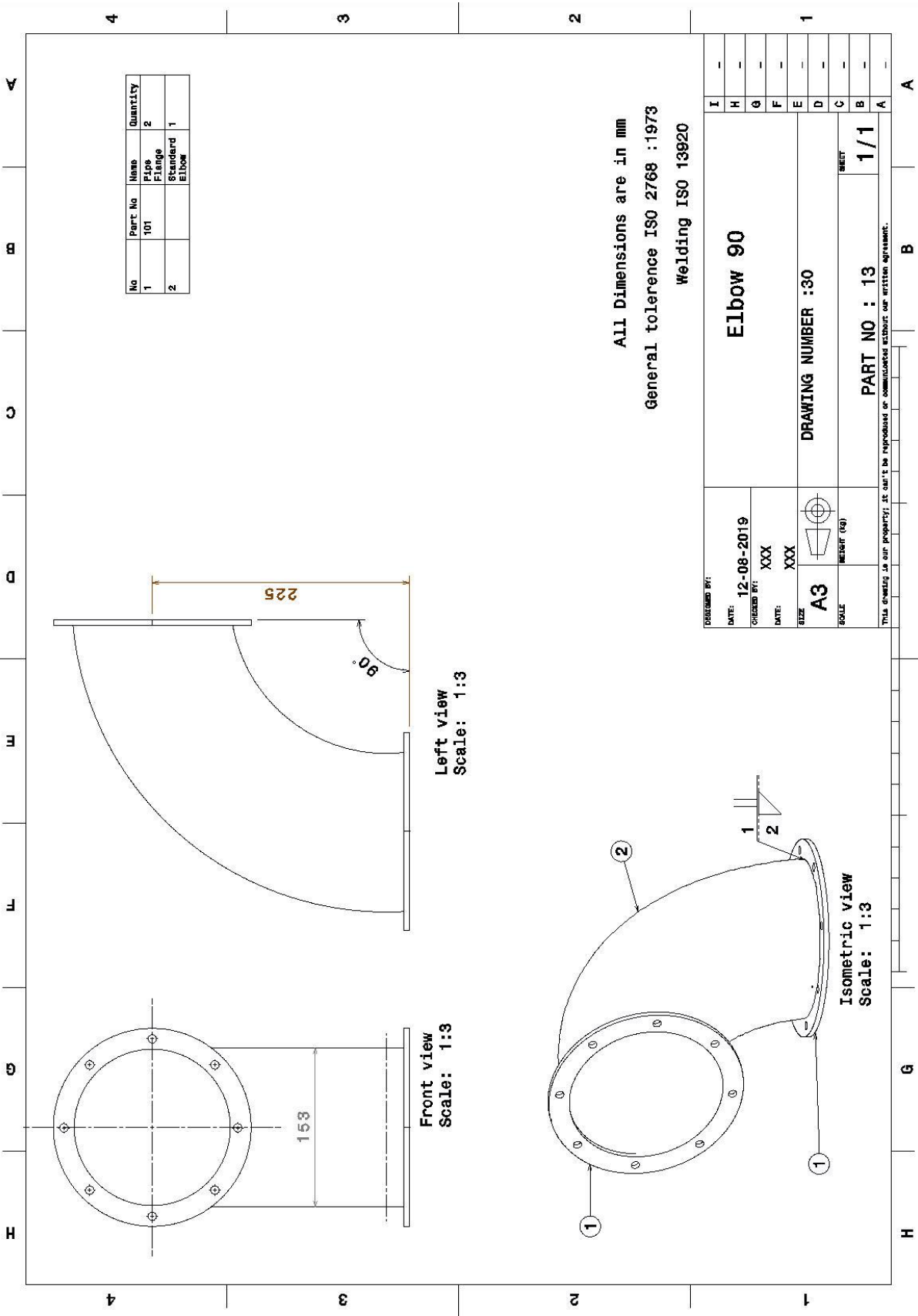
Isometric view of assembly
 Scale: 1:3
 ALL measurements are in mm
 Welding ISO 13920
 General tolerances ISO 2768 : 1973

DATE:	27-12-2018	DESIGNED BY:	
CHECKED BY:	XXX	DATE:	XXX
SIZE:	A3	SCALE:	METRIC (SI)
DRAWING NUMBER :24		SHEET	
PART NO:48		1/1	
THIS DRAWING IS OUR PROPERTY. IT CAN'T BE REPRODUCED OR COMMUNICATED WITHOUT OUR WRITTEN AGREEMENT.			

No	Part No	Name	Quantity
1	48	Chamber Back Top Flange	1
2	45	Chamber Back sheet	1





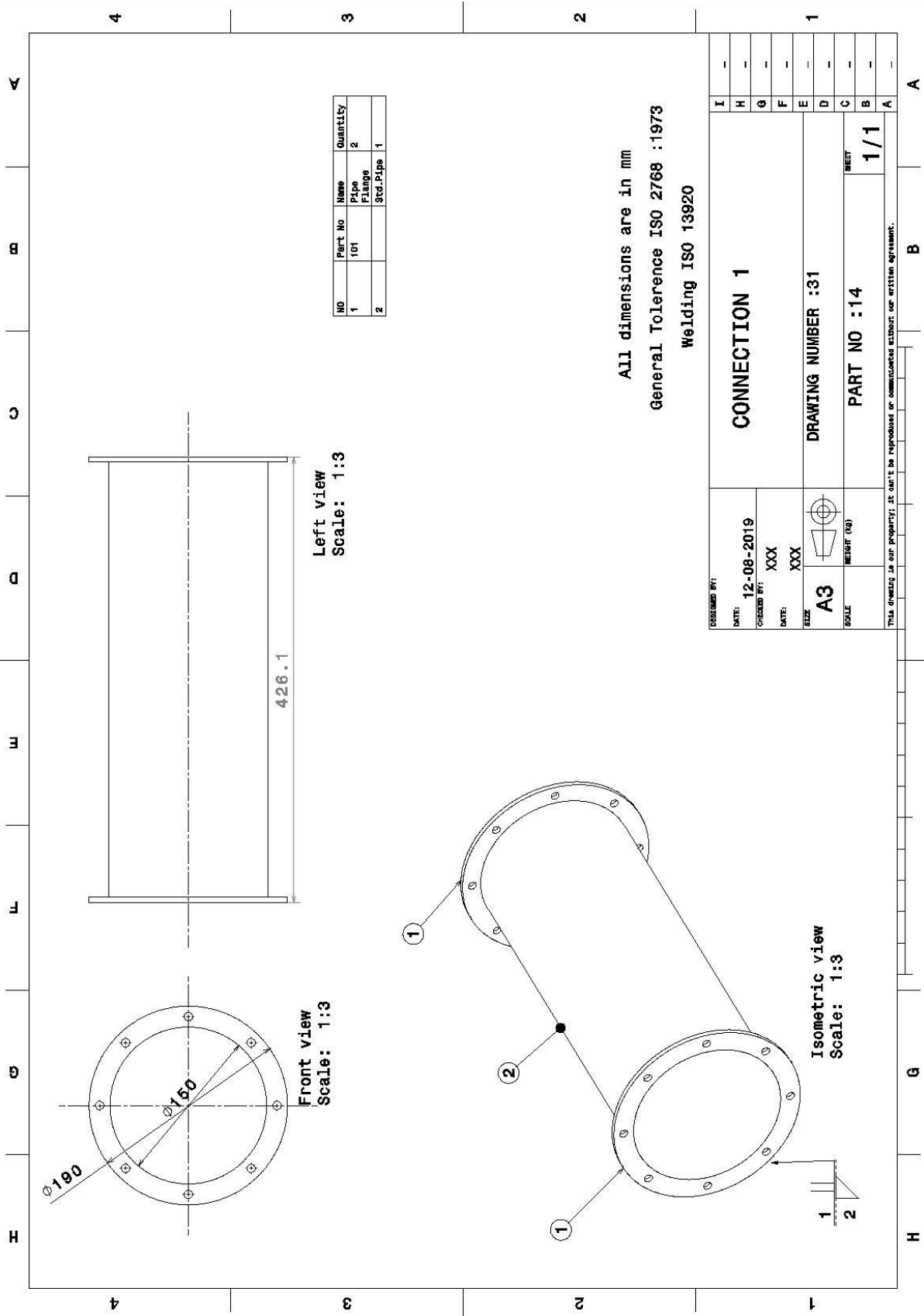


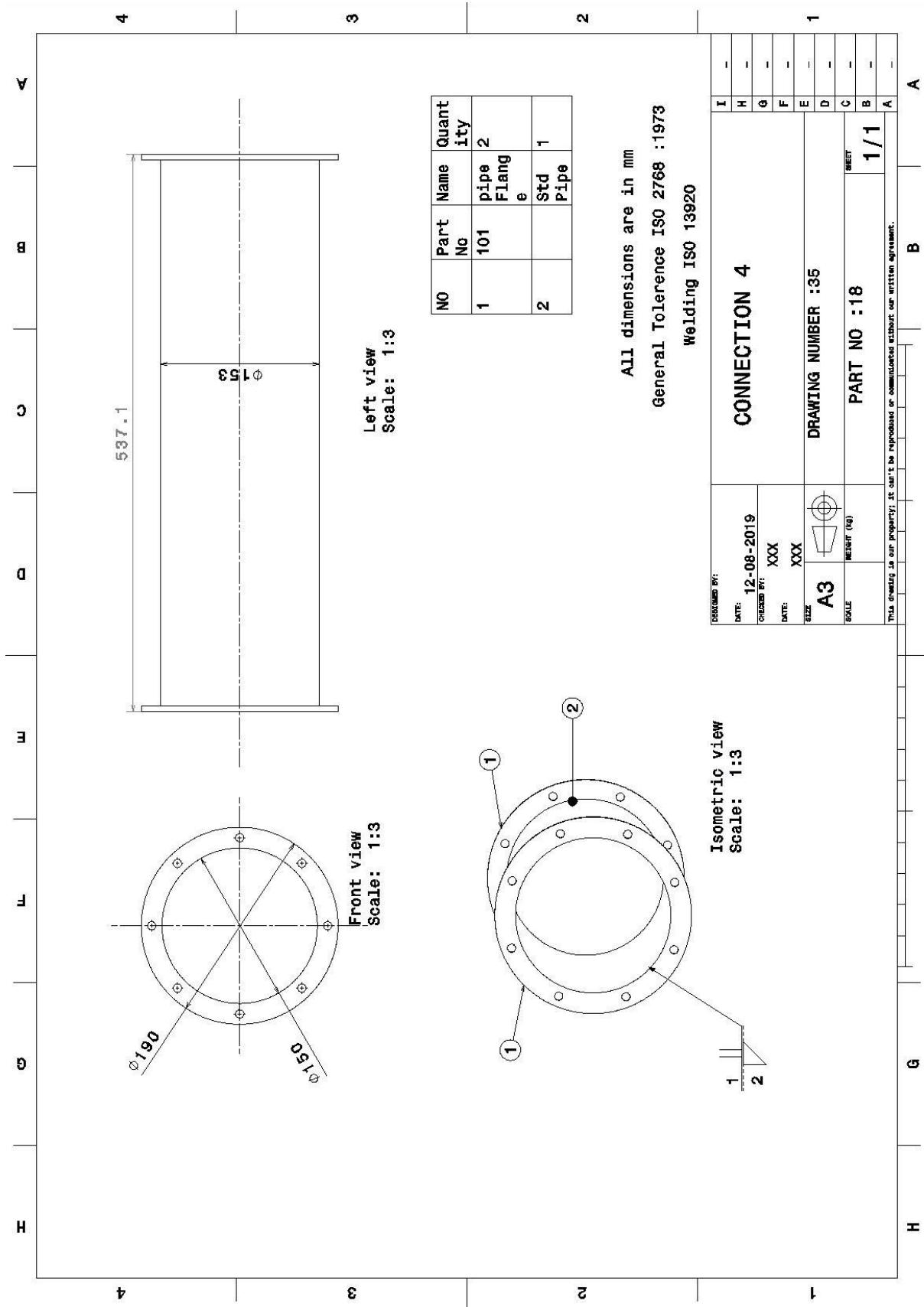
ALL Dimensions are in mm
 General tolerance ISO 2768 :1973
 Welding ISO 13920

DATE: 12-08-2019	ELBOW 90	I	-
CHECKED BY: XXX		H	-
DATE: XXX		G	-
SIZE: A3	DRAWING NUMBER :30	F	-
SCALE: METRIC (SI)		E	-
		D	-
		C	-
		B	-
		A	-

PART NO : 13
 1/1

This drawing is our property, it can't be reproduced or disseminated without our written agreement.

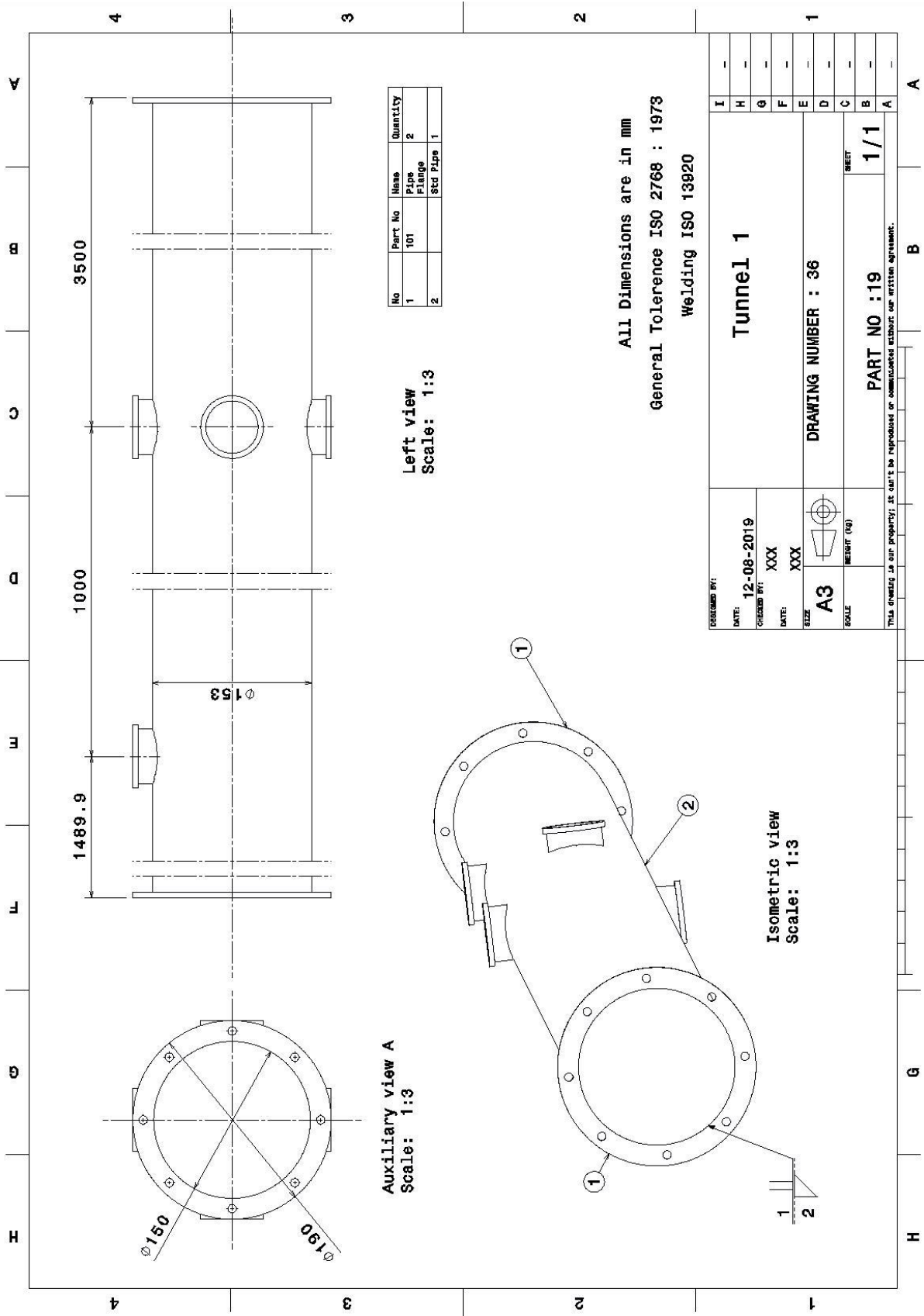


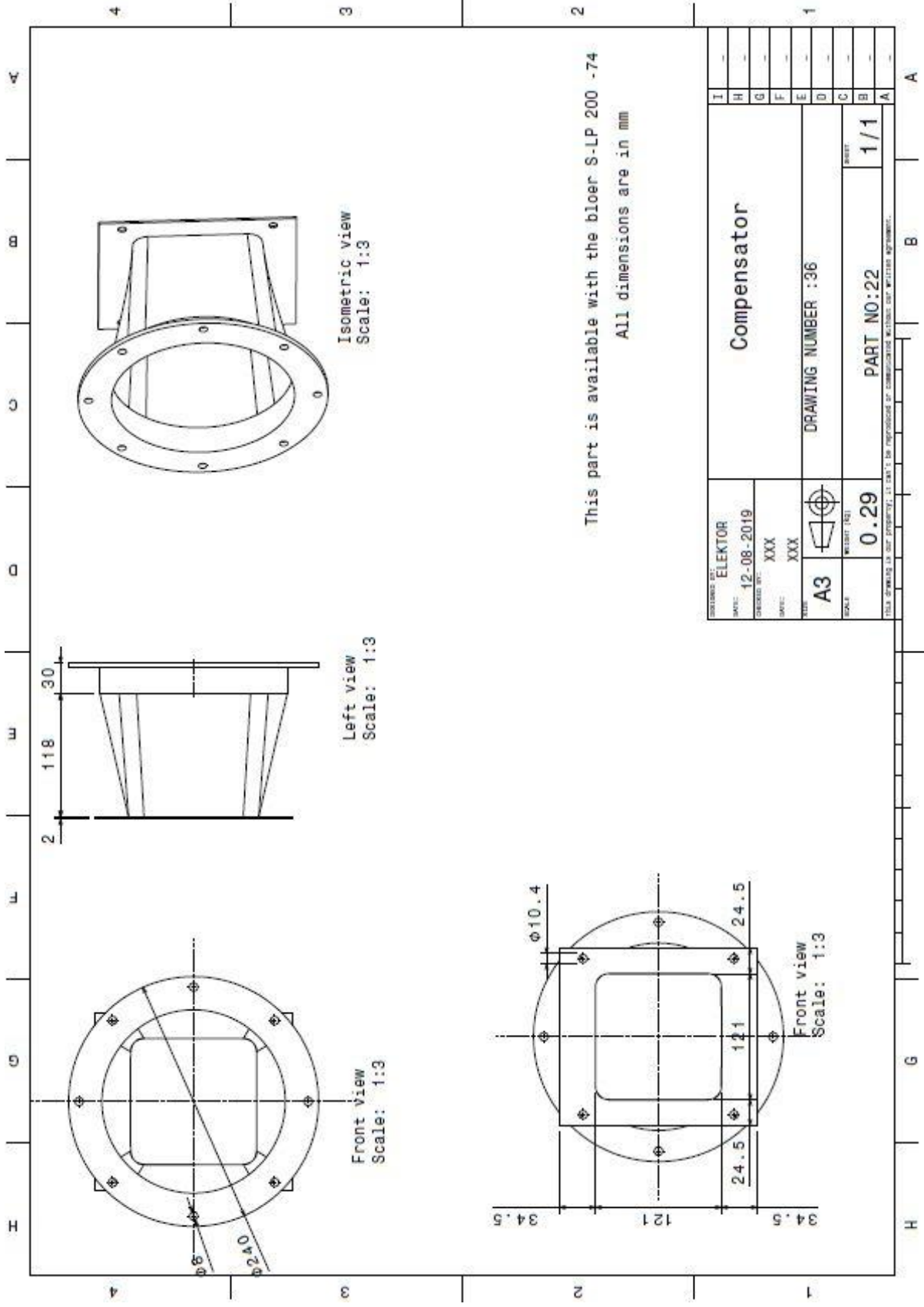


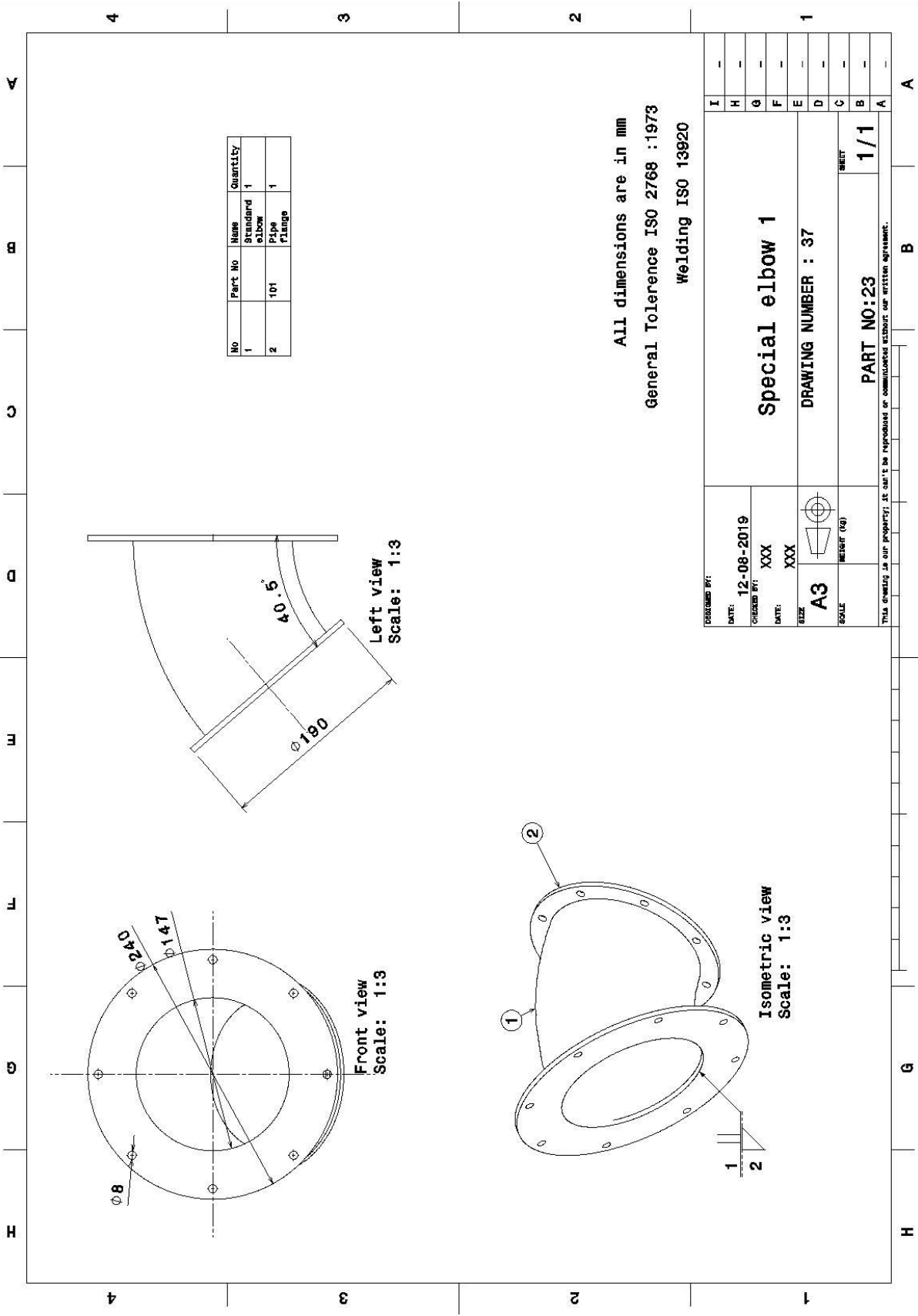
DESIGNED BY:		I
DATE:	12-08-2019	H
CHECKED BY:	XXX	G
DATE:	XXX	F
SIZE:	A3	E
SCALE:	METRIC (kg)	D
DRAWING NUMBER : 35		C
PART NO : 18		B
SHEET		A
1/1		

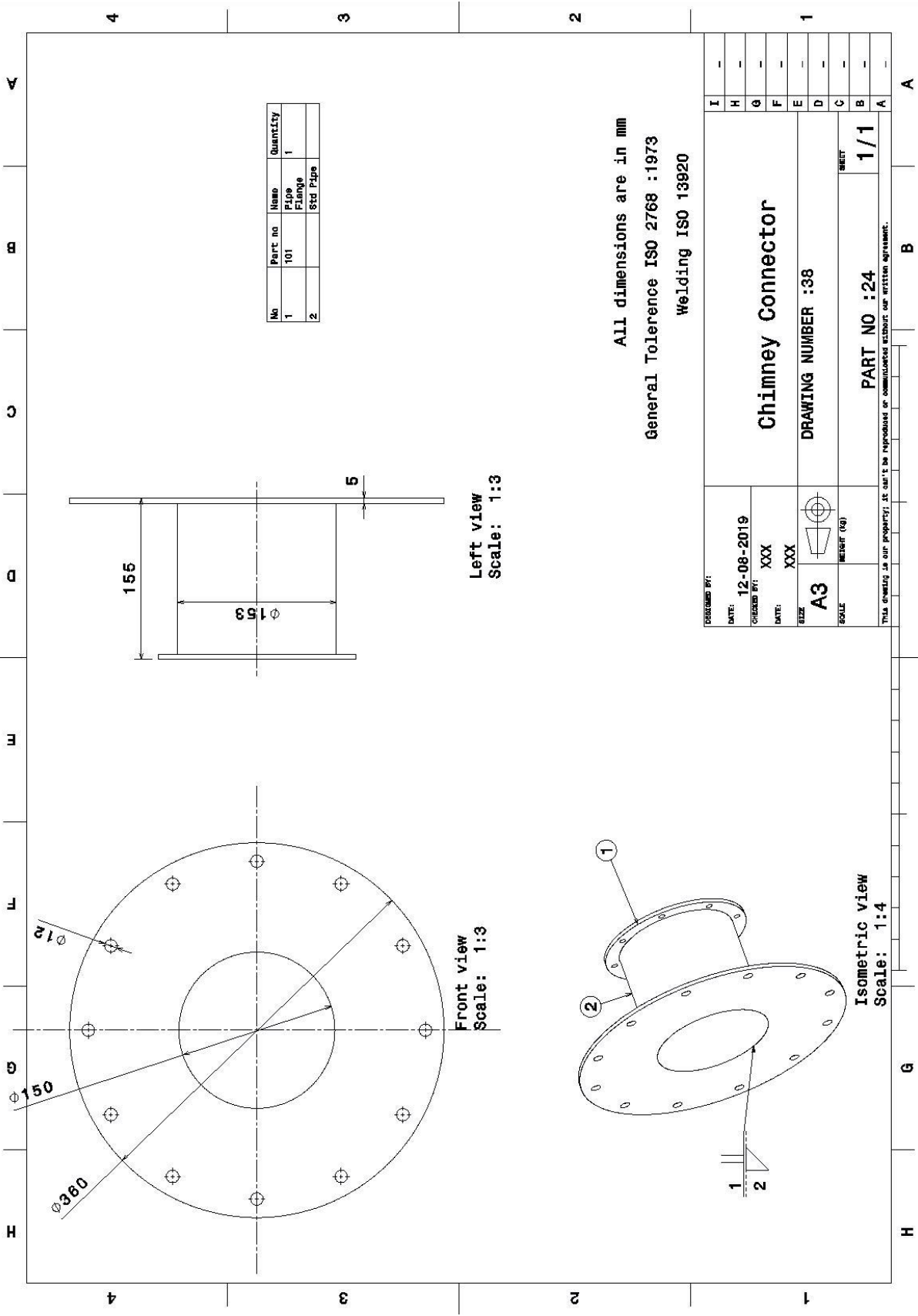
CONNECTION 4

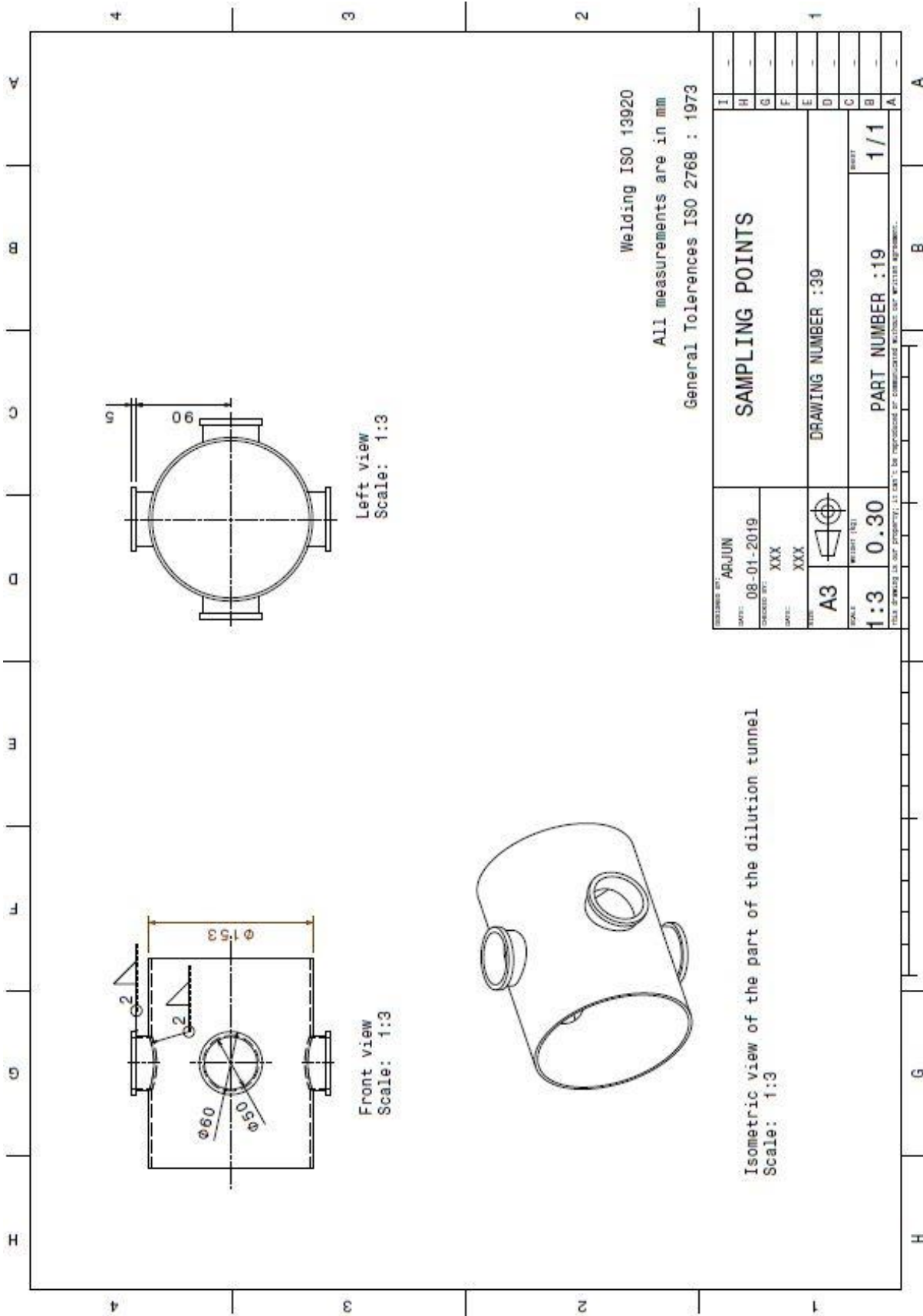
THIS DRAWING IS OUR PROPERTY. IT CAN'T BE REPRODUCED OR COMMUNICATED WITHOUT OUR WRITTEN AGREEMENT.

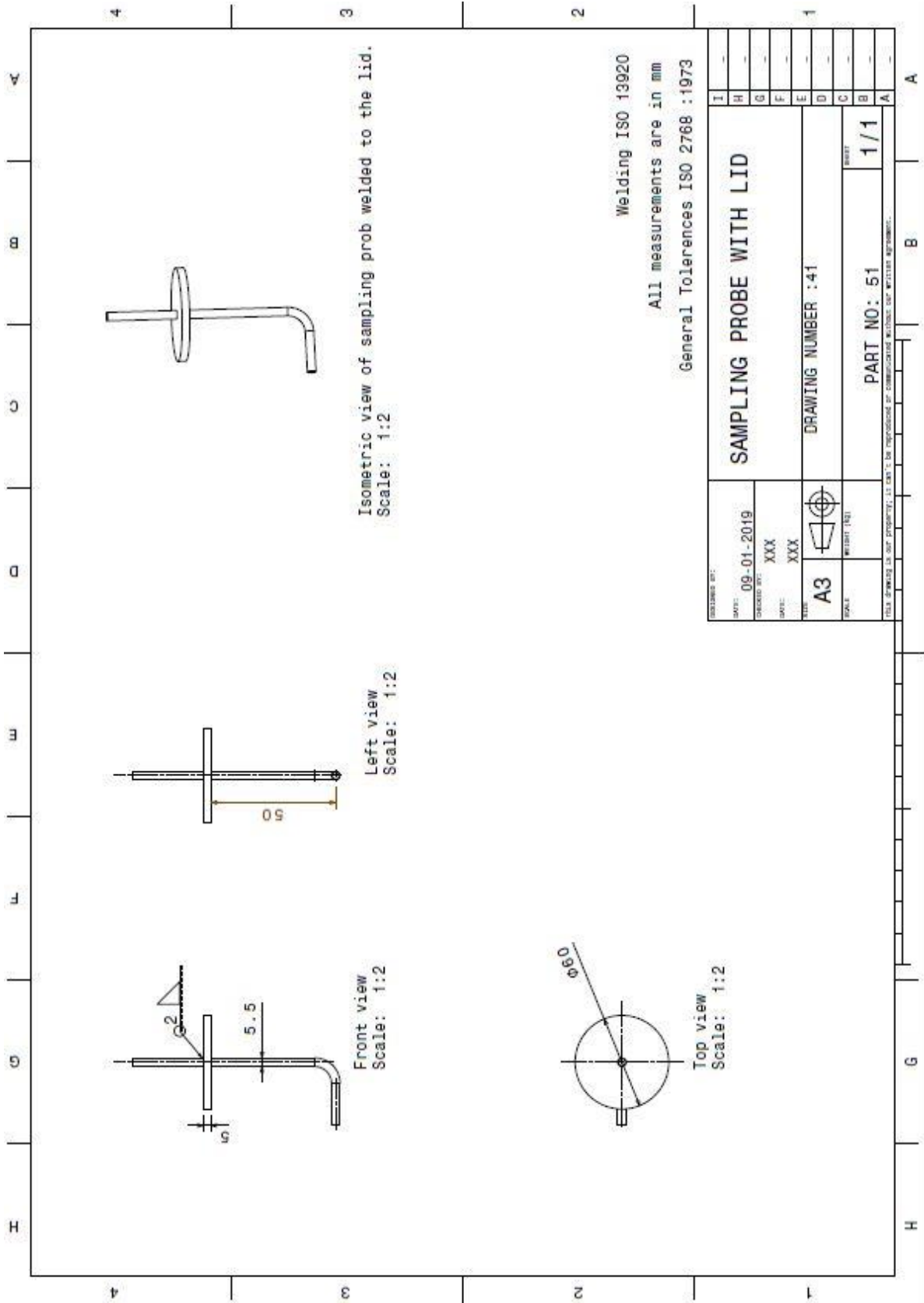


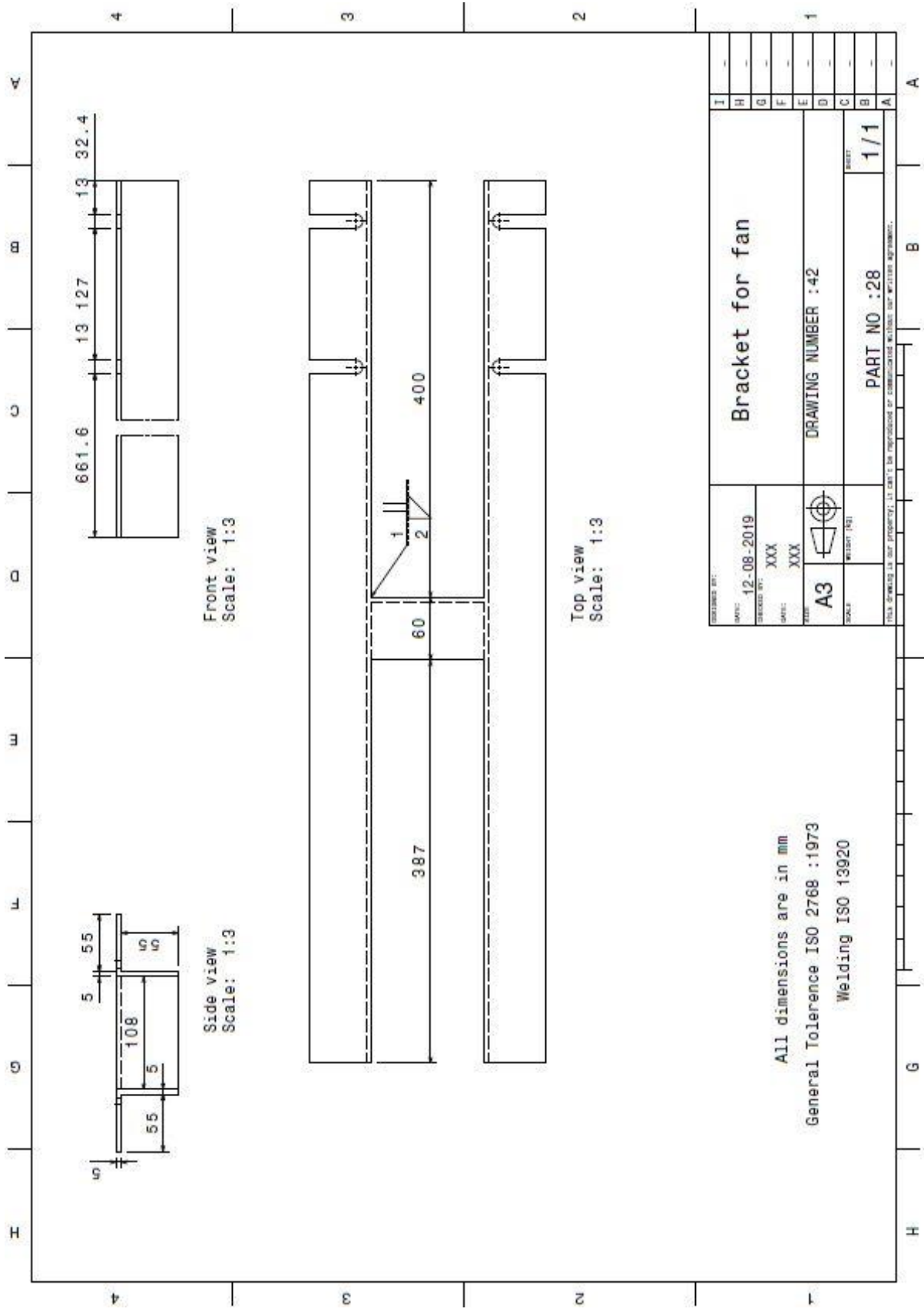


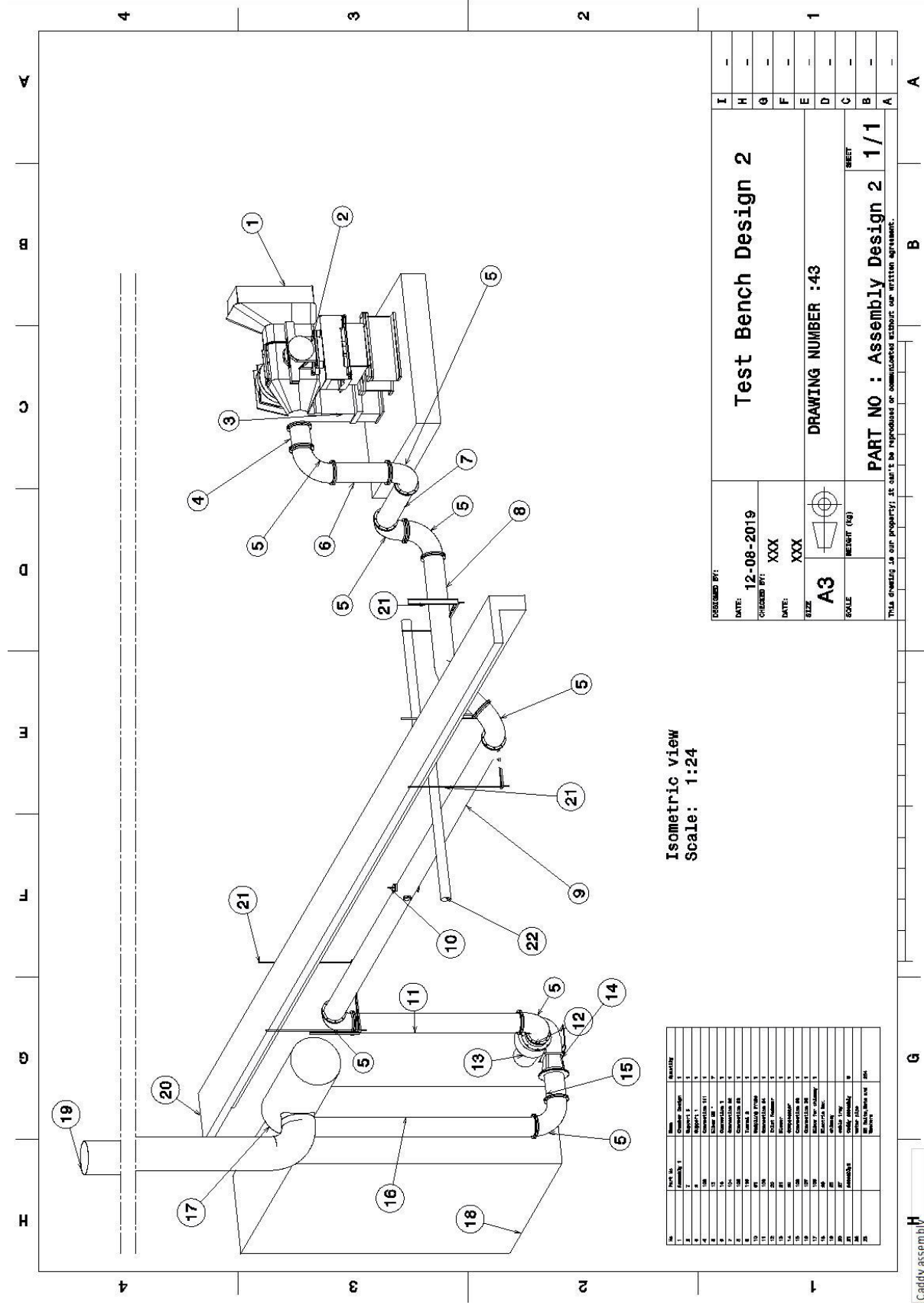




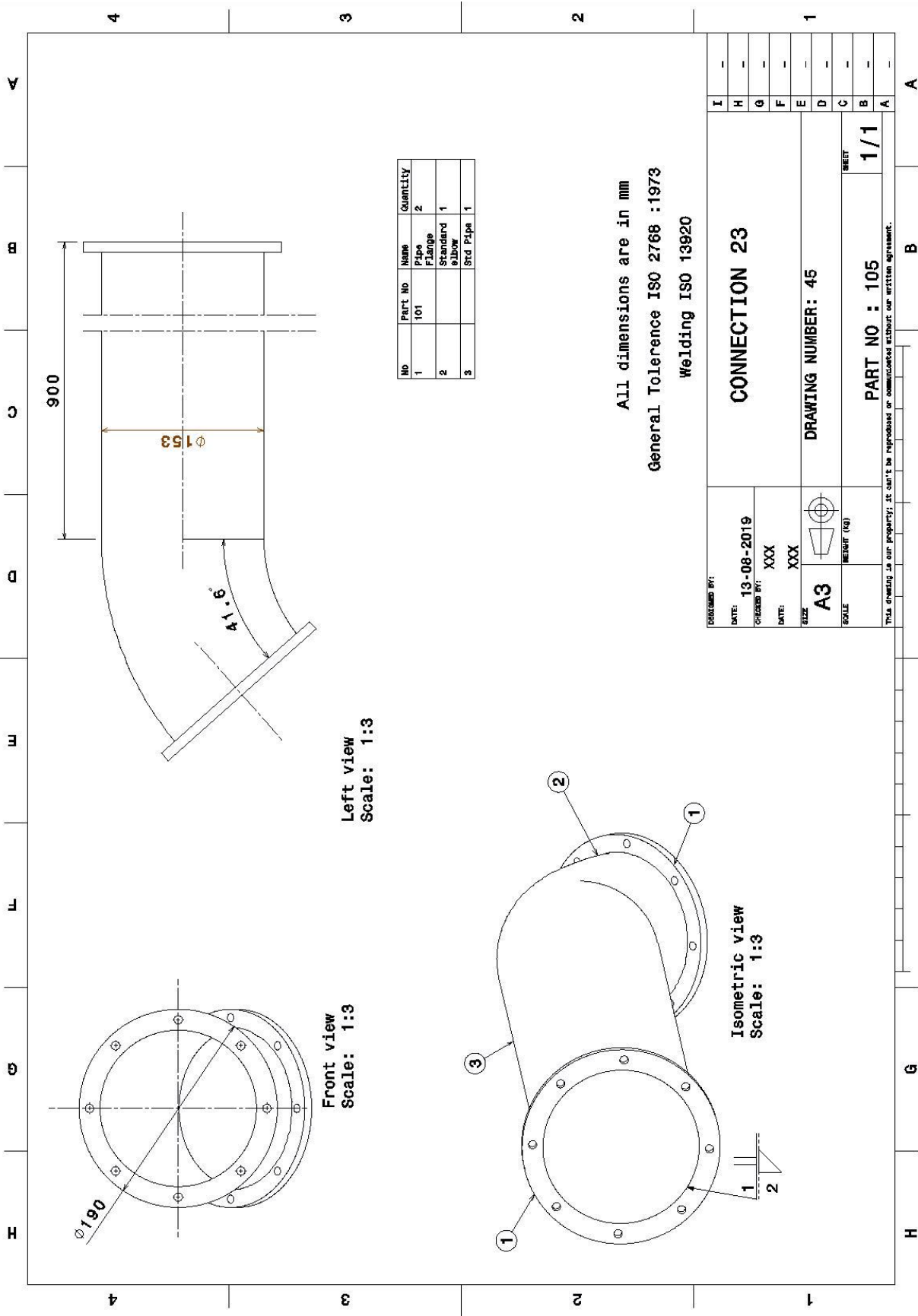


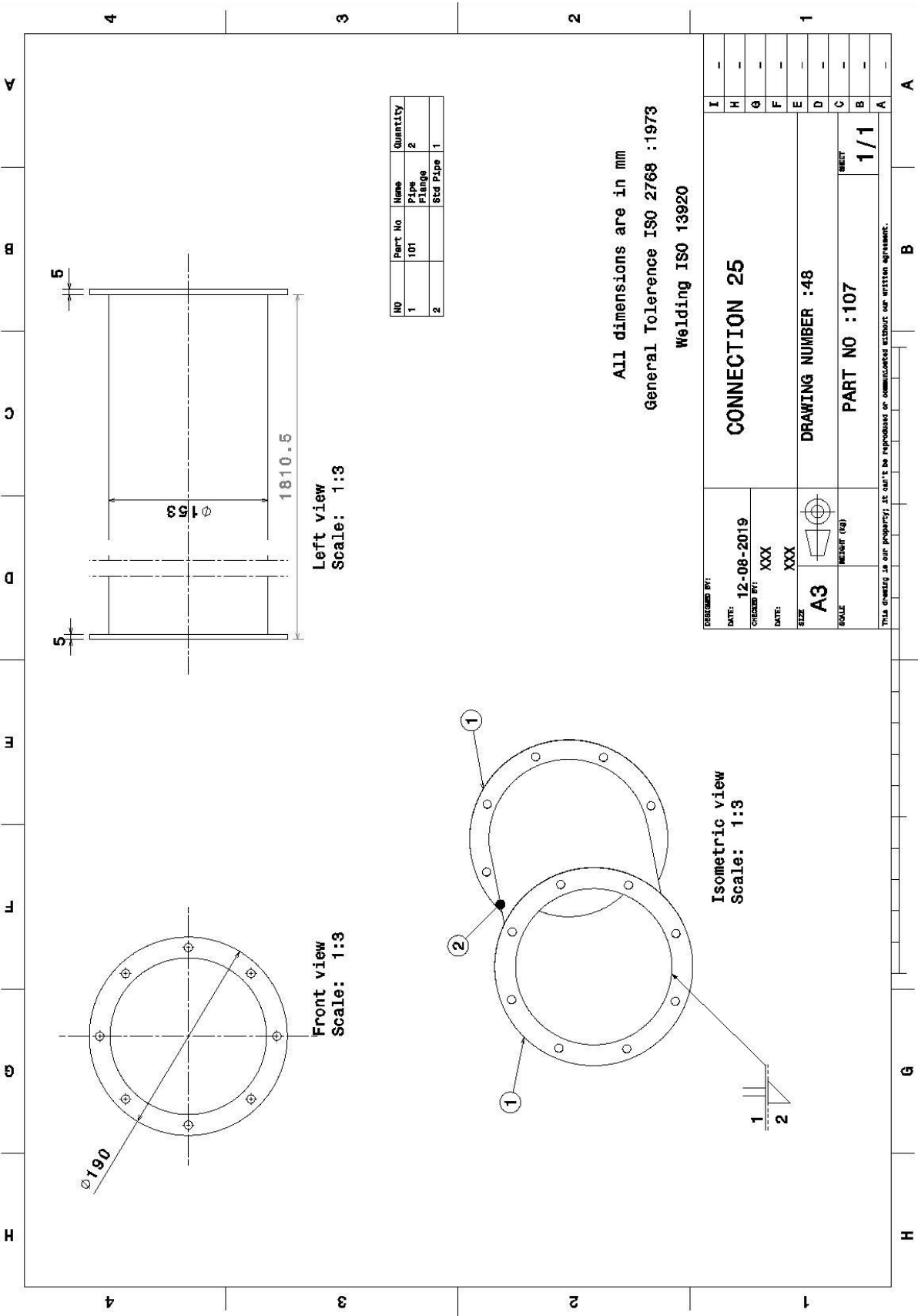


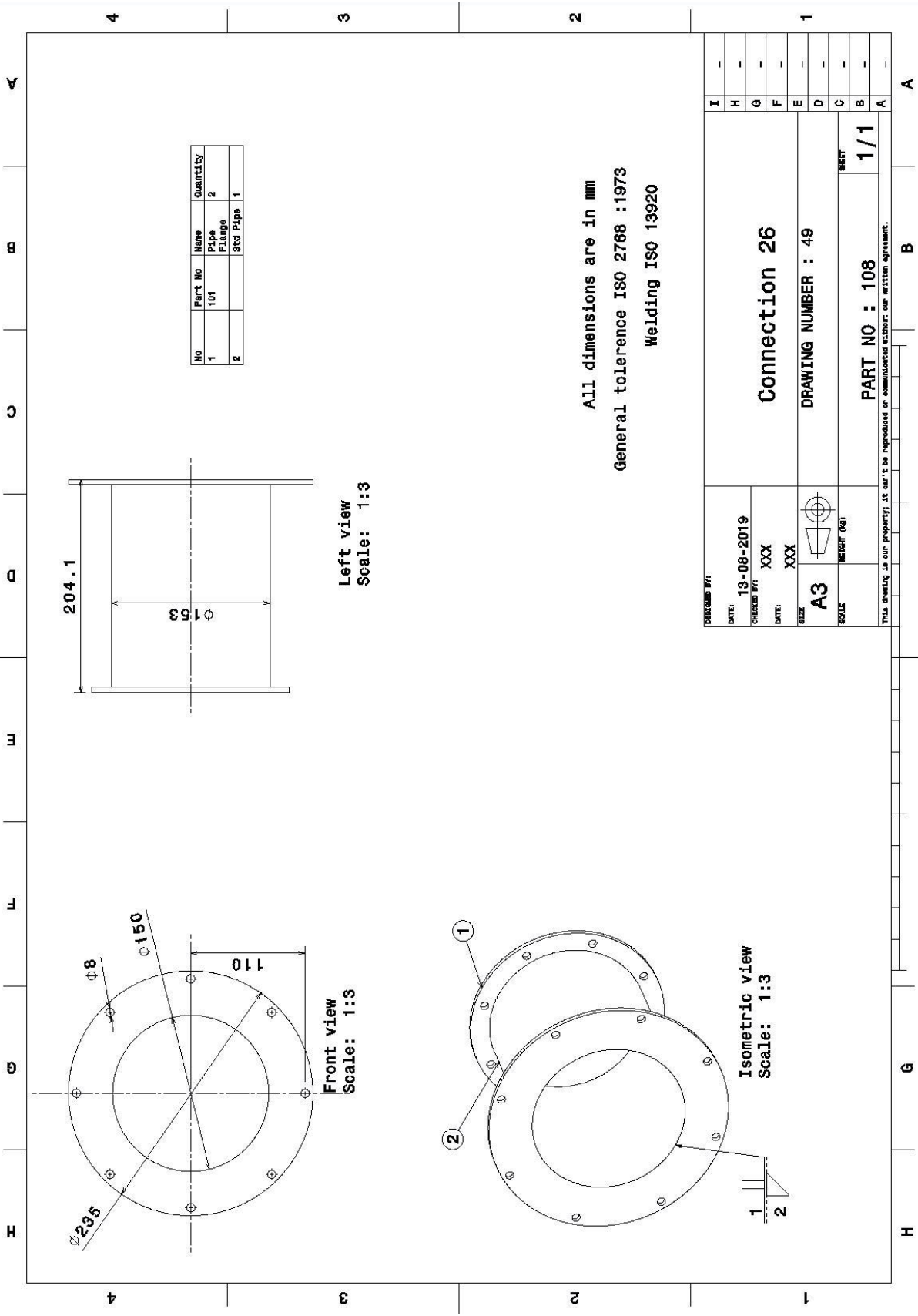


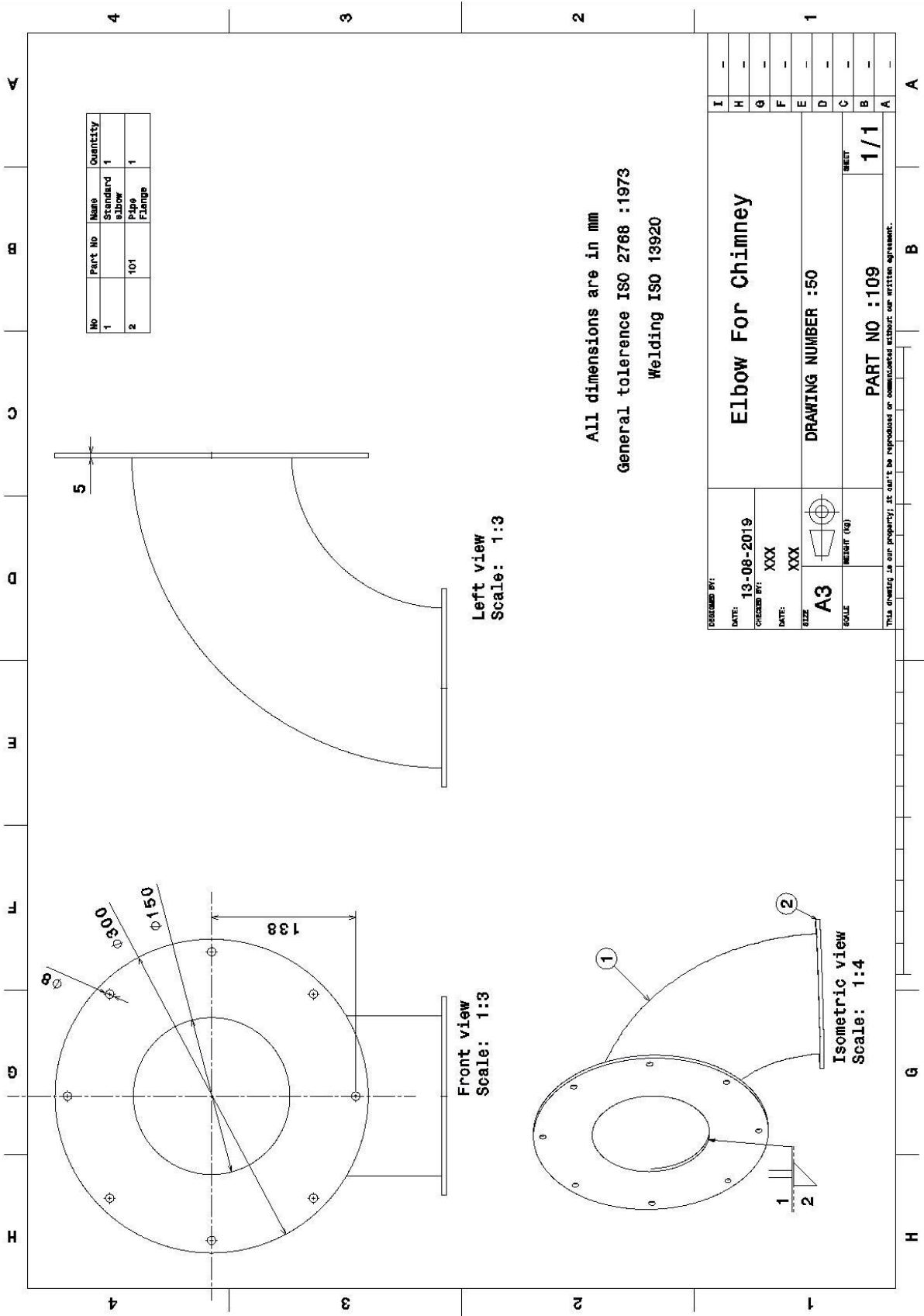


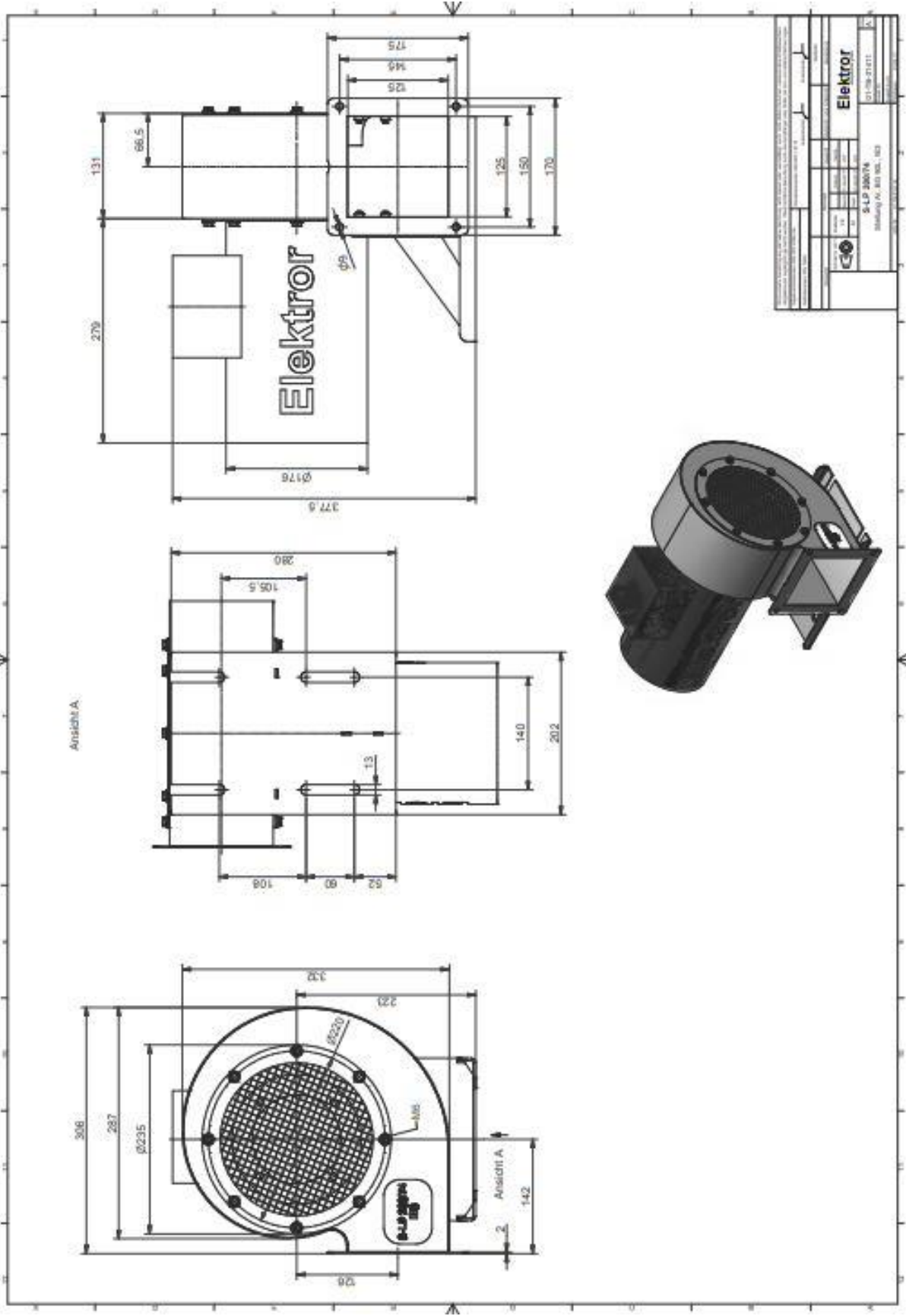
Caddy assembly



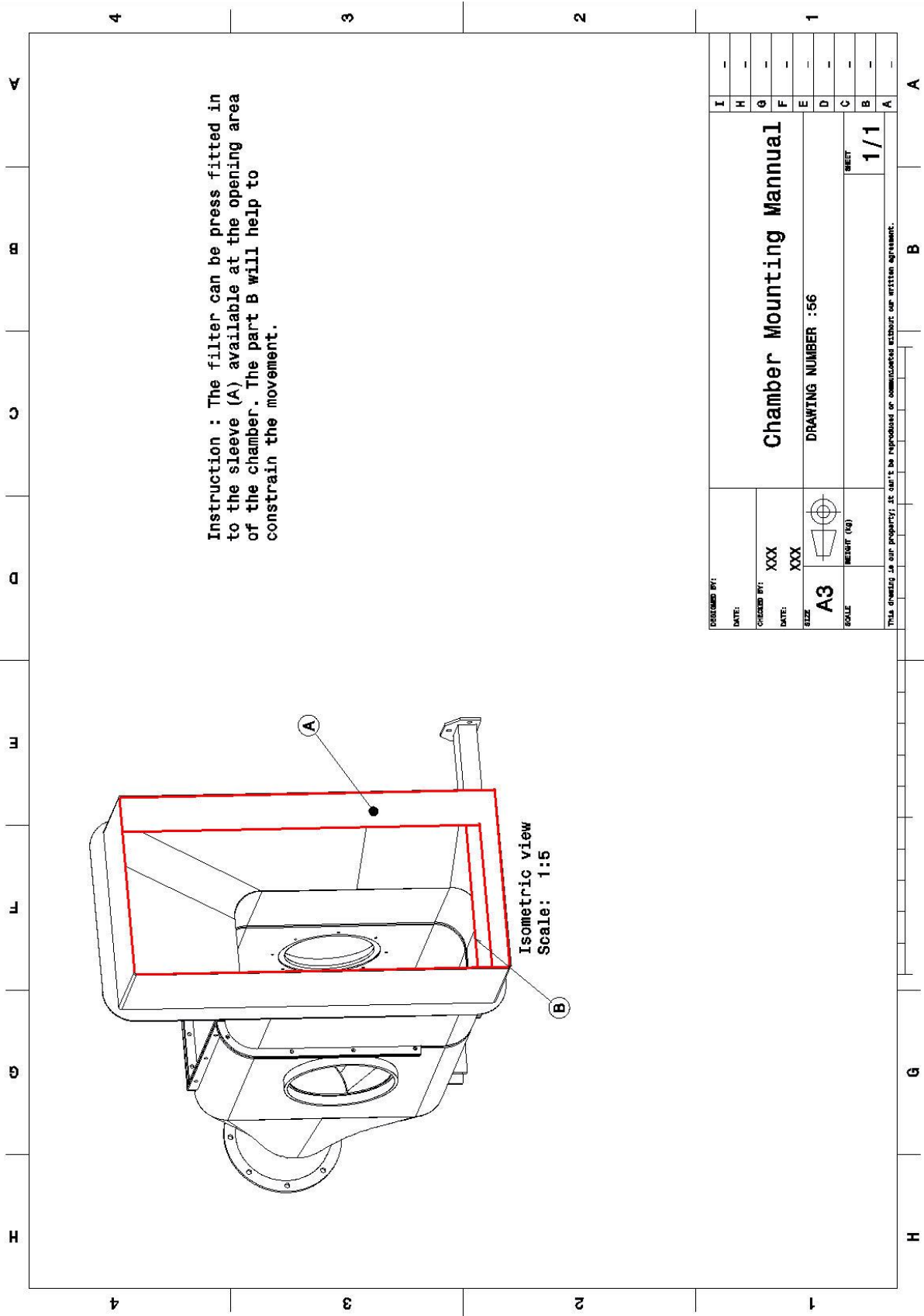








Attachment 53



Instruction : The filter can be press fitted in to the sleeve (A) available at the opening area of the chamber. The part B will help to constrain the movement.

DESIGNED BY:		I	-
DATE:		H	-
CHECKED BY:	XXX	G	-
DATE:	XXX	F	-
SIZE:	A3	E	-
SCALE:	METRIC (SI)	D	-
		C	-
		B	-
		A	-
DRAWING NUMBER : 56		SHEET	
		1 / 1	
THIS DRAWING IS OUR PROPERTY. IT CAN'T BE REPRODUCED OR COMMERCIALIZED WITHOUT OUR WRITTEN AGREEMENT.			